UNIVERSITY OF CALIFORNIA, SAN DIEGO

The Evolution of Glacial Conditions in the Southern Atlantic Ocean: A Depth Transect Approach

A dissertation submitted in partial satisfaction of the requirements for the degree of Doctor of Philosophy

in

Oceanography

by

Alan Dean Foreman

Committee in charge:

Professor Christopher Charles, Chair
Professor Jess Adkins
Professor Ralph Keeling
Professor Jennifer MacKinnon
Professor Margaret Schoeninger
Professor Jeffrey Severinghaus

2017

The Dissertation of Alan Dean Foreman is approved, and it is acceptable in quality and form for publication on microfilm and electronically:

_____

_____

_____

_____

_____

_____

Chair

University of California, San Diego

2017

EPIGRAPH

"Earth is ancient now, but all knowledge is stored up in her. She keeps a record of everything that has happened since time began. Of time before time, she says little, and in a language that no one has yet understood. Through time, her secret codes have gradually been broken. Her mud and lava is a message from the past.

Of time to come, she says much, but who listens?"

Jeanette Winterson

TABLE OF CONTENTS

LIST OF ABBREVIATIONS

AABW	Antarctic Bottom Water
AAIW	Antarctic Intermediate Water
CLIVAR	Climate Variability and Predictability
CO2	Carbon Dioxide
CPS	Counts Per Second
DIC	Dissolved Inorganic Carbon
GAABW	Glacial Antarctic Bottom Water
GNAIW	Glacial North Atlantic Intermediate Water
ICP-MS	Inductively Coupled Plasma Mass Spectrometry
LCDW	Lower Circumpolar Deep Water
LGM	Last Glacial Maximum
LSW	Labrador Sea Water
MIS	Marine Isotope Stage
NADW	North Atlantic Deep Water
NCW	Northern Component Water
PDB	Pee Dee Belemnite
SAMW	Sub-Antarctic Mode Water
SAZ	Sub-Antarctic Zone
SCW	Southern Component Water
UCDW	Upper Circumpolar Deep Water
XRF	X-Ray Fluorescence

LIST OF FIGURES

ACKNOWLEDGEMENTS

First and foremost I would like to thank my advisor, Christopher Charles. Chris has consistently put me in a position to succeed, and I appreciate his invaluable advice and unwavering support. I would not be where I am today without his guidance and mentorship. I would also like to thank the rest of my committee members: Jess Adkins, Ralph Keeling, Jennifer MacKinnon, Margaret Schoeninger, and Jeffrey Severinghaus.

In particular, Jess has been an incredibly helpful mentor for me, and this thesis would not have been possible without the support and resources that were made available to me at Cal-Tech. During my several long trips to Pasadena I was fortunate to have gotten advice, guidance, lodging, and help from the entire Adkins lab. James Rae was an amazing teacher and trace metal guru whose I could count on for support and encouragement during the many long days and late nights in the sub-basement. The rest of the Adkins lab were also excellent hosts, especially Andrea Burke, Guillaume Paris, and Ted Present, all of whom I would like to thank for helping me with my work, for their advice, and for their willingness to let me stay at their homes. Speaking of which, Emily Bockmon and Geoff Cromwell (and Milo) deserve a gigantic “Thank You!” for letting me turn a one-week stay in their guest room into a three-month temporary move-in.

None of the work presented here could have been done without the support I received at Texas A&M University from Niall Slowey. His help allowed me to get the thesis off the ground, and I appreciated his non-stop support and enthusiasm during my multiple trips there. Katherine Crabill was also an incredible help during my stays in

College Station, and without her able assistance I would not have been able to cram months worth of work into a pair of two-week trips.

I would like to thank several groups at SIO for their help. I wouldn't have been able to wash and process the samples for this project without the resources available in Richard Norris's Lab, and I am appreciative of how many hours I was allowed to spend monopolizing their ovens and sinks. Bruce Deck of the SIO Analytical facility was also incredibly helpful with any of the problems I encountered using the mass spectrometers, and I appreciate his assistance with the variety of measurements that I made while at SIO. This thesis was also made possible by the GRD and Grad Program staff members, who went out of their way to help me at the drop of a hat. In particular, Monica Bailey, Gilbert Bretado, Adam Petersen, Joshua Reeves, Denise Darling, Maureen McCormick, and Maureen McGreevy all helped me tremendously.

I had a number of sources of financial support while I was at Scripps, including the NSF Graduate Research Fellowship Program and the Integrated Ocean Drilling Program. I would also like to thank the UCSD Friends of the International Center, whose support allowed me to participate in the student-run MIST cruise, which was an incredible learning experience. I would like to thank the crews of the R/V Revelle and Ronald Brown for the their help on the two cruises that I participated in during graduate school.

Of course this thesis is largely a product of the help that I got from the Charles lab. I cannot thank Riley Gannon enough for being supportive and encouraging, for being willing to drop what he was doing and help me with anything, and most simply, for being

my friend. Life in VH109 would have been much worse without him. I would also like to thank Sara Sanchez and Niko Westphal for their help, insights, and friendship. I have been lucky to have such good lab-mates during my career at SIO.

I have had a fantastic time at Scripps because of the support of countless friends and colleagues, and so many people I met while at SIO have made San Diego feel like home. In particular I would like to thank Nick Pizzo, Sam Billheimer, Phil Bresnahan, Roland Kersten, Jenan Kharbush, Emily Trentacosta, Kelly Gallagher, Randelle Bundie, Mattias Cape, Emily Bockmon, Geoff Cromwell, Robert Petersen, Diego Melgar, Valerie Sahakian, Samer Naif, Nick Cavanaugh, Timothy Myers, and Michael Deflorio for making Scripps a place that was more than just a graduate school.

Outside of SIO I have been lucky to have friends whose support and friendship made every day brighter. Doug Collins, Sarah Smith, and (occasionally) Rutherford Smith-Collins were welcome weekly dinner companions every Thursday for 7 years, and life would have been very different without 'Dinner Thursday'. Speaking of Dinner Thursday, it is impossible to put Abbas Hussain's impact on my life in San Diego into a couple words. Suffice to say, I couldn't ask for a better friend, partner-in-crime, and roommate.

The unwavering support of my family has been a lifeline that I have turned to many times. I do not think I could have done this without their reassurance and love.

Lastly, I would like to thank Samantha Mascuch for being my partner for the last eight years. I would not be where I am without you, and I am excited to see what the

future brings. Thanks for your patience and support, and for being the best surfing buddy I could ask for.

Chapter 1, in part, will be submitted for publication to Marine Geology. Foreman, A.D., Charles, C.D., Slowey, N. C. The dissertation author was the primary investigator and author of this paper.

Chapter 2, in part, will be submitted for publication Paleoceanography. Foreman, A.D., Charles, C.D., Rae, J. W., Adkins, J.F., and Slowey, N. C. The dissertation author was the primary investigator and author of this paper.

Chapter 3, in part, will be submitted for publication to Paleoceanography. Foreman, A.D., Charles, C.D., Rae, J. W., Adkins, J.F., and Slowey, N. C. The dissertation author was the primary investigator and author of this paper.

Chapter 4, in part, will be submitted for publication to Paleoceanography. Foreman, A.D., Charles, C.D., Rae, J. W., Adkins, J.F., and Slowey, N. C. The dissertation author was the primary investigator and author of this paper.

VITA

2009 Bachelor of Science, Earth, Atmospheric & Planetary Sciences

Bachelor of Science, Chemistry, Massachusetts Institute of Technology

2011 Master of Science, Geology, University of California, San Diego

2011-2014 National Science Foundation Graduate Research Fellow

2014-2015 International Ocean Drilling Program Schlanger Fellow

2017 Doctor of Philosophy, Oceanography, University of California, San Diego

ABSTRACT OF THE DISSERTATION

The Evolution of Glacial Conditions in the Southern Atlantic Ocean:

A Depth Transect Approach

by

Alan Dean Foreman

Doctor of Philosophy in Oceanography

University of California, San Diego, 2017

Professor Christopher D. Charles, Chair

Understanding the role of the deep ocean in governing glacial/interglacial cycles has been a central theme of paleoceanography since its inception. Historically attempts at resolving the changes that occurred in the deep ocean have focused on tying together sedimentary time series from disparate locations. However, the sparse geographic distribution and variable depositional conditions of the sedimentary cores that make up such compilations have been significant obstacles for the creation of a detailed picture of changes in circulation and carbon storage over ice-age cycles.

Vertical tracer profiles represent an alternative approach that circumvents a number of these problems. These profiles ('depth transects') compile proxy measurements from sediment cores collected at multiple depths in a single geographic area into a single 'steady-state' picture. By densely sampling the water column in a single location, vertical profiles act as 'paleo-CTD' casts that provide detailed observations of changes in water mass geometry using sediment cores that have experienced nearly identical depositional conditions.

In this thesis I present proxy observations from a depth transect in the Southeastern Atlantic Ocean for 6 different time points over the last glacial/interglacial cycle. Together these observations provide information about the timing and magnitude of changes in deep ocean temperature, salinity, and carbon storage as glacial conditions evolved over the last 140,000 years.

The efficacy of the vertical depth transect approach depends entirely on how accurately the cores that comprise the depth transect can be correlated and dated. In Chapter 1, I present X-Ray Fluorescence (XRF) observations of bulk sedimentary elemental abundances for the 20 sediment cores that comprise the core collection. In this chapter I demonstrate that these XRF-derived elemental traces have characteristic variability that can be used to correlate cores across the entire range of depths in the collection, and that they can be used to develop a precise stratigraphic framework.

With this knowledge in hand, Chapter 2 focuses on documenting the evolution of the deep ocean temperature structure over the last ice age cycle using paired measurements of benthic foraminiferal Mg/Ca and $\delta^{18}O$. From these measurements I

infer that both a change in structure and a significant cooling occurred in the Southern Atlantic between 2-3 km across the Marine Isotope Stage (MIS) 5E/5D transition. At MIS 5A/4 a second cooling took place at mid-depths, and was likely accompanied by an increase in the production of cold, salty southern-sourced water. The deep South Atlantic appears to have mostly cooled to LGM temperatures by MIS 4, though the gradient between northern- and southern-sourced water continued to sharpen between MIS 4 and the LGM.

The changes in stratification implied by the conservative tracers presented in Chapter 2 should have had consequences for the cycling of carbon and nutrients in the deep ocean. Chapter 3 presents concurrent measurements of 7 different tracers ($\delta^{13}C$, U/Ca, Mn/Ca, Nd/Ca, B/Ca, Sr/Ca, and Na/Ca) that provide a way to infer the relative significance of remineralization, air-sea gas exchange, and other nonconservative properties over the last glacial/interglacial cycle. Taken together, the vertical profile measurements in Chapter 3 are consistent with the phenomenon of nutrient deepening in the South Atlantic during cold episodes of the full glacial cycle, and suggest that the increased production of cold, salty southern-sourced water trapped nutrients and carbon at depth in the Southern Atlantic glacial conditions strengthened.

Chapter 4 outlines a complimentary perspective by using newly developed records of the $\delta^{13}C$ of atmospheric CO_2 in tandem with two time series of deep ocean $\delta^{13}C$ from this core collection to document the amount of excess carbon stored in the deep South Atlantic ocean during cold episodes. The magnitude and timing of the $\delta^{13}C$ divergence record match other independent attempts to calculate vertical $\delta^{13}C$ gradients

in the Subantarctic South Atlantic and can be tied directly to the ice core atmospheric CO_2 records. Each of these comparisons suggests that enhanced carbon storage at depth in the ocean was indeed responsible for much of the atmospheric $\delta^{13}C$ CO_2 record, and, by extension, the atmospheric concentration of CO_2. Additionally, the similarity of the record of $\delta^{13}C$ divergence and a time-series record of circumpolar deep water temperature suggests that carbon trapping in the deep South Atlantic ocean was associated with colder, saltier water, consistent with the mechanisms proposed in Chapters 2 and 3.

Introduction

Cyclic oscillations between colder 'ice age' and warmer 'interglacial' periods over the Late Pleistocene are well documented and have been statistically linked to changes in Earth's orbit [*J D Hays et al.*, 1976]. While these orbital changes seem to fundamentally drive glacial/interglacial changes by altering incident radiation, the magnitude of the variations in energy are too low to account for the amplitude of the observed climatic alterations recorded by a wide variety of measurements and proxies. Instead, positive feedbacks within Earth's climate system must amplify orbital forcing to produce the rapid, large-scale changes seen in proxy records.

Given its global distribution and strength as a greenhouse gas, carbon dioxide (CO_2) stands as the primary positive feedback working in concert with orbital forcing. Data from ice cores has placed CO_2 concentrations at 180-200 p.p.m.v. during peak glacial episodes, and at roughly 280 p.p.m.v. during interglacial periods [*J-R Petit et al.*, 1999]. It is widely agreed that the recurring 80-100 p.p.m.v. changes in CO_2, which correlate strongly with records of orbital forcing, temperature, and global ice volume, must have played a significant role in driving glacial/interglacial cycles. Despite this consensus, there has been difficulty in describing the fundamental mechanism(s) behind the CO_2 variations over long timescales, leading their description as the 'holy grail' of glacial/interglacial research [*D M Sigman and E A Boyle*, 2000].

One popular concept in this respect is that the underlying mechanisms governing atmospheric CO_2 concentrations must be dominated by changes in the internal 'plumbing' of the ocean. This theme arises mainly from consideration of the relative size of the deep

ocean reservoir of inorganic carbon: the deep ocean holds 10 times as much carbon as the terrestrial biosphere, surface ocean, and atmospheric reservoirs combined [*D M Sigman and E A Boyle*, 2000]. Moreover, the rate of exposure of the deep ocean to the atmosphere is on the order of 1000 years, meaning that any changes in pools of carbon other than that of the deep ocean would be 'diluted' on glacial/interglacial timescales. It has also been shown that the deep ocean dominates inorganic carbon burial on thousand year timescales through control of calcium carbonate dissolution and burial on the ocean floor [*W S Broecker and T-H Peng*, 1982].

It seems clear then that an understanding of the glacial/interglacial 'holy grail' depends on divining the changes that occurred in the deep ocean. This has been the subject of much research over the past several decades, and a large base of evidence now exists supporting the notion that the deep ocean was drastically different at the peak of the Last Glacial Maximum (LGM) [*J Lynch-Stieglitz et al.*, 2007]. In the modern Atlantic Ocean, for instance, surface and intermediate waters lose buoyancy in the North Atlantic and flow south as North Atlantic Deep Water (NADW). This southward-flowing water extends to 40°S and is bracketed in the Southern Hemisphere above and below by Antarctic Intermediate Water (AAIW) and Antarctic Bottom Water (AABW). During the LGM, however, it is generally accepted that AABW extended northward to 60°N, forcing NADW to shoal roughly 2 km to create a water mass known as Glacial North Atlantic Intermediate Water (GNAIW) [*W B Curry and D W Oppo*, 2005; *T M Marchitto and W S Broecker*, 2006]. Other lines of evidence reinforce the idea of a dramatically different

deep ocean at the LGM, suggesting that the deep ocean was near both saltier and near to freezing [*J F Adkins et al.*, 2002; *D P Schrag et al.*, 2002].

While a comprehensive picture of the abyssal LGM Atlantic ocean has begun to emerge, relatively little is known about how the ocean arrived at that state from the previous interglacial. Understanding the mechanisms involved in the evolution of ice age conditions is more than just an academic exercise, as the ability of coupled ocean-atmosphere models to simulate glacial/interglacial conditions is often used as a test to determine the confidence in that model's predictions of future climate. This type of model assessment can only be made if there are observations in place for a full ice age cycle.

Much of the past work in documenting the evolution of ice ages has focused on reconstructing paleo-proxies from high-resolution individual time series at various scattered locations. The relatively sparse distribution of these sedimentary records makes it difficult to draw detailed conclusions about changes in the patterns of overturning circulation and the corresponding fluctuations in oceanic carbon storage and global climate. The comparison of sediment cores from diverse locations is further hampered by the different sedimentation rates and depositional conditions experienced by the cores.

Vertical tracer profiles, in which proxy measurements from sediment cores collected at multiple depths in a single geographic area are compiled into a single 'steady-state' picture, represent an alternative approach that circumvents a number of these problems. By densely sampling the water column in a single location, vertical profiles act as 'paleo-CTD' casts that provide detailed observations of changes in water

mass geometry at key time points during glacial evolution. The tight geographic distribution of the cores in these sedimentary depth transects also ensures that sediment and organic rain from the surface ocean should be nearly identical for the cores, which removes a key confounding factor that generally exists for sedimentary time series. The current 'canonical' picture of water mass geometry in Atlantic during the Last Glacial Maximum (LGM) is derived from interpreting two sedimentary depth transects [*W B Curry and D W Oppo*, 2005], and vertical profiles of tracers have formed the basis for reconstructions of the LGM Pacific [*J Herguera et al.*, 1992], Indian [*N Kallel et al.*, 1988], and Southern Oceans [*U S Ninnemann and C D Charles*, 2002].

In this dissertation I take advantage of the tight geographic distribution of a collection of sediment cores spanning intermediate and deep water depths along the Namibian Margin to create vertical profiles at six key time points over the evolution of the last glacial/interglacial cycle. This collection of cores is particularly suitable for creating sedimentary depth transects, as the principal water masses involved in Atlantic meridional circulation intersect the seafloor in this location, and can be distinguished by their varying nutrient contents and densities. I supplement these 'steady-state' vertical profiles with paleo-proxy measurements from two time series at intermediate and deep water depths in the same collection sampled at millennial scale resolution. Taken together, the vertical profiles and time series allow me to reconstruct changes in bottom water temperature, salinity, and carbon storage at multiple points during the evolution of glacial conditions, and to infer the role of temperature and salinity stratification in trapping carbon in the deep ocean. Furthermore, the parallel measurement of different

paleoproxies from the same samples allows for the characterization of the controls on various tracers by comparing tracers that should behave in similar ways. The extent to which tracers are altered by so-called non-conservative effects is an open question that commonly impedes the interpretation of paleo-records.

The utility of the depth transect approach depends on whether accurate stratigraphic correlation can be achieved between cores contained in the collection. Chapter 1 demonstrates that stratigraphic correlation of sedimentary variables implies chronological consistency over the length of the glacial interglacial cycle at millennial-scale resolution. This conclusion can be drawn for the younger sections of these cores using radiocarbon-dated samples; for example, stratigraphic identification of the close of the Last Glacial Maximum (LGM) interval from different sedimentary variables all date to within 500-1000 years with radiocarbon. Stratigraphic correlation for the deeper sections of the cores that extend beyond the age range of radiocarbon is achieved using scanning X-Ray Fluorescence (XRF) measurements. These measurements, which are generated by bombarding the sediment core with x-ray radiation and measuring the resulting fluorescence spectrum, provide two-centimeter resolution of the relative abundances of various elements in the sediment core. Using XRF measurements I show that there is shared variability in the time series of the iron (Fe) to calcium (Ca) ratio for each of the cores in the collection, which allows me to align the ratios of different cores in order to achieve stratigraphic consistency. I verify the validity of this approach in two ways. First, aligning the Fe/Ca ratios for the cores creates a matching age horizon for the previously measured radiocarbon ages at the last glacial maximum. Second, the

correlation of these ratios in the older parts of the core aligns a well-known bio-stratigraphic marker at the last interglacial period. Together these two independent tests, along with the strong correlation between Fe/Ca ratios across the cores, suggest that stratigraphic consistency is achieved for this core collection, and that the vertical transect approach is valid.

Given the evidence that stratigraphic consistency is achieved for this core collection, an obvious pair of questions is whether changes in deep water mass geometry can be detected as glacial conditions evolve, and how these changes are associated with changes in atmospheric carbon dioxide. This is the focus of Chapter 2, which presents the results of co-occurring measurements of the stable oxygen isotopes ($\delta^{18}O$) and magnesium calcium ratios (Mg/Ca) of benthic foraminiferal calcite. Benthic stable oxygen isotope ratios respond to changes in both bottom water salinity and temperature. Efforts to separate these components within marine $\delta^{18}O$ records has been an area of significant focus for the paleoceanographic community [*J Chappell and N J Shackleton*, 1986; *K Cutler et al.*, 2003], as there is evidence that salt and temperature stratification both play a role in trapping carbon in the deep ocean on glacial time scales [*J Toggweiler*, 1999; *J F Adkins et al.*, 2002; *D P Schrag et al.*, 2002; *J F Adkins*, 2013]. By making simultaneous measurements of Mg/Ca, which responds to changes in temperature but not to changes in salinity, it is possible to discriminate between the dual effects of temperature and salinity on $\delta^{18}O$ calcite within the same samples.

Several key observations arise from this approach. First, the data suggest large-scale cooling occurred in the deep ocean across in the first step-down from interglacial

conditions (commonly known as the MIS 5E/5D transition), consistent with proxy records from corals [*K Cutler et al.*, 2003] and ice cores [*M A Headley*, 2008]. Simultaneous with this cooling, the boundary between northern component water (NCW) and southern component water (SCW) shoaled in the South Atlantic.

The vertical profiles also show a significant set of changes in ocean temperature and salinity across the second major step-down towards glacial conditions (e.g. the MIS 5A/4 boundary) over the last glacial/interglacial cycle. The profiles suggest that the cooling of the interior of the ocean over this transition was limited to the mid-depths, and that the gradient between SCW and NCW likely shoaled further. The observations from both transitions are consistent with a mechanism first proposed by Adkins [2013], in which cooling of NCW creates saltier SCW, ultimately driving the NCW/SCW boundary upwards in the water column and allowing for the storage of CO_2 in the deep ocean.

A final point that arises from this chapter is that the time slices from Chapter 2 confirm the picture of the South Atlantic at the LGM suggested by Curry and Oppo [2005] and Lynch-Stieglitz [2007]. The LGM time slice shows that the boundary between NCW and SCW shoaled to similar water depths as those collected along the Brazil margin at roughly the same latitude. The $\delta^{18}O$ and Mg/Ca data also indicate that much of the remaining changes in $\delta^{18}O$ observed as the ocean slid into its maximum glacial state took place as result of changes in sea level, and that the deep ocean had already cooled to LGM conditions during the previous cold period (MIS 4).

Given the observations made in Chapter 2, an interesting and related question is how closely proxies that respond to changes in the chemistry and biology of the ocean

(i.e. non-conservative tracers) mirror those that are in theory sensitive only to changes in the density structure of the deep ocean (i.e. conservative tracers). In particular, the question of how significant the redistribution of tracers via particle transport is relative to advection and diffusion has hindered the development of biogeochemical models. Chapter 3 addresses this question by analyzing vertical profiles of non-conservative tracers sensitive to carbon cycling and particle transport ($\delta^{13}C$, Nd/Ca, U/Ca, Mn/Ca, B/Ca, Sr/Ca, Na/Ca) in relation to the profiles of conservative tracers ($\delta^{18}O$, Mg/Ca) presented in Chapter 2.

Of particular interest in Chapter 3 is that the vertical gradients of $\delta^{13}C$, a nutrient-like tracer that is sensitive to both particle redistribution and air-sea gas exchange, build steadily across the evolution of the glacial cycle, with the strongest gradients observed during glacial periods (MIS4 and the LGM). The $\delta^{13}C$ gradients are constant over the length of a given profile in the vertical, in contrast to the tracers of physical circulation, which show sharp boundaries between water masses during these periods. It seems likely that this difference in behavior is an expression of nutrient deepening [*E A Boyle*, 1988], in which a transfer of nutrients and carbon from the upper and mid-depth ocean to the deep reduces atmospheric CO_2.

The vertical profiles of other non-conservative elements shine light on how this nutrient deepening could have arisen. In particular, the profiles of Nd/Ca, which mirror the $\delta^{13}C$ profiles, suggest that the strength of particle redistribution relative to advection grew much more significant during glacial periods, given that dissolved Nd is highly particle reactive in the modern ocean. The strong correlation between the Nd/Ca and $\delta^{13}C$

profiles also suggest that air-sea gas exchange did not significantly impact the distribution of $\delta^{13}C$ for these profiles, as there is no mechanism in place for why dissolved Nd concentrations would vary with air-sea gas exchange.

If the deep ocean grew more stratified and mixing became more sluggish, it would also have experienced lowered dissolved oxygen concentrations, which would in turn be reflected in the profiles of elements sensitive to changes in redox conditions. This is shown to be the case for the profiles of U/Ca and Mn/Ca, which both suggest that the deep ocean was experiencing much lower concentrations of dissolved oxygen during glacial periods. The transfer of carbon to the deep ocean via nutrient deepening should also decouple the tracers sensitive to carbonate ion concentrations from the profiles $\delta^{13}C$, as the process of carbonate compensation should keep the carbonate ion concentrations roughly constant for the vertical depth profiles. The profiles of B/Ca and Sr/Ca, which both have been shown to respond to changes in carbonate ion [*J Yu et al.*, 2008; *J Yu et al.*, 2014] suggest that this was the case, and that the carbonate ion concentrations did not significantly change across any of the glacial profiles. Instead, the only changes in carbonate ion concentrations evident in these profiles were limited to an apparent elevation in deep ocean carbonate ion during the last interglacial period. An interesting final observation from this chapter is that measurements of Na/Ca, whose controls are not well understood, show a remarkable correlation with those of Sr/Ca, suggesting perhaps that Na/Ca might closely track carbonate ion concentrations. This would be of considerable interest for future work, as Na/Ca is significantly easier to measure than

B/Ca, the current tracer most commonly used to infer changes in carbonate ion concentrations.

Taken together, the observations from Chapters 2 and 3 suggest that the stable carbon isotope distribution in the South Atlantic during glacial periods is consistent with phenomenon of nutrient deepening, and that this deepening occurred in conjunction with heightened stratification of the deep ocean. In Chapter 4 I use two millennial-resolution time series developed from South Atlantic mid-depth and deep cores to explore in more detail how the $\delta^{13}C$ gradient evolved in the vertical over the last glacial/interglacial cycle, and compare this evolution to records of $\delta^{13}C$ of atmospheric CO_2 [*S Eggleston et al.*, 2016], $\delta^{13}C$ surface-deep gradients from the sub-Antarctic [*M Ziegler et al.*, 2013], and deep ocean temperature from the Pacific [*H Elderfield et al.*, 2010]. The time series I developed show that intervals of maximal vertical gradient in $\delta^{13}C$ in the deep South Atlantic ocean correspond with maxima in $\delta^{13}C$ of atmospheric CO_2 record over the entire buildup of glacial conditions, reinforcing the conclusion from Chapter 3 that the $\delta^{13}C$ gradient is strengthened by the movement of carbon from the atmosphere to the deep ocean during nutrient deepening. The comparison of this South Atlantic record and the Pacific temperature record (inferred from benthic foraminiferal Mg/Ca) shows the gradient in $\delta^{13}C$ is highly correlated with changes in the inferred temperature of Circumpolar Deep Water, suggesting that stratification played a key role in bottling-up carbon in the deep ocean. This comparison also implies that changes in surface production may not be responsible for the evolution of nutrient deepening. Further supporting this conclusion is the observation that the record of the $\delta^{13}C$ gradient from the

South Atlantic is strongly correlated with the surface-deep gradient in $\delta^{13}C$ in the sub-Antarctic published by Ziegler et al. [2013]. Ziegler et al. attributed the strengthening of the vertical $\delta^{13}C$ gradient in their record to iron-fertilization in the sub-Antarctic zone. Yet the similarities between their record and mine would demand that the iron fertilization must have been basin-wide, which seems improbable. Clearly more work remains to fully understand the mechanisms involved in producing nutrient deepening, although both the time series and vertical profiles from this thesis suggest that stratification played an important role. An obvious first step for future work is to develop models of how the $\delta^{13}C$ gradient in the deep ocean evolved in tandem with the $\delta^{13}C$ signal of atmospheric CO_2. The analysis in Chapter 4 emphasizes several key intervals that should serve as targets for this pursuit.

I.1 References

Adkins, J. F. (2013), The role of deep ocean circulation in setting glacial climates, *Paleoceanography*, *28*(3), 539-561.

Adkins, J. F., K. McIntyre, and D. P. Schrag (2002), The salinity, temperature, and δ18O of the glacial deep ocean, *Science*, *298*(5599), 1769-1773.

Boyle, E. A. (1988), Vertical oceanic nutrient fractionation and glacial/interglacial CO2 cycles, *Nature*, *331*(6151), 55-56.

Broecker, W. S., and T.-H. Peng (1982), *Tracers in the Sea*.

Chappell, J., and N. J. Shackleton (1986), Oxygen isotopes and sea level, *Nature*, *324*(6093), 137-140.

Curry, W. B., and D. W. Oppo (2005), Glacial water mass geometry and the distribution of δ13C of ΣCO2 in the western Atlantic Ocean, *Paleoceanography*, *20*(1).

Cutler, K., R. Edwards, F. Taylor, H. Cheng, J. Adkins, C. Gallup, P. Cutler, G. Burr, and A. Bloom (2003), Rapid sea-level fall and deep-ocean temperature change since the last interglacial period, *Earth and Planetary Science Letters*, *206*(3), 253-271.

Eggleston, S., J. Schmitt, B. Bereiter, R. Schneider, and H. Fischer (2016), Evolution of the stable carbon isotope composition of atmospheric CO2 over the last glacial cycle, *Paleoceanography*, *31*(3), 434-452.

Elderfield, H., M. Greaves, S. Barker, I. R. Hall, A. Tripati, P. Ferretti, S. Crowhurst, L. Booth, and C. Daunt (2010), A record of bottom water temperature and seawater δ 18 O for the Southern Ocean over the past 440kyr based on Mg/Ca of benthic foraminiferal Uvigerina spp, *Quaternary Science Reviews*, *29*(1), 160-169.

Hays, J. D., J. Imbrie, and N. J. Shackleton (1976), Variations in the Earth's orbit: pacemaker of the ice ages, *Science*, *194*(4270), 1121-1132.

Headley, M. A. (2008), Krypton and xenon in air trapped in polar ice cores: Paleo-atmospheric measurements for estimating past mean ocean temperature and summer snowmelt frequency, Ph.D thesis.

Herguera, J., E. Jansen, and W. Berger (1992), Evidence for a bathyal front at 2000-M depth in the glacial Pacific, based on a depth transect on Ontong Java Plateau, *Paleoceanography*, *7*(3), 273-288.

Kallel, N., L. D. Labeyrie, A. Juillet-Leclerc, and J.-C. Duplessy (1988), A deep hydrological front between intermediate and deep-wafpr, masses in the glacial Indian Ocean, *Nature*, *333*(6174), 651-655.

Lynch-Stieglitz, J., J. F. Adkins, W. B. Curry, T. Dokken, I. R. Hall, J. C. Herguera, J. J.-M. Hirschi, E. V. Ivanova, C. Kissel, and O. Marchal (2007), Atlantic meridional overturning circulation during the Last Glacial Maximum, *science*, *316*(5821), 66-69.

Marchitto, T. M., and W. S. Broecker (2006), Deep water mass geometry in the glacial Atlantic Ocean: A review of constraints from the paleonutrient proxy Cd/Ca, *Geochemistry, Geophysics, Geosystems*, *7*(12).

Ninnemann, U. S., and C. D. Charles (2002), Changes in the mode of Southern Ocean circulation over the last glacial cycle revealed by foraminiferal stable isotopic variability, *Earth and Planetary Science Letters*, *201*(2), 383-396.

Petit, J.-R., J. Jouzel, D. Raynaud, N. I. Barkov, J.-M. Barnola, I. Basile, M. Bender, J. Chappellaz, M. Davis, and G. Delaygue (1999), Climate and atmospheric history of the past 420,000 years from the Vostok ice core, Antarctica, *Nature*, *399*(6735), 429-436.

Schrag, D. P., J. F. Adkins, K. McIntyre, J. L. Alexander, D. A. Hodell, C. D. Charles, and J. F. McManus (2002), The oxygen isotopic composition of seawater during the Last Glacial Maximum, *Quaternary Science Reviews*, *21*(1), 331-342.

Sigman, D. M., and E. A. Boyle (2000), Glacial/interglacial variations in atmospheric carbon dioxide, *Nature*, *407*(6806), 859-869.

Toggweiler, J. (1999), Variation of atmospheric CO2 by ventilation of the ocean's deepest water, *Paleoceanography*, *14*(5), 571-588.

Yu, J., H. Elderfield, and A. M. Piotrowski (2008), Seawater carbonate ion-δ 13 C systematics and application to glacial–interglacial North Atlantic ocean circulation, *Earth and Planetary Science Letters*, *271*(1), 209-220.

Yu, J., H. Elderfield, Z. Jin, P. Tomascak, and E. J. Rohling (2014), Controls on Sr/Ca in benthic foraminifera and implications for seawater Sr/Ca during the late Pleistocene, *Quaternary Science Reviews*, *98*, 1-6.

Ziegler, M., P. Diz, I. R. Hall, and R. Zahn (2013), Millennial-scale changes in atmospheric CO2 levels linked to the Southern Ocean carbon isotope gradient and dust flux, *Nature Geoscience*, *6*(6), 457-461.

Chapter 1. Stratigraphic and chronological consistency for 20 cores from the Southeastern Atlantic achieved using XRF-derived bulk elemental abundances

Abstract

The construction of past ocean vertical profiles ("depth transects") - proxy observations collected across multiple water depths from a tightly constrained geographic region - represents one of the most promising avenues for progress in paleoceanography. The efficacy of this approach, however, depends entirely on how accurately the cores that comprise the depth transect can be correlated and dated. The depth transect approach has typically been limited to the interval between the Holocene and the Last Glacial Maximum, which can be radiocarbon dated. However, it is important to establish how glacial conditions may have evolved, and this objective requires the identification of coeval time horizons in multiple sediment cores prior to the constraints of radiocarbon. Here I present x-ray fluorescence observations of bulk sedimentary elemental abundances for 20 sediment cores from a collection along the Namibian margin in the Southeastern Atlantic. I demonstrate that these XRF-derived elemental traces show characteristic variability that can be used to correlate cores across the entire range of depths in the collection. I then examine whether it is possible to use XRF to develop a precise stratigraphic framework using two independent tests. First, using radiocarbon, I show that the stratigraphic indicators for the close of the LGM (from planktonic foraminiferal $\delta^{18}O$ and XRF) in a subset of the cores all date to within a relatively narrow 500-1000 year range. Second I use the well-known biostratigraphic marker *G. menardii* to show that the alignment of scanning XRF traces between cores also aligns the first appearance of *G. menardii* during the penultimate deglaciation and its abundance history throughout the

last interglacial period, with a decorrelation depth scale of approximately 5 cm (equivalent to roughly 1000 years for these cores). Together these two tests give me confidence that chronological and stratigraphic consistency within a ~1000 year window can be achieved for the vertical profiles presented in this thesis. There are, however, long period features in the XRF traces that seem to vary with water depth. I use this and other observations to speculate on the origin of the XRF-derived elemental abundance history in the region.

1.1 Introduction

The role of the deep ocean in governing Earth's climate on ice age time scales has been one of the long-standing questions in paleoceanography. Historically this question has been addressed by compiling paleo-proxy observations from high-resolution individual sediment cores. Yet observations made for the global ocean using this approach are hampered by the relatively sparse distribution of sedimentary tracer observations in the global oceans over glacial/interglacial cycles. Further complicating this problem is that sediment cores are subject to different sedimentation rates and deposition conditions in different ocean basins, which cofounds the interpretation of various tracer distributions.

Compiling tracer profiles from different depths in a single area represents an alternative approach that addresses many of these problems. Constructing these vertical profiles can be thought of as compiling a series of "paleo-CTD" casts that densely sample the water column at specific time points. This strategy has two main benefits, as it both allows for finer-scale observations to be made about water mass geometry in the vertical, and it utilizes cores that have been exposed to near-identical sedimentation rates and depositional conditions that depend only on the water depth, thus eliminating many of the confounding factors in interpreting differences in tracer behavior. These advantages are such that vertical profiles form much of the basis for the current understanding of paleo-tracer distribution during the Last Glacial Maximum (LGM) in the Atlantic [*L D Keigwin*, 2004; *W B Curry and D W Oppo*, 2005] Pacific [*J Herguera et al.*, 1992],

Indian [*N Kallel et al.*, 1988], and Southern Oceans [*U S Ninnemann and C D Charles*, 2002]

The efficacy of the depth transect approach depends entirely on the accurate correlation of well-dated time points between different sediment cores. For vertical profiles of the LGM, radiocarbon measurements are most often used to provide stringent dating and correlation between cores in a given collection. Radiocarbon is limited in stratigraphic utility by its half-life, however, and cannot be used as a correlative tool for the majority of the profiles that are the subject of this thesis. Thus a different means of ensuring stratigraphic consistency for this core collection is required.

Various non-destructive core logging methods that record changes in physical sediment properties are often used to provide initial shipboard stratigraphic interpretations of marine sediment cores. These tools include magnetic susceptibility loops and gamma ray attenuation estimates of porosity (GRAPE). The resulting measurements are dependent on a combination of sediment parameters (e.g. grain-size, terrigenous fraction) and do not always show diagnostic variability with optimal signal to noise ratio that can be correlated among multiple cores [*R H Wilkens et al.*, 2017]. In contrast, scanning X-Ray Fluorescence (XRF) [*J Jansen et al.*, 1998; *T O Richter et al.*, 2006] measures changes in the bulk sediment elemental composition at cm- to mm- scale resolution for major, minor and trace elements. These records of variability are potentially high-resolution and semi-quantitative. They record diagnostic changes in elemental abundances that can be used to correlate sediment cores in the same collection. By combining the stratigraphic correlation of these elemental time series derived from

scanning XRF with that of independent variables (e.g. stable isotope records) from the same core, it is theoretically possible to achieve stratigraphic and chronologic consistency for a collection of multiple cores.

The observations that form the basis for multiple chapters of this thesis come from a set of sediment cores that were collected along the Namibian margin and that span the full glacial/interglacial cycle. Most of the important transitions of the last ice age cycle fall outside the useful time window of radiocarbon, and it is therefore necessary to instead turn to scanning XRF traces to create accurate stratigraphic ties between the 20 cores in the collection.

The following sections are devoted to examining the methods used to construct the vertical profiles in this thesis. I begin by describing the core collection and the modern surface and deep oceanographic conditions along the Namibian margin. Subsequent discussion focuses on the variations in elemental abundance time series measured by scanning XRF, and examines how these measurements provide a framework that can be used to create vertical profile measurements.

Implicit in using scanning XRF for stratigraphic purposes is that the changes in elemental ratios measured for these cores are diagnostic of the rain of sediment from above and that their behavior is governed by the same set of processes for each of the cores. The final part of this chapter assesses the validity of these assumptions in two ways. First, using a subset of the core collection I compare the parts of the cores designated by XRF measurements as marking the close of the LGM with radiocarbon age measurements for those core subsections. Second I use the well-documented spike in the

South Atlantic population of the planktonic foraminiferal species *G. menardii* near the beginning of the last interglacial MIS 5E [*W Berger and G Wefer*, 1996; *F J Peeters et al.*, 2004] as a biostratigraphic marker to compare the timing of the appearance of *G. menardii* between several cores upon alignment of the scanning XRF traces. Together the radiocarbon ages and the appearance of *G. menardii* in the cores I analyzed provide two independent tests that corroborate the stratigraphic ties that I have developed for the cores. I then finish this chapter by briefly discussing the possible drivers for the elemental variations seen in the core collection.

1.2 Core Collection and Methods

The cores that make up the basis for this thesis were collected aboard the R/V Melville in March 2003 between 130 km and 350 km offshore just south of the Walvis Ridge. All but 3 of the cores were collected along two depth transects within a narrow area defined by 19° 43.3´S and 21° 33.1´S and 9° 54.1´E and 12° 48.1´E (Figure 1.1, A and B), and range in depth from 1405 to 3678 meters. The remaining cores were taken further south along a transect at 24° 28.0´S, 12° 26.0´E and range in depth from 2200 to 2600 m (Figure 1.1, C).

The sampling region for these cores is at the intersection of the principal water masses involved in meridional circulation. At the surface, the Benguela Oceanic Current flows equatorward roughly 300 km offshore. Primary production in this area is driven by a combination of periodic upwelling of cold nutrient-rich waters due to south-southeasterly winds [*J Lutjeharms and J Meeuwis*, 1987] and perennial shelf-edge upwelling [*C Summerhayes et al.*, 1995]. Terrigenous material is supplied to the area

mainly through eolian input [*N Lancaster*, 1981; *B Jahn et al.*, 2003], though it has been suggested that riverine sources varied significantly enough to make an imprint on terrigenous inputs during glacial periods [*J-B W Stuut et al.*, 2002].

Deeper in the water column the different northern- and southern- sourced water masses are stacked vertically and can be distinguished by their varying nutrient contents and densities (Figure 1.2). Antarctic Intermediate Water (AAIW) and Upper Circumpolar Deep Water (UCDW) make up part of the water column between 500-1500 meters depth, and overlie constituents of North Atlantic Deep Water. In particular, Labrador Sea Water (LSW) occupies the 1700-2000 meter depth range [*R Schlitzer*, 2000]. Moving even deeper, North Atlantic Deep Water (NADW) borders the southern-sourced Lower Circumpolar Deep Water (LCDW) at roughly 3600 meters depth.

The cores were brought aboard ship and immediately split into 1-1.5 meter segments that were labeled and capped. Core sections were stored under refrigerated conditions onboard the R/V Melville before being transported to the refrigerated core repository at the Integrated Ocean Discovery Program facility at Texas A&M University. At Texas A&M University the core sections were split longitudinally and visually inspected. The subsampling discussed below was performed on one half of the core subsections (the “sampling” half), while the XRF measurements were made on the undisturbed half of the core (the “archive” half).

10 cc samples were taken from core subsections at 5 cm resolution along the full length of 20 cores. These samples, roughly 2000 in total, were oven dried at 50°C and

then washed through a 63 μm sieve with distilled water. The remainder was dried again at 50°C and then dry-sieved at 200 μm for picking individual specimens.

Stable carbon and oxygen isotope measurements for the benthic foraminifer *Cibicidoides wuellerstorfi* were made using a Finnigan MAT 253 mass spectrometer at Scripps Institution of Oceanography. The following chapters of this thesis describe two sets of stable isotope measurements: vertical profile measurements and time series measurements. Vertical profile measurements (Chapters 2 and 3) refer to measurements made by collecting all *C. wuellerstorfi* specimens from the >200μm size fraction and then measuring 2-3 splits of the crushed and sonically cleaned specimens. Time series measurements (Chapters 1 and 4) refer to measurements made by analyzing 3 *C. wuellerstorfi* specimens picked from the >200μm size fraction at 5 cm intervals along the length of the core. For both sets of measurements stable isotope values were measured using a Kiel IV carbonate device. The samples were targeted with 3 droplets of 104% phosphoric acid at 70°C. Analytical precision, estimated from measurements of NBS 19 standards, was 0.07 per mil and 0.04 per mil for $\delta^{18}O$ and $\delta^{13}C$ respectively. Carbon and oxygen isotopes are reported relative to the Vienna Pee Dee Belemnite (VPDB) standard.

There is evidence that different morphotypes of a nominal benthic foraminiferal species tend to have differences in trace metal incorporation (and possibly stable isotopic composition) in their $CaCO_3$ tests [*J. W. Rae, pers. communication*]. To eliminate this possibility and to ensure maximum precision I picked individual *C. wuellerstorfi* specimens according to the guidelines laid out by Rae et al. [*J W Rae et al.*, 2011]. This

resulted in the exclusion of an average of roughly 5-10 individuals for a given sample for the vertical profile measurements.

Stable carbon and oxygen isotope analysis of specimens of the planktonic foraminifer *Globigerina bulloides* were made by Jenna Munson [*Unpublished*] at the Scripps Institution of Oceanography. Samples were picked from the 355-425μm size fraction and isotopic analyses were performed using a common acid-bath, Carousel-48 automation carbonate preparation device coupled to a Finnigan MAT 252 mass spectrometer. Estimated analytical precision, deduced from the concurrent measurement of NBS 19 standards, was 0.05 to 0.07 per mil for $\delta^{13}C$ and $\delta^{18}O$, respectively.

Radiocarbon measurements were made by Jenna Munson [*Unpublished*] at the Center for Accelerator Mass Spectrometry at Lawrence Livermore National Laboratory on *Globigerina bulloides* and mixed benthic samples. Foraminifera tests were sonicated in a .0001N HCl solution; planktonics were sonicated briefly to avoid having the shells explode, whereas benthics were sonicated for 1 minute. The HCl was then pipetted off and the samples were dried, weighed, and graphitized. Sample sizes varied between 0.4 and 8 mg. The $\delta^{13}C$ of the samples used for radiocarbon analysis was not measured by Munson et al. [*unpublished]*, but were assigned a $^{13}C/^{12}C$ ratio of 1.0‰ for planktonic samples, and 0‰ for the benthic samples to correct for the mass-dependent fractionation.

Foraminiferal census counts of *G. menardii* were carried out on the >250μm size fraction of cores MV09-PC21 and MV09-PC43 every 5 cm down the length of the core. Each sample was divided using a microsplitter to facilitate counting, and all counts of

abundance were based on the identification and taxonomic assignment of at least 300 specimens per sample.

XRF core scanning data was collected for the undisturbed halves of 20 cores from the sediment core collection, using a third-generation AvaaTech XRF core scanner at Texas A&M University. XRF scanning uses x-ray radiation to induce the expulsion of an electron from the inner energy shell of a targeted atom. The loss of an electron puts the target atom into an unstable excited state and results in the transfer of an electron from the outer shell of the atom to the vacancy created in the inner shell. This transition to the inner shell is accompanied by the release of energy in the form of a photon with a characteristic wavelength for the specific element. Overall, the determination of the relative elemental abundance is made by measuring the intensities of the energy released when a small section of the core is irradiated with x-ray energy of a particular wavelength. The abundance data presented below was generated by scanning at 2 cm resolution, using generator settings of 10 kV, a current of 0.5 mA, and a sampling time of 20 seconds on the core surface. Prior to a scan, each core surface was covered with 4 μm Ultralene foil to prevent sediment desiccation and contamination of the XRF detector.

Elemental abundances (in the form of counts per second) were generated for Al, Si, Cl, K, Ca, Ti, and Fe. The resulting depth series were aligned with one another using the software AnalySeries [*D Paillard et al.*, 1996].

1.3 Results

The core MV09-PC21 was chosen as a benchmark for stratigraphic correlation because it lies close to the middle of the depth transect, and because its sedimentation rate

history appears to have been relatively uniform. The benthic foraminiferal $\delta^{18}O$ record for MV09-PC21 was tied to the LR04 oxygen isotopic stack [*L E Lisiecki and M E Raymo*, 2005] to develop a chronology for this core and, thereby, the entire collection (Figure 1.3). This age-depth determination in the benchmark core allowed conversion of the elemental abundance depth series to time series for all the cores. The transferal of the LR04 chronology can be justified on the basis of good agreement with the LR04 stack across the length of the record. Sedimentation rates in MV09-21 derived from this approach are on the order of 5 cm/kyr, with a slight apparent peak near the LGM. It is important to emphasize that the assumption of the LR04 chronology does not affect the stratigraphic correlation of the cores in the depth transect, as this correlation is performed in the depth domain.

Relative sedimentary elemental concentrations were measured on the remaining 19 cores from three geographically adjacent collection areas (locations A, B, C Figure 1.1) to develop stratigraphic ties with core MV09-21. In other studies, stratigraphic correlation was achieved using either Fe/Ca or Ti/Ca ratios [*J-B W Stuut*, 2001; *J A Collins et al.*, 2014; *R G Rothwell*, 2015], with changes in Ca interpreted as a altered biogenic production and Fe and Ti as indicators of changing terrigenous input [*G H Haug et al.*, 2001; *G H Haug et al.*, 2003]. Other elements that have also been used to infer changes in terrigenous inputs include Al, K, and Si [*R G Rothwell*, 2015].

Given that Atlantic $CaCO_3$ records are well-characterized and show common variability over glacial interglacial cycles, ratios of proxies for terrigenous input (e.g. Fe, Ti, Al, K, and Si) to proxies for biogenic carbonate (e.g. Ca) from cores collected in close

geographic proximity to each other should show coherent variability for these elements between cores within each collection area (e.g. A, B, C in Figure 1.1). This is indeed the case, as the elemental abundance data for the cores show an obvious correlation in the behavior of the terrigenous elements Al, K, Fe, and Ti over the glacial/interglacial cycle (Figure 1.4 and 1.5). Generally, the abundance of these elements peak during glacial periods and reach minima during warmer interglacial periods. Si shows a nearly identical pattern to these elements except during the deglaciation, when Si peaks while the other elemental abundances exhibit a relative decrease. This Si maximum on the deglaciation is most likely the result of enhanced biogenic opal deposition during the deglaciation [*C Summerhayes et al.*, 1995].

Ca abundance is generally anti-correlated with the elements listed above, showing maxima in Ca during interglacial periods and minima in Ca during glacial periods. This behavior, which is consistent across each of the cores, is shown for MV09-PC21 in Figure 1.6. Work done by collaborators at Texas A&M University shows that discrete measurements of $CaCO_3$ content along the length of the cores are inversely related to the Fe signal from XRF data, as predicted by the Fe/Ca traces [*K Crabill*, 2017].

Normalizing the Fe signal with Ca provides a diagnostic signal that can be correlated across the entire sediment core collection. In particular, the Fe/Ca ratio is at a maximum during MIS 2 and MIS 4 (high Fe, low Ca) and at a minimum during the Holocene and MIS 5E. The Fe/Ca signal for these cores is also consistent with the Fe/Ca signal reported in nearby cores (Figure 1.7), which has been used previously as a

stratigraphic tool in the region [*J-B W Stuut*, 2001; *B Jahn et al.*, 2003; *J A Collins et al.*, 2014].

The Fe/Ca signal must be able to be linked between the neighboring collection areas. The differences in the Fe/Ca signal between cores appear to be related to the distance offshore and depth that the cores were collected in (e.g. Figure 1.8, Figure 1.9, and Figure 1.10). Cores from the A and C regions can be tied quite closely to core MV09-21 (Figures 1.8 and 1.10). Cores from depth transect area B are not as strongly correlated with the Fe/Ca signal of core MV09-PC21 as the cores from the A or C depth transect areas are, particularly near MIS 4. (Figure 1.9)

Given the importance of developing an accurate stratigraphy for the core collection, two tests were used to ensure that the cores from the core collection A and C match those of B. First, radiocarbon age measurements provide a stringent test of stratigraphic and chronological consistency for the core collection. Radiocarbon dates for 6 of the cores show that dates identified as the close of the LGM from XRF traces fall into a ~500-year window [*Jenna Munson, Unpublished*]. These are plotted in on top of *G. bulloides* $\delta^{18}O$ measurements from the same cores [*Jenna Munson, Unpublished*] (Figure 1.11). Both the time series of G. *bulloides* $\delta^{18}O$ and the radiocarbon-dated time points show good agreement across the cores from collection areas A, B, and C, which suggests that accurate stratigraphic correlation was achieved using tie points based on the elemental abundance profiles of Fe/Ca for these cores.

The recorded population fluctuations of *G. menardii* in the South Atlantic are well-documented and synchronous [*W Berger and G Wefer*, 1996; *A Rau et al.*, 2002; *F J*

Peeters et al., 2004; *T Caley et al.*, 2012]. As such, records of *G. menardii* abundance provide a second stratigraphic test beyond the bounds of radiocarbon. Abundances of *G. menardii* are highly correlated and spike before Termination II in both the shallower MV09-PC43 and deeper MV09-PC21 cores according to the stratigraphy I have developed (Figure 1.12). This accumulation pattern is consistent with the published records of the reappearance of *G. menardii* in the South Atlantic, which show a resurgence in population at the close of glacial periods stretching back 800 kyr [*F J Peeters et al.*, 2004; *T Caley et al.*, 2012].

Despite the stratigraphic closure that can be achieved for the core collection over specific intervals of the last ice age cycle, there are a couple prominent intervals for which the elemental behavior in the shallow cores is different than in the deeper cores. In particular, differences in the maxima of Fe/Ca during glacial intervals (i.e. MIS 4 and LGM) are evident in the comparison of cores collected from shallower depths (e.g. Area B; Figure 1.9) and those collected at depths deeper than 2000 meters (e.g. Area A and C; Figure 1.8 and Figure 1.10). There is also evidence for a depth-dependent trend in Fe/Ca minima near the MIS 5B/5A boundary. While none of these observations prevent stratigraphic closure from being achieved, they have interesting implications for the source of XRF elemental abundance variability that are discussed in the following section.

1.4 Discussion

The vertical transect approach is a departure from the traditional approach of collecting geographically-diverse time series of paleoproxies. As a sampling strategy it

has distinct advantages over time series in its ability to make fine-scale observations in the vertical and to minimize errors associated with changes in boundary conditions. However, as discussed earlier, for the vertical transect approach to be valid it must be possible to demonstrate accurate stratigraphic and chronologic consistency amongst the entire core collection. Below I discuss the implications of my results with respect to this criterion, and examine the possible drivers for the elemental variability observed for these cores.

The centimeter-scale measurements made using XRF demonstrate characteristic variability that suggests that Fe/Ca signals can be used to ensure stratigraphic consistency amongst all of the cores. This approach has been applied several times with nearby cores [*J-B W Stuut*, 2001; *J A Collins et al.*, 2014], which show a similar diagnostic signal. The agreement in the Fe/Ca ratio between the cores in this collection and those analyzed in other papers suggests that the signal is coherent in this region and gives confidence in this approach as a correlative tool.

Radiocarbon dates on a subset of cores show that the Fe/Ca data can be used to as a stratigraphic tie for the core collection to denote the close of the LGM. The 500-year difference between the dated cores implies that the XRF measurements are accurate for cross-correlation on the order of 2-4 cm resolution, given the calculated sedimentation rates for these cores. Additionally the radiocarbon measurements provide reassurance that measurements I have made for the LGM vertical profiles are representative of the close of the LGM and do not fall in a period representing the deglaciation.

The sudden population increase of *G. menardii* in these cores provides a second test of the stratigraphic accuracy of the Fe/Ca traces. Although ubiquitous in the modern Southern Atlantic, *G. menardii* has exhibited characteristic population changes across the Southern Atlantic over glacial-interglacial cycles [*F J Peeters et al.*, 2004; *T Caley et al.*, 2012] perhaps driven by the cessation and resumption of interocean exchange between the Indian and Atlantic oceans. Given that the timing of these changes is well-known and that they should be synchronous for closely spaced sediment cores, the appearance of *G. menardii* in the core collection is a stringent stratigraphic test outside of the bounds of radiocarbon. Figure 1.12 shows that when sedimentary sequences are aligned with scanning XRF traces, the *G. menardii* abundance records are also then highly correlated within a lag/lead window of ~4-6 cm.

The combination of these two observations provides confidence that the stratigraphy developed for the core collection is correct. The radiocarbon measurements suggest that the younger sections of the cores are accurately correlated to within a 500-1000 year window. (Figure 1.10) Beyond the limits of radiocarbon, the correlation from the *G. menardii* records suggest that the cores are correctly aligned and that changes in the stratigraphic ties beyond 5 cm (~750 years) in either direction significantly reduce the strength of the correlation (Figure 1.11). While the resolution of XRF measurements (2 cm) prevents finer detail stratigraphic correlations, the two stratigraphic tests suggest that the stratigraphy is accurate to within 500 years for the younger sections of the cores and 1500 years for the older sections. This is a critical observation, as the depth transect

approach developed in subsequent chapters assumes the sampling of ocean properties at pseudo ‘steady-state’ conditions.

The strong correlation in the behavior of Al, K, Fe, Ti, and Si suggests that there is a common process governing the abundance of all of these elements. This has often been attributed to terrigenous input [*F X Gingele*, 1996; *J-B W Stuut et al.*, 2002; *J A Collins et al.*, 2014], given that grain-size records show a significant strengthening of the trade winds [*B Jahn et al.*, 2003] and an increase in fluvial inputs during glacial periods [*J-B W Stuut et al.*, 2002]. If this is the case, then it seems likely that the changes in this diagnostic signal are at least partially driven by changes in the local climate in response to variations in insolation.

The anti-correlation between the Fe and Ca records and the depth dependence of the XRF traces (particularly during MIS 4 and MIS 5B/5A) imply that the Fe/Ca XRF ratios could be related to either the depth of the core or its distance offshore. Cores closer to the coastline would likely experience larger changes in upwelling-driven productivity, which could explain the differences in the maxima and minima between shallower and deeper cores. Likewise, proximity to the coast could result in heightened contributions of both terrigenous or eolian material [*J-B W Stuut et al.*, 2002]. The presence of elevated quartz measurements in the cores during glacial periods [*K Crabill*, 2017] suggests that eolian contributions may have been stronger during times of elevated Fe, but more work needs to be done to substantiate this conclusion.

Changes in local export productivity and changes in terrigenous/eolian input would not explain a difference in elemental abundance with water depth (e.g. the

difference between cores above and below 1800-2000 meters depth). An alternative possibility would be that differences in the Fe/Ca records are a result of changes in water mass properties. For instance, shallow cores could experience variable carbonate dissolution relative to deeper cores, which could potentially give rise to a change in behavior of the XRF records between 1800-2000 meters. However, $\%CaCO_3$ data [*K Crabill*, 2017] and proxies related to carbonate ion concentrations (e.g. B/Ca and Sr/Ca from Chapter 3 of this thesis) do not support a difference in carbonate dissolution across the 1800-2000 meter boundary.

A final possibility is that the difference in behavior across the 1800-2000 meter boundary in the XRF elemental abundances reflects a shoaling of the boundary between different water masses. In this scenario, the differences between the shallow and deep cores would be driven by some combination of changes in the advection of fine particles to the core location and/or by changes in the redox state of sediment porewaters [*R S Robinson et al.*, 2002]. Given that the change in behavior for these cores appears during the shift to glacial conditions, this would imply that the boundary between Northern and Southern Source water masses started to strongly shoal across the MIS 5A/4 boundary, consistent with the proxy data from this thesis (e.g. Chapter 2 and 3).

1.5 Conclusion

Here I have presented a set of elemental abundance records that show coherent variability over glacial/interglacial time scales. The similarity of these records implies that a common process is governing the distribution of these elements, and that the downcore records of elemental variability (in particular Fe/Ca) can be used as

stratigraphic tools beyond the limits of radiocarbon. The coherence of the Fe/Ca signal for use in the stratigraphy of these cores is confirmed by both radiocarbon and biostratigraphic markers. This gives confidence in the stratigraphic consistency of the depth profile results presented in Chapters 2, 3, and 4.

The core collection provides several avenues for future research. Most obviously, the development of higher-resolution elemental abundance records could potentially clarify the drivers of local elemental variability. For instance, high-resolution records of change in eolian input shown by changes in dust end-member reconstruction [*J-B W Stuut*, 2001] should be reflected in changing elemental ratios (Si/Al, for example). The development of other types of records might also shed light on local oceanographic processes and the drivers of the differences in elemental variability between the shallow and deep cores. In particular, radiocarbon dating the fine fraction of shallow and deep cores would help resolve whether the change in behavior of the elemental variability centered around 2000 meters during glacial conditions was driven by a shoaling of a southern-sourced water mass. Additionally the creation of a comprehensive XRF dataset of Barium (Ba) variability for these cores could shed light on the extent of local changes in productivity over glacial cycles and whether these changes drove any difference in behavior between shallow and deep cores. Unfortunately, this was not possible to achieve for this thesis due to a problem with the X-ray tube that prevented the acquisition of heavier element abundances, but a resampling of the cores could provide interesting information regarding the extent of productivity changes and the relation of these changes to local climatic processes.

Chapter 1, in part, will be submitted for publication to Marine Geology. Foreman, A.D., Charles, C.D., Slowey, N. C. The dissertation author was the primary investigator and author of this paper.

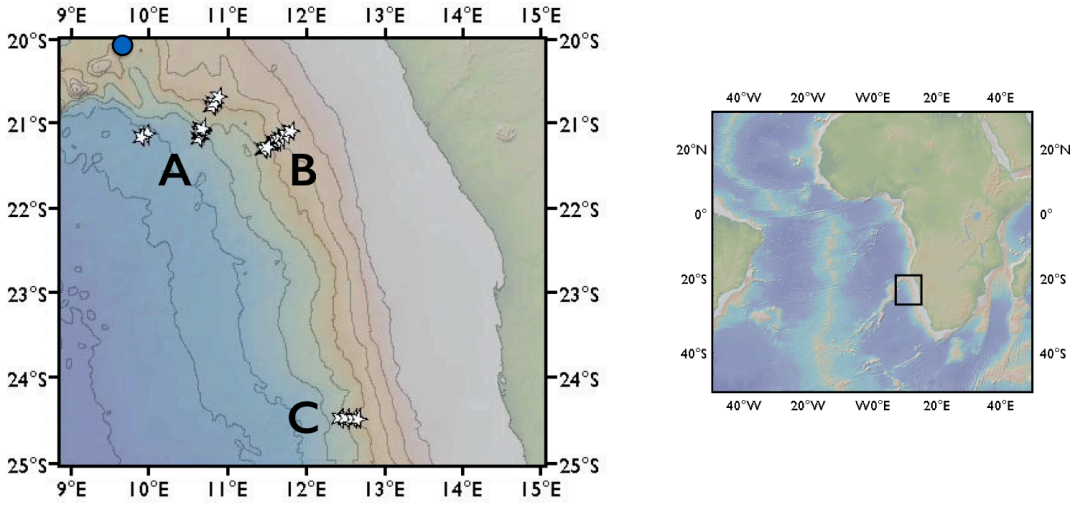

Figure 1.1 Cores were collected along 3 transects near the Walvis Ridge (A, B, C). Elemental abundances vary coherently downcore in each of the 3 locations, allowing stratigraphic correlation to be achieved. The blue circle represents the location of core MD96-2094 [*J-B W Stuut*, 2001], used to compare XRF Fe/Ca traces.

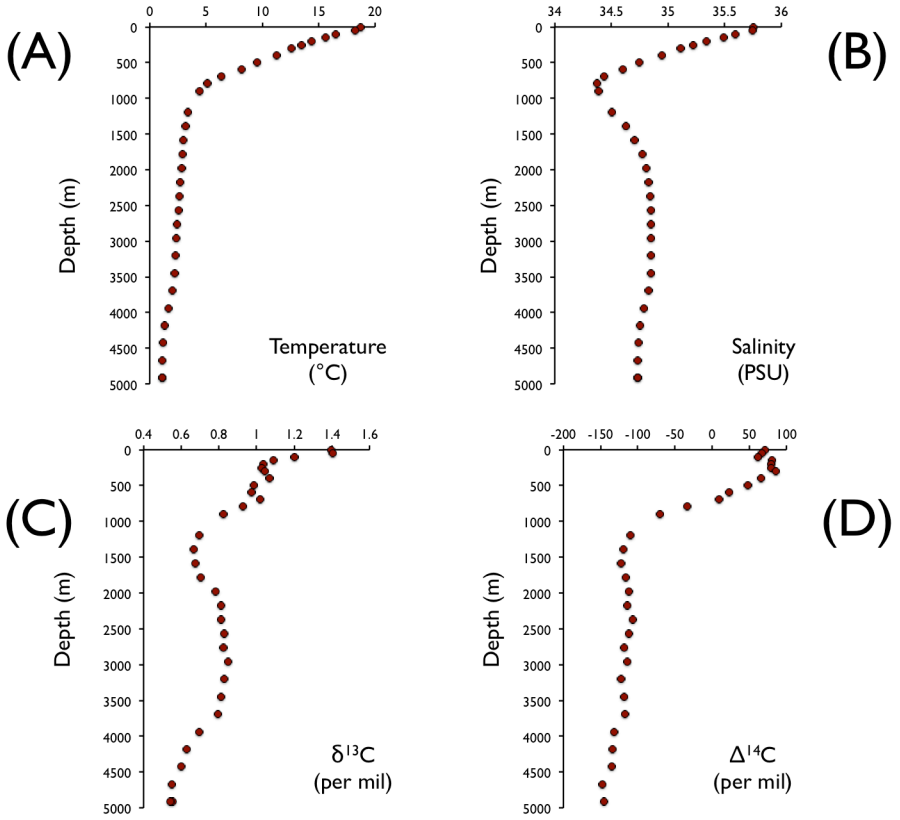

Figure 1.2 Profiles from the CLIVAR A10 cruise at 30°S show small gradients in (A) Temperature and B) Salinity and larger gradients in (C) the $\delta^{13}C$ of the dissolved inorganic carbon (DIC) and (D) $\Delta^{14}C$. The observed foraminiferal $\delta^{13}C$ for the core top profile (Figure 3.4) mirrors the water mass distribution seen in (C). The $\delta^{13}C_{DIC}$ measurements suggest that the northern- and southern- sourced water masses that are stacked vertically in the water column in this area can be distinguished by their varying nutrient contents. In particular, North Atlantic Deep Water (NADW) borders the southern-sourced Lower Circumpolar Deep Water (LCDW) at roughly 3600 meters depth.

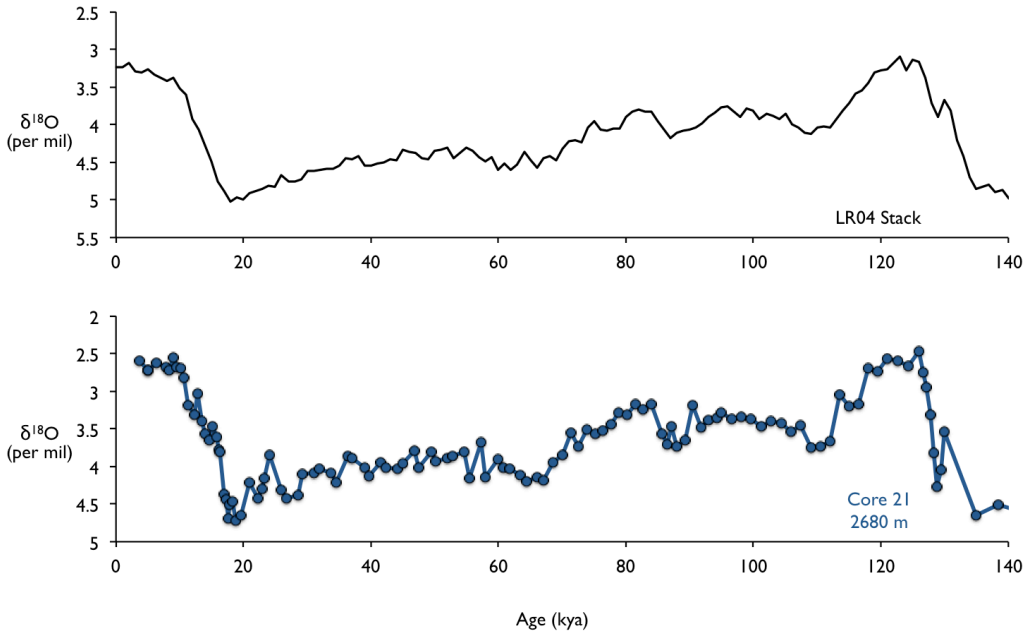

Figure 1.3 Core MV09-PC21 was aligned with the LR04 stack to create an age model for the core. Downcore elemental variability measured by XRF was used to create age models for the rest of the core collection.

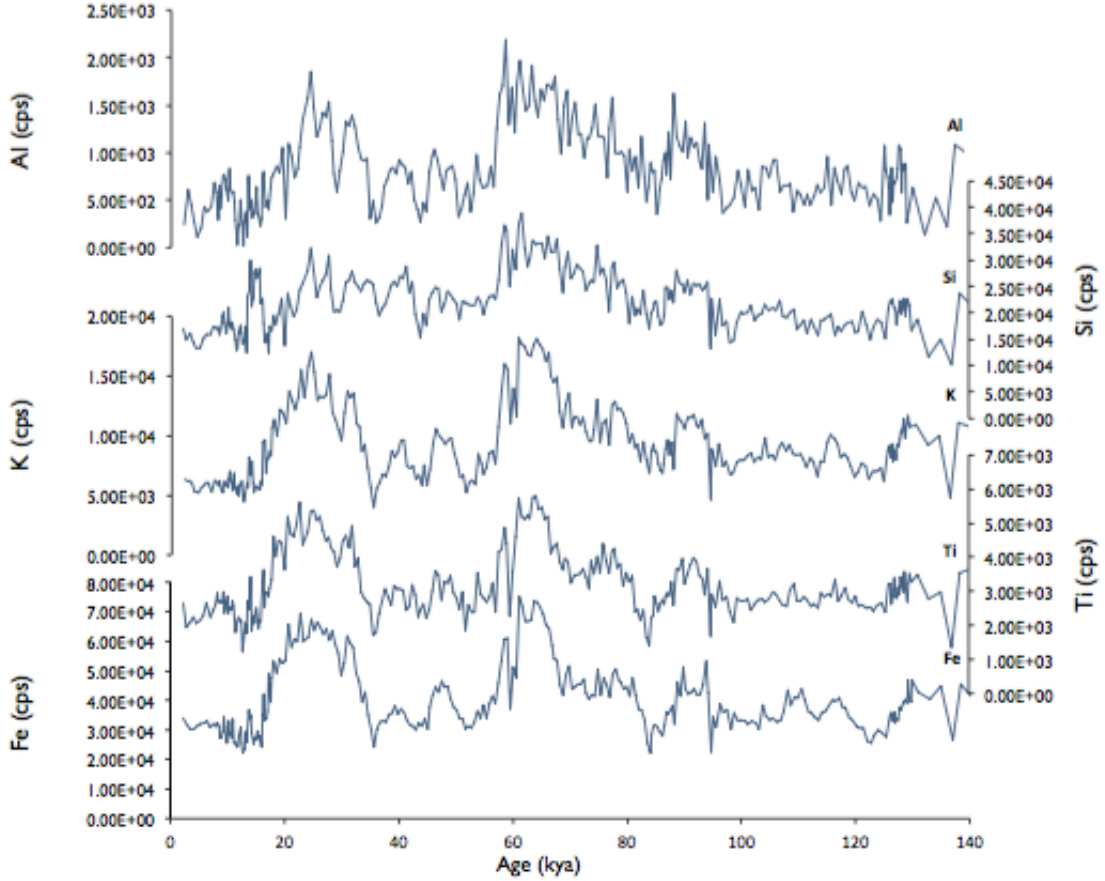

Figure 1.4 Abundances (in CPS) of Al, Si, K, Ti, and Fe in MV09-PC21 as measured by XRF. These elements show a common variability throughout the cores collected from the shallow cores collected in area A and C, and can be tied with the elemental variability of cores from collection areas B. Within the cores, all of these elements show common variability except for Si, which shows a different behavior during the deglaciation.

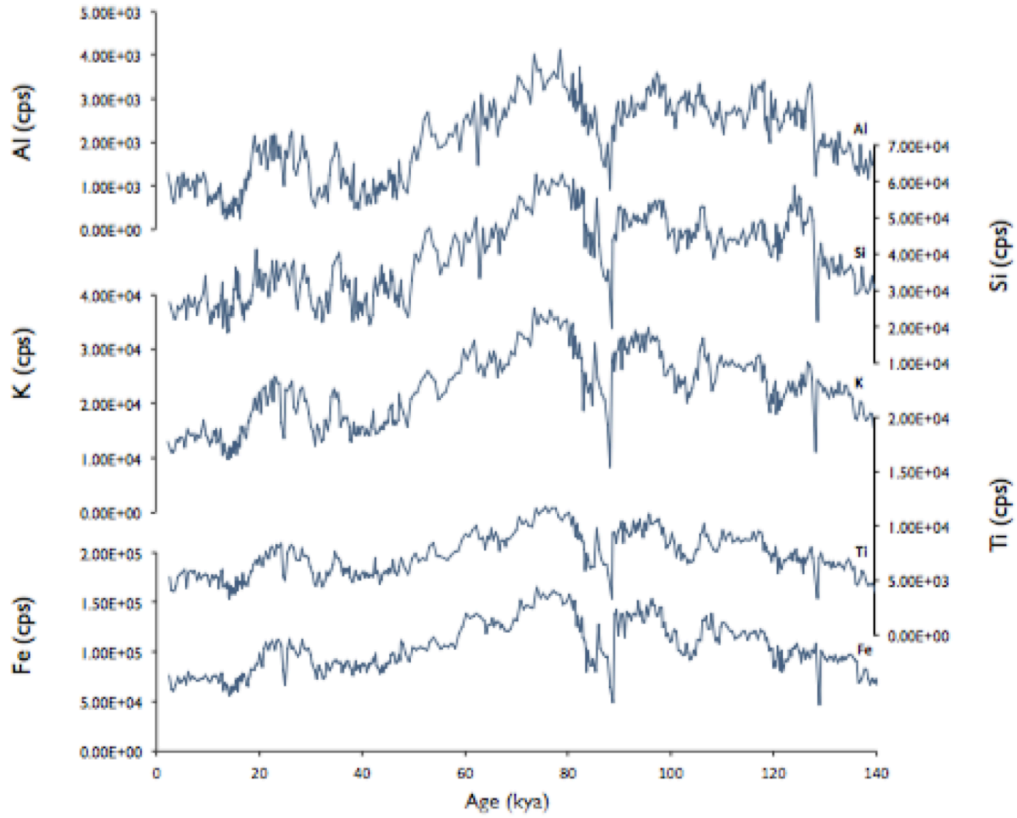

Figure 1.5 Abundances (in CPS) of Al, Si, K, Ti, and Fe in MV09-PC43 as measured by XRF. These elements show a common variability throughout the shallow cores collected from the in area B, and can be tied with the elemental variability of cores from collection areas A and C. Within the cores, all of these elements show common variability except for Si, which shows a different behavior during the deglaciation.

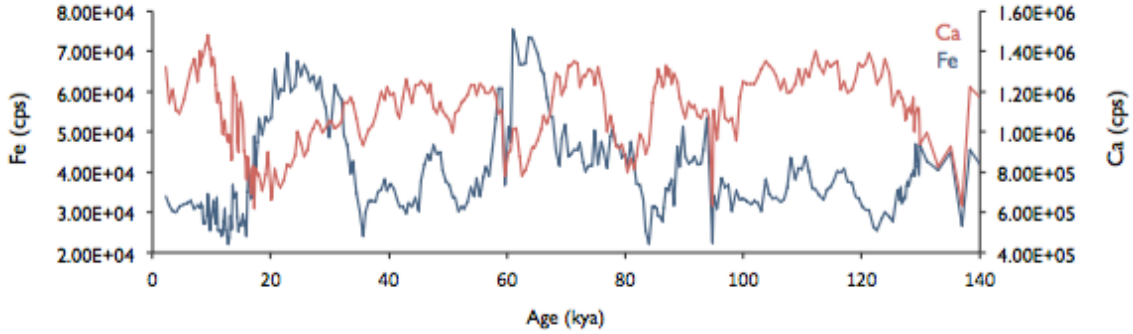

Figure 1.6 Abundances of Ca and Fe for MV09-PC21. The behavior of Ca is opposite to that of Fe, showing elevated values during interglacials and reduced values during glacial periods.

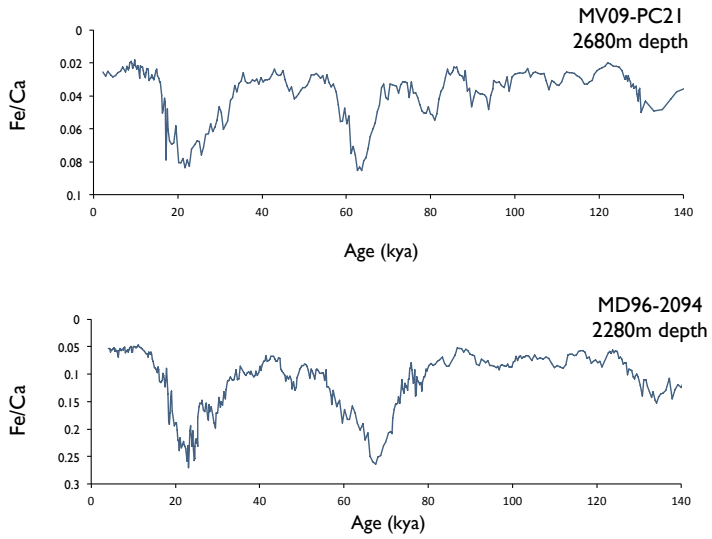

Figure 1.7 Fe/Ca ratios (inverted) for (a) core MV09-PC21 (this study) and (b) core MD96-2094 [*J-B W Stuut*, 2001]. The close agreement between these cores, whose age models were developed independently, suggests that Fe/Ca can be used as a stratigraphic correlation tool.

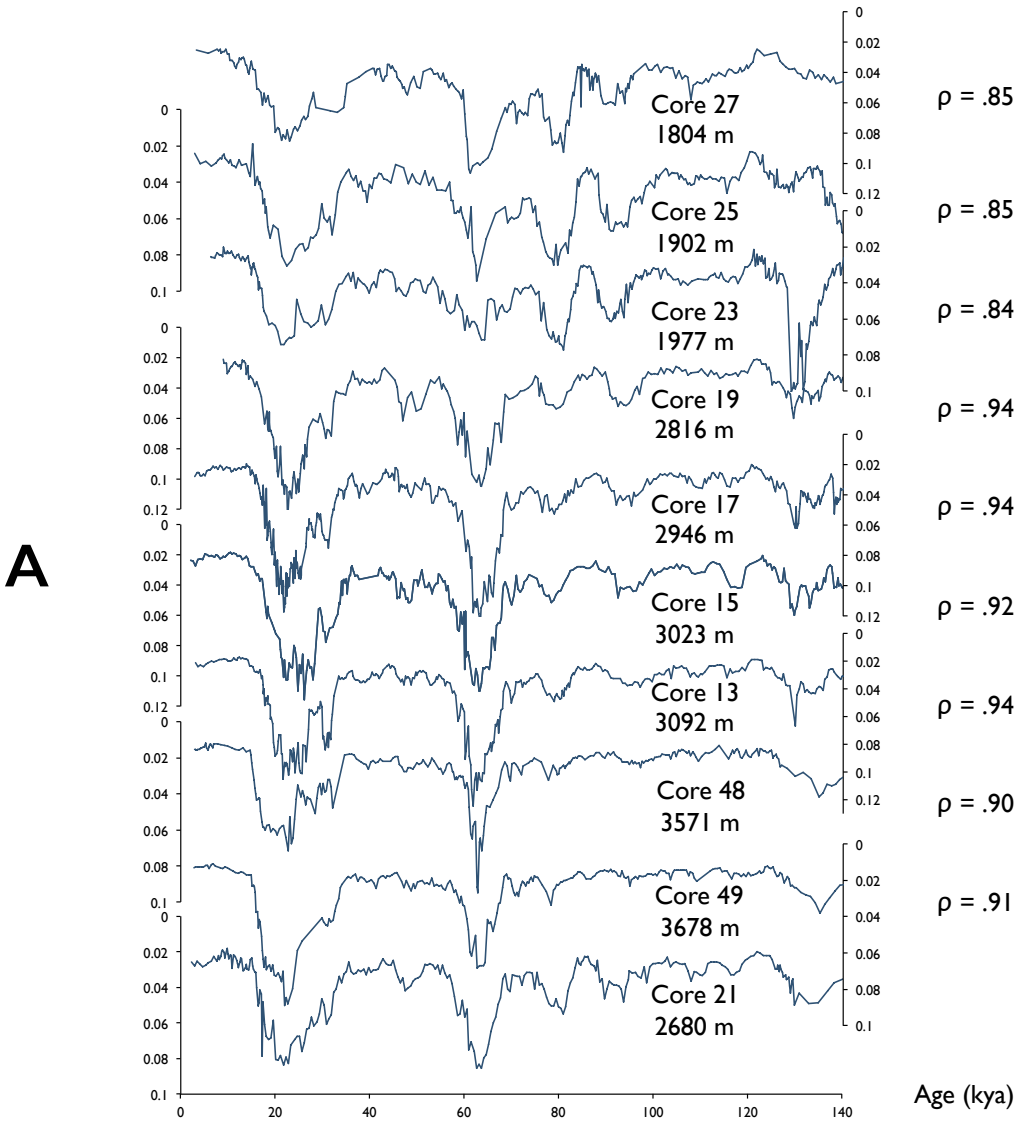

Figure 1.8 Fe/Ca ratios (inverted) for cores collected in the A transect region, sorted by depth. Core MV09-PC21, which was tied to the $\delta^{18}O$ LR04 stack, is shown at the bottom as a comparison. Correlation coefficients for between each core and core MV09-PC21 are shown to the right of the XRF traces. These cores show a coherent signal marked by elevated values of Fe/Ca during glacial periods, and reduced values during interglacials.

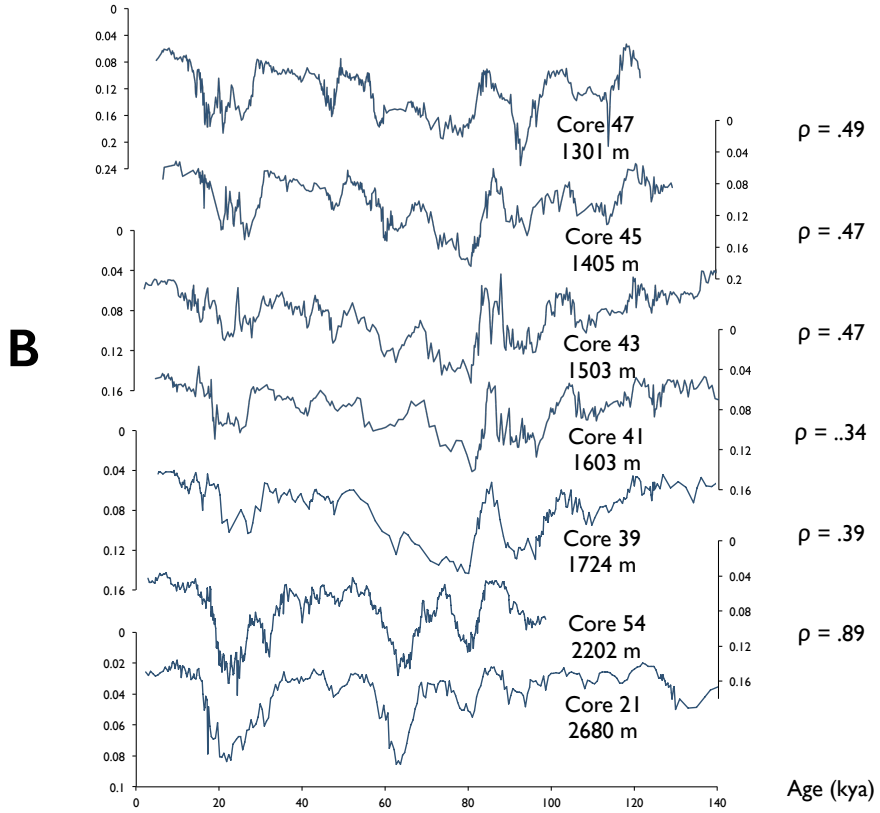

Figure 1.9 Fe/Ca ratios (inverted) for cores collected in the B transect region, sorted by depth. Core MV09-PC21, which was tied to the $\delta^{18}O$ LR04 stack, is shown at the bottom as a comparison. Correlation coefficients between each core and core MV09-PC21 are shown to the right of the XRF traces. These cores show a coherent signal marked by elevated values of Fe/Ca during glacial periods, and reduced values during interglacials.

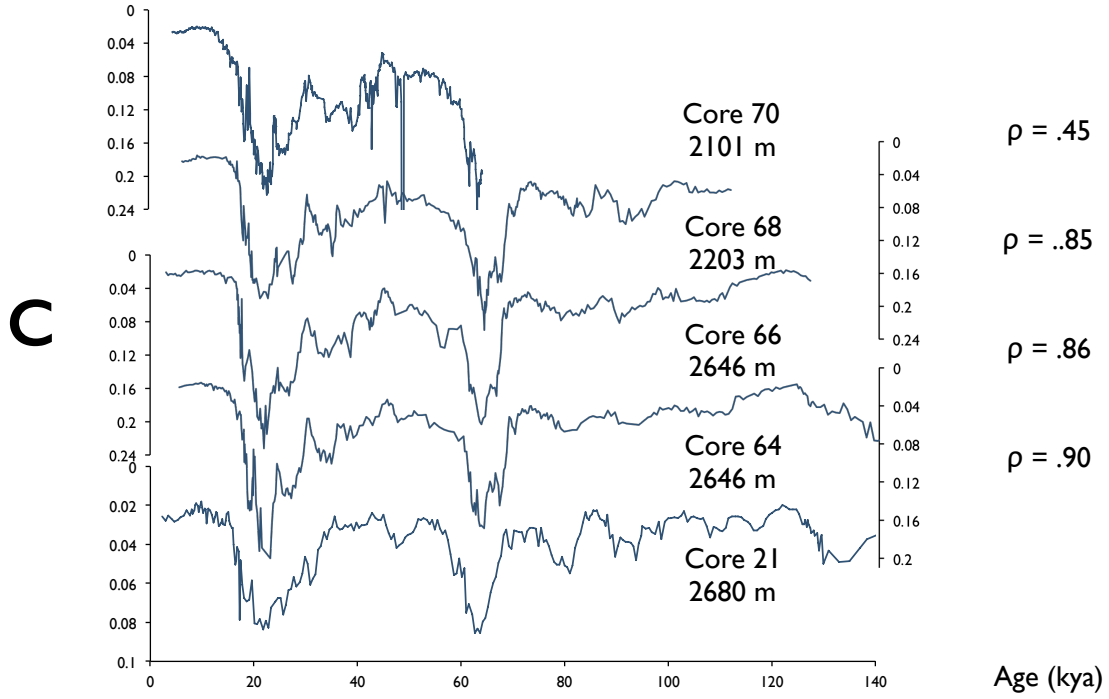

Figure 1.10 Fe/Ca ratios (inverted) for cores collected in the C transect region, sorted by depth. Core MV09-PC21, which was tied to the $\delta^{18}O$ LR04 stack, is shown at the bottom as a comparison. Correlation coefficients for between each core and core MV09-PC21 are shown to the right of the XRF traces. These cores show a coherent signal marked by elevated values of Fe/Ca during glacial periods, and reduced values during interglacials.

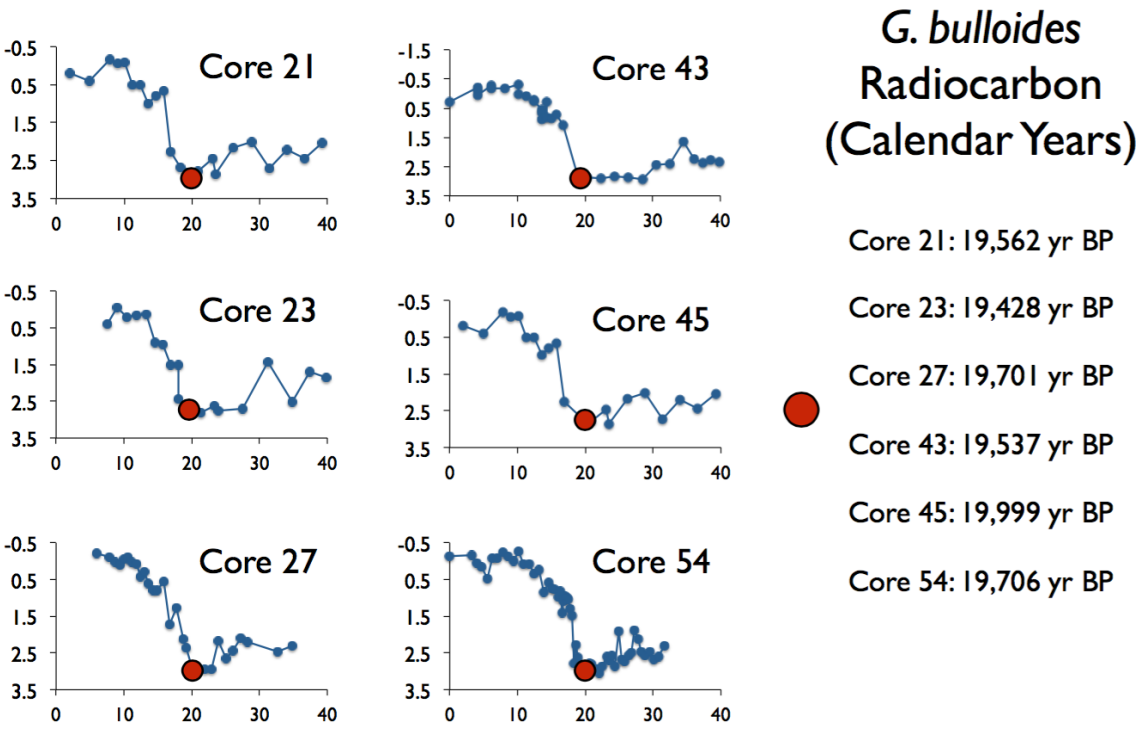

Figure 1.11 The correlation between cores from the A region and B region can be checked by examining proxies that are independent of Fe/Ca for two representative cores. The $\delta^{18}O$ values of *G. bulloides* specimens (Jenna Munson, pers. communication) for cores from the A region (MV09-PC21, MV09-PC23, MV09-PC27) and B region (MV09-PC43, MV09-PC45, Core MV09-PC54) show good agreement after tie-points were developed using Fe/Ca traces. Radiocarbon values for the close of the LGM fall within a 500-year window and are denoted by red circles.

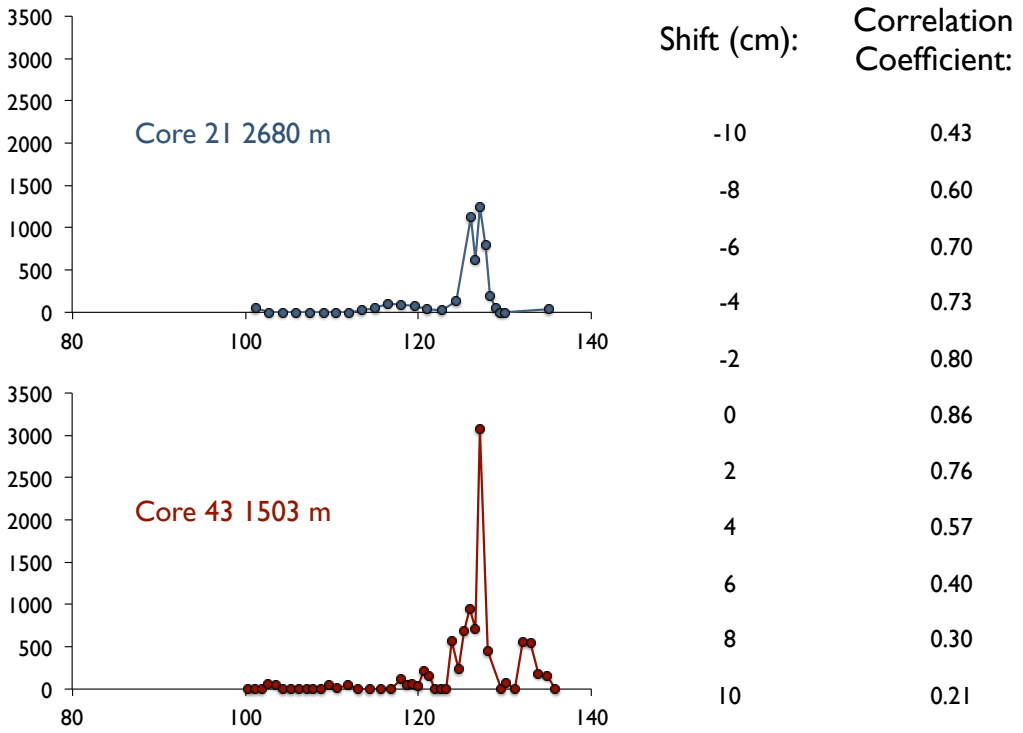

Figure 1.12 Beyond the limits of radiocarbon, the correlation between cores from the A and B regions can be checked by using the appearance of *G. menardii* as a biostratigraphic marker. The two cores show good agreement in the timing of the *G. menardii* population burst just prior to MIS 5E. The correlation coefficients for the two records of *G. menardii* population abundance are shown to the right of the time series. The stratigraphy developed from Fe/Ca traces appears to maximize the correlation of the two records, and correlation drops off significantly if the MV09-PC43 record lags or leads beyond 4 cm from the current stratigraphy.

1.6 References

Berger, W., and G. Wefer (1996), Expeditions into the past: paleoceanographic studies in the South Atlantic, *The South Atlantic: present and past circulation*, 363-410.

Caley, T., J. Giraudeau, B. Malaizé, L. Rossignol, and C. Pierre (2012), Agulhas leakage as a key process in the modes of Quaternary climate changes, *Proceedings of the National Academy of Sciences*, *109*(18), 6835-6839.

Collins, J. A., E. Schefuß, A. Govin, S. Mulitza, and R. Tiedemann (2014), Insolation and glacial–interglacial control on southwestern African hydroclimate over the past 140 000 years, *Earth and Planetary Science Letters*, *398*, 1-10.

Crabill, K. (2017), Late Quaternary carbonate deposition and oceanographic processes in the Southeast Atlantic Ocean, Texas A&M University.

Curry, W. B., and D. W. Oppo (2005), Glacial water mass geometry and the distribution of δ13C of ΣCO2 in the western Atlantic Ocean, *Paleoceanography*, *20*(1).

Gingele, F. X. (1996), Holocene climatic optimum in Southwest Africa—evidence from the marine clay mineral record, *Palaeogeography, Palaeoclimatology, Palaeoecology*, *122*(1-4), 77-87.

Haug, G. H., K. A. Hughen, D. M. Sigman, L. C. Peterson, and U. Röhl (2001), Southward migration of the intertropical convergence zone through the Holocene, *Science*, *293*(5533), 1304-1308.

Haug, G. H., D. Günther, L. C. Peterson, D. M. Sigman, K. A. Hughen, and B. Aeschlimann (2003), Climate and the collapse of Maya civilization, *Science*, *299*(5613), 1731-1735.

Herguera, J., E. Jansen, and W. Berger (1992), Evidence for a bathyal front at 2000-M depth in the glacial Pacific, based on a depth transect on Ontong Java Plateau, *Paleoceanography*, *7*(3), 273-288.

Jahn, B., B. Donner, P. J. Müller, U. Röhl, R. R. Schneider, and G. Wefer (2003), Pleistocene variations in dust input and marine productivity in the northern

Benguela Current: evidence of evolution of global glacial–interglacial cycles, *Palaeogeography, Palaeoclimatology, Palaeoecology*, *193*(3), 515-533.

Jansen, J., S. Van der Gaast, B. Koster, and A. Vaars (1998), CORTEX, a shipboard XRF-scanner for element analyses in split sediment cores, *Marine Geology*, *151*(1), 143-153.

Kallel, N., L. D. Labeyrie, A. Juillet-Leclerc, and J.-C. Duplessy (1988), A deep hydrological front between intermediate and deep-wafpr, masses in the glacial Indian Ocean, *Nature*, *333*(6174), 651-655.

Keigwin, L. D. (2004), Radiocarbon and stable isotope constraints on Last Glacial Maximum and Younger Dryas ventilation in the western North Atlantic, *Paleoceanography*, *19*(4).

Lancaster, N. (1981), Paleoenvironmental implications of fixed dune systems in southern Africa, *Palaeogeography, Palaeoclimatology, Palaeoecology*, *33*(4), 327-346.

Lisiecki, L. E., and M. E. Raymo (2005), A Pliocene-Pleistocene stack of 57 globally distributed benthic δ18O records, *Paleoceanography*, *20*(1).

Lutjeharms, J., and J. Meeuwis (1987), The extent and variability of South-East Atlantic upwelling, *South African Journal of Marine Science*, *5*(1), 51-62.

Ninnemann, U. S., and C. D. Charles (2002), Changes in the mode of Southern Ocean circulation over the last glacial cycle revealed by foraminiferal stable isotopic variability, *Earth and Planetary Science Letters*, *201*(2), 383-396.

Paillard, D., L. Labeyrie, and P. Yiou (1996), Macintosh program performs time-series analysis, *Eos, Transactions American Geophysical Union*, *77*(39), 379-379.

Peeters, F. J., R. Acheson, G.-J. A. Brummer, W. P. De Ruijter, R. R. Schneider, G. M. Ganssen, E. Ufkes, and D. Kroon (2004), Vigorous exchange between the Indian and Atlantic oceans at the end of the past five glacial periods, *Nature*, *430*(7000), 661-665.

Rae, J. W., G. L. Foster, D. N. Schmidt, and T. Elliott (2011), Boron isotopes and B/Ca in benthic foraminifera: Proxies for the deep ocean carbonate system, *Earth and Planetary Science Letters*, *302*(3), 403-413.

Rau, A., J. Rogers, J. Lutjeharms, J. Giraudeau, J. Lee-Thorp, M.-T. Chen, and C. Waelbroeck (2002), A 450-kyr record of hydrological conditions on the western Agulhas Bank Slope, south of Africa, *Marine Geology*, *180*(1), 183-201.

Richter, T. O., S. Van der Gaast, B. Koster, A. Vaars, R. Gieles, H. C. de Stigter, H. De Haas, and T. C. van Weering (2006), The Avaatech XRF Core Scanner: technical description and applications to NE Atlantic sediments, *Geological Society, London, Special Publications*, *267*(1), 39-50.

Robinson, R. S., P. A. Meyers, and R. W. Murray (2002), Geochemical evidence for variations in delivery and deposition of sediment in Pleistocene light–dark color cycles under the Benguela Current Upwelling System, *Marine Geology*, *180*(1), 249-270.

Rothwell, R. G. (2015), Twenty years of XRF core scanning marine sediments: What do geochemical proxies tell us?, in *Micro-XRF Studies of Sediment Cores*, pp. 25-102, Springer.

Schlitzer, R. (2000), Electronic atlas of WOCE hydrographic and tracer data now available, *Eos, Transactions American Geophysical Union*, *81*(5), 45-45.

Stuut, J.-B. W. (2001), Late Quaternary southwestern African terrestrial-climate signals in the marine record of Walvis Ridge, Ph.D Thesis

Stuut, J.-B. W., M. A. Prins, R. R. Schneider, G. J. Weltje, J. F. Jansen, and G. Postma (2002), A 300-kyr record of aridity and wind strength in southwestern Africa: inferences from grain-size distributions of sediments on Walvis Ridge, SE Atlantic, *Marine Geology*, *180*(1), 221-233.

Summerhayes, C., D. Kroon, A. Rosell-Melé, R. Jordan, H. Schrader, R. Hearn, J. Villanueva, J. Grimalt, and G. Eglinton (1995), Variability in the Benguela Current upwelling system over the past 70,000 years, *Progress in Oceanography*, *35*(3), 207-251.

Wilkens, R. H., T. Westerhold, A. J. Drury, L. Mitchell, T. Gorgas, and J. Tian (2017), Revisiting the Ceara Rise, equatorial Atlantic Ocean: isotope stratigraphy of ODP Leg 154 from 0 to 5 Ma, *Climate of the Past*, *13*(7), 779.

Chapter 2. The evolution of deep ocean temperature and salinity in the Southeastern Atlantic over the last glacial/interglacial cycle

Abstract

The deep ocean temperature structure over the last ice age cycle represents an essential aspect of ice age climate sensitivity, yet the documentation of its evolution has thus far been limited to scattered time series from the global ocean. Here I present vertical profile measurements of benthic foraminiferal Mg/Ca and $\delta^{18}O$ at six time points throughout the evolution of glacial conditions, derived from a rigorously controlled depth transect of sediment cores. From these measurements I infer that both a change in structure and a significant cooling occurred in the Southern Atlantic between 2-3 km across the MIS 5E/5D transition. At MIS 5A/4 a second cooling took place at mid-depths, and was likely accompanied by an increase in the production of cold, salty southern-sourced water. The deep South Atlantic appears to have mostly cooled to LGM temperatures by MIS 4, though the gradient between northern- and southern-sourced water continued to sharpen between MIS 4 and the LGM. I suggest that the changes at MIS 5E/5D are linked to a whole ocean cooling and either an expansion of sea-ice or a cooling of northern source water, while the transition of MIS 5A/4 is linked to a cooling of northern source water and a resulting expansion of cool, salty southern source water. The paired Mg/Ca and $\delta^{18}O$ observations also provide constraints on ice volume-induced changes in seawater $\delta^{18}O$ during intervals such as MIS 5D that currently lack sea level estimates.

2.1 Introduction

The separation of the temperature and seawater oxygen isotopic components of the marine oxygen isotope record has been a theme of significant interest for the paleoceanographic community, given the existing body of evidence that salt and temperature stratification have both played a role in trapping carbon in the deep ocean on glacial time scales [*J Toggweiler*, 1999; *J F Adkins et al.*, 2002; *D P Schrag et al.*, 2002; *J F Adkins*, 2013]. Evidence of sea level variation from coral records has been combined with benthic calcite $\delta^{18}O$ records to produce records of temperature change in the deep Pacific [*J Chappell and N J Shackleton*, 1986] and the deep Atlantic [*K Cutler et al.*, 2003; *J F Adkins*, 2013]. For the Last Glacial Maximum, the combination of sea level data and porewater constraints allow a reasonable separation of the temperature component of the benthic foraminiferal $\delta^{18}O$ signal. Reconstructions from earlier times suffer, however, from a lack of well-constrained sea level data over the entire glacial cycle, particularly for Marine Isotope Stage (MIS) 5D and 4. Given that the transitions between MIS 5E-5D and MIS 5A-4 experienced large changes in temperature, sea level, and atmospheric CO_2, it is vital to fill in the gaps of existing observations to confidently reconstruct the behavior of the deep ocean.

The magnesium to calcium (Mg/Ca) ratio in foraminifera has been commonly used as a proxy for the temperature of the seawater in which the foraminifera developed, and as such has the potential to be combined with measurements of foraminiferal calcite $\delta^{18}O$ to reconstruct the oxygen isotopic composition of seawater. A combination of core-top [*H Elderfield et al.*, 2000; *D W Lea et al.*, 2000] and laboratory culture [*D W Lea et*

al., 1999; *S Barker et al.*, 2005] studies have been able to constrain the relationship between temperature and Mg/Ca ratios in planktonic foraminiferal calcite. For benthic foraminifera that live at abyssal depths, this relationship is less well constrained in part because of the difficulty in sampling and culturing. In practice this has meant that the temperature relationship of Mg/Ca in benthic foraminifera has only been developed from empirical calibrations in core top sediments for the most commonly analyzed taxa, e.g. *C. wuellerstorfi* [*C H Lear et al.*, 2002; *P A Martin et al.*, 2002; *S P Bryan and T M Marchitto*, 2008]. These calibrations are made more difficult because 1.) the exact mechanisms of Mg incorporation into the foraminiferal calcite are not known, and the observed relationships tend to be taxon specific; 2.) the observed nature of the relationship between temperature and Mg/Ca seems to be exponential across the full range of temperatures in the ocean; and 3.) the sensitivity of Mg/Ca to changes in temperature is lowest in colder waters. The problem is further complicated by studies that have shown that Mg/Ca is reduced at low carbonate ion saturation [*J Yu and H Elderfield*, 2008]. As a result, it has been difficult to know whether any given sedimentary record of paired benthic foraminiferal Mg/Ca and $\delta^{18}O$ calcite (and by extension, $\delta^{18}O_{sw}$) is quantitatively meaningful.

Vertical depth transects, which compile results from multiple cores from a tight geographical area, represent an approach that potentially circumvents many of the confounding influences by allowing for a multiproxy comparison of multiple sediment cores at specific time points. The dense sampling in the vertical provides essential context for the distribution of sedimentary temperature and salinity proxies. Here I present paired

observations of Mg/Ca and $\delta^{18}O$ for 6 time slices throughout the last glacial interglacial cycle from a collection of cores spanning depths between 1500-3600 meters along the Southeastern Atlantic margin. These observations allow for inferences regarding the timing and magnitude of changes in the vertical structure of temperature in the South Atlantic. In particular I document both the large scale cooling and the change in the vertical structure of the Southern Atlantic that occurred between 2-3 km across the MIS 5E/5D and the MIS 5A/4 transitions. The paired Mg/Ca and $\delta^{18}O$ measurements also provide some new constraints on ice volume-induced $\delta^{18}O_{sw}$ changes across these intervals that currently lack definitive sea level observations.

2.2 Methods and Oceanographic Setting

The southeastern Atlantic is an especially suitable place to observe changes in the depth distribution of deep-water properties because it is at the intersection of the principal water masses involved in meridional circulation. The different northern- and southern-sourced water masses are stacked vertically in this location, and can be distinguished by their varying nutrient contents and densities. Antarctic Intermediate Water (AAIW) and Upper Circumpolar Deep Water (UCDW), for example, make up part of the water column between 500-1500 meters depth, and overlie constituents of North Atlantic Deep Water. In particular, Labrador Sea Water (LSW) occupies the 1700-2000 meter depth range [*R Schlitzer*, 2000]. Deeper in the water column, North Atlantic Deep Water (NADW) borders the southern-sourced Lower Circumpolar Deep Water (LCDW) at roughly 3600 meters depth (Figure 1.2).

The cores presented here were collected aboard the R/V Melville in March 2003. All but 3 of the cores were collected along two depth transects within an area defined by 19° 43.3´S and 21° 33.1´S and 9° 54.1´E and 12° 48.1´E, and range in depth from 1405 to 3678 meters. The remaining cores were taken further south along a transect at 24° 28.0´S, 12° 26.0´E and range in depth from 2200 to 2600 m.

The stratigraphy for the cores used in the vertical profiles presented in this chapter is discussed in significantly greater detail in Chapter 1. Briefly, measurements for core top (i.e. presumably "near modern ocean") profiles were collected within the top 3 centimeters of each of the cores. A combination of radiocarbon measurements and downcore XRF elemental ratio measurements were used to develop a common tie point for the close of the Last Glacial Maximum (LGM). For older vertical profiles where radiocarbon cannot provide an age constraint, the benthic $\delta^{18}O$ record of MV09-PC21 (2680m depth) was tied to the LR04 stack [*L E Lisiecki and M E Raymo*, 2005] to develop a chronology for core MV09-PC21. Down core measurements of various elemental ratios (Fe/Ca and Si/Ti) for each of the other cores in the collection were then tied to the MV09-PC21 record between Marine Isotope Stage (MIS) 5E and the LGM. This approach led to good agreement between several different, semi-independent variables in down-core records (see Chapter 1). I sought to collect vertical profiles for marine isotope stages 5E, 5D, 4, 2 (LGM), and 1 (Core Tops) that most nearly reflected "steady state" intervals at various key points along the ice age cycle. I collected a sixth profile close to MIS 5A, which presented the clearest stratigraphic tie from the XRF data;

however, subsequent isotopic analyses shows that this profile falls closer to the MIS5B/5A boundary.

Stable carbon and oxygen isotope measurements for the vertical profiles were made on splits from the crushed *Cibicidoides wuellerstorfi* specimens mentioned above. These splits were taken after the ultrasonication step, to ensure the removal of clays. Stable isotope values for $\delta^{13}C$ and $\delta^{18}O$ were measured on a Thermo Finnigan MAT 253 mass spectrometer equipped with a Kiel IV carbonate device. Analytical precision, estimated from measurements of concurrently analyzed NBS 19 standards, was 0.07 per mil and 0.04 per mil for $\delta^{18}O$ and $\delta^{13}C$ respectively.

Analysis of trace elemental ratios followed Rae et al [2011], which combined the techniques used by Foster [2008] with oxidative cleaning methods developed by Barker et al [2003]. *Cibicidoides wuellerstorfi* specimens >200μm were selected for a single morphotype (according to guidelines established by Rae et al. [2011]), before being crushed between clean glass slides and transferred to acid-cleaned centrifuge tubes. The samples were subjected to repeated ultrasonication and rinses with MilliQ >18.2 MΩ-cm water to remove clays. The samples were then treated with a 1% hydrogen peroxide solution buffered with 0.1M ammonium hydroxide at 70°C to oxidize organic matter. Following oxidation, samples were treated with a weak acid leach (0.0005M nitric acid) for 30 seconds to remove any adsorbed contaminants, and then dissolved in 250μl of 0.075 M nitric acid. No reductive cleaning step was used, as reductive cleaning has been shown to alter the Mg/Ca ratio in cleaned biogenic carbonate [*S Barker et al.*, 2003; *J Yu and H Elderfield*, 2008]. Samples were centrifuged immediately after dissolution, and

transferred to Teflon vials for storage, leaving a residual (~10µl) amount in the centrifuge tube to exclude any remaining dissolved contaminants. All nitric acid used in these procedures was trace metal clean (SEASTAR brand, ultra pure), and work was carried out in a dedicated flow hood within an over-pressured clean lab using water generated by a boron-free MilliQ package.

Aliquots of the dissolved samples were analyzed for trace elements (Li, B, Na, Mg, Al, Ca, Mn, Sr, Cd, Ba, Nd, U) on an Agilent ICP-MS, matching sample and standard concentration at 1 mmol/L. More details on the trace element analysis can be found in Chapter 3. There is a strong linear correlation in measurements of Na/Ca and Sr/Ca for the dataset as a whole (cf. Figure 3.8). The exact origins of this correlation are unclear, as the processes governing the concentrations of Na in foraminiferal tests are not well characterized [*J C Wit et al.*, 2013]. However, the tight correlation between Na and Sr provides a means of discriminating against samples that have been contaminated or altered during the measurement process. Four total samples (two in the MIS 4 vertical profile and two in the MIS 5D profile) fell off of the Na/Sr relationship defined by the rest of the core collection, and were therefore excluded from this analysis.

2.3 Results

The co-occurring measurements of $\delta^{18}O$ and Mg/Ca demonstrate how the temperature and salinity structures of the intermediate and deep South Atlantic likely evolved over the last full glacial cycle. Starting at the last interglacial (MIS 5E), the MIS 5E profile of $\delta^{18}O$ is slightly lower in comparison to the modern core top profile, but otherwise is largely similar in vertical structure. In contrast to $\delta^{18}O$, the Mg/Ca

measurements below 1800 meters at MIS 5E are strongly elevated, on average nearly 25% higher in Mg/Ca relative to core top values. Stepping forward in time, the MIS 5D $\delta^{18}O$ profile is on average ~0.7‰ higher relative to core top measurements, while the Mg/Ca vertical profile almost exactly matches the core top profile in structure and magnitude. The MIS 5A $\delta^{18}O$ and Mg/Ca profiles mirror their MIS 5D counterparts, showing almost no change between MIS 5D and 5A over the length of the time slices. In contrast, the profiles from MIS 4 show both significantly higher values for $\delta^{18}O$ and a reduction in Mg/Ca, with the latter change localized at mid-depths between 2200-2700 meters. Both $\delta^{18}O$ and Mg/Ca profiles continue to evolve between MIS 4 and the LGM, with a further enrichment in $\delta^{18}O$ and a large decrease in Mg/Ca above 2200 meters. These LGM profiles are consistent with previous evidence from the Brazil margin suggesting a significant discontinuity (enhanced stratification) existed near 2 km in the Southern Atlantic [*W B Curry and D W Oppo*, 2005].

In the following sections I elaborate on these results. I begin by outlining the structure of the $\delta^{18}O$ and Mg/Ca core top profiles, and examine the relationship between those variables and the modern water column. I then describe in detail the changes in structure for the $\delta^{18}O$ and Mg/Ca profiles that can be seen during the stepwise evolution of glacial conditions represented by these profiles. Finally, I discuss the conclusions that can be drawn regarding changes in the sea level and deep ocean temperature records for this time period, and the implications of published calibrations of Mg/Ca for *C. wuellerstorfi* for this dataset.

2.3.1 Core Top Profiles of Stable Isotopes and Mg/Ca

The $\delta^{18}O$ values for the core top profile do not show a pronounced trend below 1500 meters, presumably because gradients in temperature and salinity below this depth are not strong enough to be recorded by *C. wuellerstorfi* (Figure 2.3 A). $\delta^{18}O$ values between 1500 meters and 3600 meters depth average 2.92 +/- 0.06 per mil. Specimens of *C. wuellerstorfi* were not present in the core tops above 1500 meters, but measurements of $\delta^{18}O$ in *Planulina arimenensis* show a gradient between 1500 and 1000 meters depth consistent with a transition to warmer, fresher water above the Labrador Sea Water mass. The lack of change observed in the cores below 1500 meters depth is in agreement with the predicted foraminiferal $\delta^{18}O$ (predicted from the combination of inferred $\delta^{18}O_{sw}$, measured CTD temperature and the paleotemperature equation for $\delta^{18}O$), from which one would expect only a slight trend towards higher $\delta^{18}O$ values between 1500-3600 meters.

Co-occurring measurements of Mg/Ca in *C. wuellerstorfi* were made for the same set of core top samples. Mg/Ca measurements in these samples range between 0.98 and 1.30 and show a nearly linear decrease in values that are below 1600 meters depth. A single point at 1500 meters appears anomalously low compared with Mg/Ca values for the nearby depths. Temperature data from a nearby CTD cast taken on the MV09 cruise suggest that the linearly-decreasing structure observed in Mg/Ca is likely a response to the approximately 2°C change in temperature from shallowest to deepest water observed at this location (Figure 2.1).

2.3.2 Evolution of $\delta^{18}O$ and Mg/Ca During the Buildup to Glacial Conditions

The stable isotope profile for MIS 5E is made up of $\delta^{18}O$ measurements from 14 cores that range in depth between 1503-3678 meters. The $\delta^{18}O$ values show significantly

more scatter than for core top and LGM profiles, but average 2.63 +/- 0.15 per mil (Figure 2.2). In general the $\delta^{18}O$ profile appears to mimic the core top profile in structure, with no obvious gradient appearing in the vertical. The co-occurring measurements of Mg/Ca for the MIS 5E samples show a substantial increase in Mg/Ca compared to each of the other time slices in this dataset (Figure 2.2). Measurements for Mg/Ca in cores above 1750 meters water depth are reduced in Mg/Ca compared to deeper samples, measuring on average 1.37 +/- .06. Below this water depth, there is a substantial increase in the average Mg/Ca values to 1.57 +/- .09.

The MIS 5D $\delta^{18}O$ profile is compiled from 15 cores that range in depth between 1503-3678 meters. The $\delta^{18}O$ profile for MIS 5D shows a similar structure to that of MIS 5E above 1700 meters, with values of $\delta^{18}O$ roughly 0.3 per mil higher than those between 1700 and 2000 meters. Below 2000 meters $\delta^{18}O$ values are higher about 0.35 per mil, moving from an average value of 3.29 +/ .08 per mil to an average value of 3.65 +/- 0.08 around 3000 meters. The Mg/Ca profile for this substage shows a substantial reduction in Mg/Ca compared to MIS 5E at every core in the profile below 1800 meters depth, dropping on average by nearly 0.4 (Figure 2.2). Above 1800 meters, however, this difference largely is erased, and values in general are reduced in Mg/Ca by less than 0.1. The vertical structure of Mg/Ca at MIS 5D is similar to that observed for MIS 5E in that samples from cores above 1700 meters depth exhibit reduced Mg/Ca values compared to cores in the 1800-2000 meter depth range. Cores between 1800-2000 meters show a strong gradient in Mg/Ca of 0.3 across these depths. Below 2000 meters the cores show a linear decrease in Mg/Ca of 0.16 between 2000-3000 meters (Figure 2.3E).

The profile collected along the transition between MIS 5B and MIS 5A (referred to as MIS 5A) is made up of $\delta^{18}O$ measurements from 15 cores ranging between 1405-3678 meters depth, and closely mimics the MIS 5D profile (Figure 2.3D). Above 1500 meters the values of $\delta^{18}O$ for the MIS 5A transition show an average value of 3.21 per mil. Immediately below 1500 meters depth the values are higher by ~0.2 per mil, and remain roughly constant between 1600-2200 meters, averaging 3.39 +/- 0.05 per mil. Below 2200 meters depth the values shift towards a slightly higher average value of 3.56+/- 0.22 per mil. (Figure 2.2) The Mg/Ca values for the MIS 5A vertical profile are very close in both structure and magnitude to the MIS 5D profile. Cores above 1700 meters are substantially reduced in Mg/Ca compared to the cores in the 1800-2000 meter depth range, averaging 1.28 +/- 0.04. The cores between 1800-2000 meters display elevated values compared to the rest of the profile, similar to the MIS 5D profile. Below 2000 meters the cores show a linear decrease in depth of Mg/Ca down through 3000 meters.

The MIS 4 profile is made up of $\delta^{18}O$ measurements compiled from 16 cores ranging between 1405-3678 meters depth. There is a nearly 0.2 per mil decrease in $\delta^{18}O$ between 1405 meters depth and 1900 meters depth. Below 1900 meters the values of $\delta^{18}O$ for the profile are roughly constant, averaging 4.25+/-0.05 per mil. (Figure 2.2) In contrast, the Mg/Ca profile shows a varied vertical structure (Figure 2.2). The shallowest point in the Mg/Ca profile, at 1405 meters depth, is depleted in Mg/Ca compared to the cores between 1800-2000 meters. Values measured for cores for the rest of the profile show a strong transition to lower values between 2000-2500 meters depth (Figure 2.3C).

Below 2200 meters the values of Mg/Ca align closely with those from the LGM profile, with the exception of a single point at 2866 meters depth that shows significantly elevated Mg/Ca values (Figure 2.3B).

Measurements from 13 piston cores spanning water depths between 1603 and 3678 meters make up the LGM vertical profile of $\delta^{18}O$ (Figure 2.2). (The lack of *C. wuellerstorfi* specimens in shallower cores precludes stable isotope analysis further up the water column.) The shallowest point in the water column profile is roughly 0.3 per mil lower than the rest of the profile. Below this point there is evidence of a small (~0.15 per mil) linear gradient in $\delta^{18}O$ between 1700-2200 meters; and further below the $\delta^{18}O$ values remain roughly constant around an average value of 4.66 +/- 0.06 per mil. Co-occurring measurements of Mg/Ca for the LGM time slice show a distinct vertical structure at the LGM. Shallower values show a linear decrease from 1.26 to 0.97 between 1600 and 2200 meters depth. Below this depth the values of Mg/Ca stay nearly constant, averaging 0.95 +/- 0.03.

2.3.3 Implied changes in temperature and ice volume

Constraints from global sea level records [*K Cutler et al.*, 2003] and porewater measurements [*J F Adkins et al.*, 2002] show that sea level decreased by 120 meters and that the deep ocean was near freezing at the LGM. Likewise, measurements of sea level at the last interglacial have constrained the maximum sea level rise (relative to modern) to +10 meters [*A Dutton and K Lambeck*, 2012]. However, there is a relative lack of evidence for the manner in which the global volume of ice and the global ocean temperature may have changed between MIS 5E and the LGM. In particular, the most

commonly cited estimates for MIS 5D and MIS 4 sea level [*K Cutler et al.*, 2003] lack enough data for robust determination of the magnitude and timing of sea-level change. In this section I begin by discussing the application of existing Mg/Ca temperature calibrations for *C. wuellerstorfi* to these profiles to help constrain sea level and temperature at MIS 5D and MIS 4. I then examine the implied changes in sea level and deep sea temperature at MIS 5D and MIS 4 in the data by comparing the MIS 5D and 4 profiles with profiles that have well-constrained sea level and deep ocean temperature estimates. Subsequently I use the sea-level estimates from Cutler et al. [2003] and a scaling of seawater $\delta^{18}O$ for sea level [*J F Adkins et al.*, 2002] to examine the implications of the profiles for deep ocean temperature during the major steps toward glaciation.

An important caveat in the calculation of the changes in ice volume and temperature implied by the paired $\delta^{18}O$ and Mg/Ca measurements is that the $\delta^{18}O$ signal of *C. wuellerstorfi* can be significantly altered by changes in the $\delta^{18}O$ of the source waters [*L Labeyrie et al.*, 2005; *L Skinner and N Shackleton*, 2005; *C Waelbroeck et al.*, 2008; *C Waelbroeck et al.*, 2011]. In the modern ocean, the difference in $\delta^{18}O_{sw}$ of NADW and AABW is on the order of 0.5 per mil [*H Craig and L I Gordon*, 1965]. Given the suggested changes in northern/southern source water mass geometry between the LGM and present day [*W B Curry and D W Oppo*, 2005; *J Lynch-Stieglitz et al.*, 2007], a shift in the source waters for a given core could be enough to influence any estimates of sea level by as much as 50 meters. Such a strong influence is unlikely, however, as evidence points to southern sourced waters at the LGM being much saltier than present day [*J F*

Adkins et al., 2002]. This would potentially "buffer" observations from a single vertical profile against significant water-mass $\delta^{18}O_{sw}$ effects, but it does imply that the $\delta^{18}O_{sw}$ deductions might show a combination of ice volume-related and deep ocean circulation-related effects. The extent to which the change in salinity of the southern source waters would have altered these measurements is dependent on the mechanisms of deep water formation. For example, increased sea-ice formation would not be expected to substantially change the $\delta^{18}O_{sw}$ [*R Weiss et al.*, 1979; *J F Adkins et al.*, 2002], while a change in the amount of melt water from land-based ice sheets would strongly alter the $\delta^{18}O$ signal [*J Toggweiler and B Samuels*, 1995; *J F Adkins et al.*, 2002]. Without surface constraints on the $\delta^{18}O$/salinity relationship it is impossible to adequately constrain these potential changes. For the following simple calculations, I assume that the changes in the source $\delta^{18}O_{sw}$ are largely protecting the profiles against large changes in water-mass $\delta^{18}O_{sw.}$ However, the possibility of changes in source water is examined further in the discussion section.

A first obvious step is to examine whether any existing calibrations for Mg/Ca and temperature can be applied to this dataset. The empirical calibration of the Mg/Ca ratio to temperature for *Cibicidoides spp.* proposed by Lear et al. [2002] yields a relationship of Mg/Ca = 0.867*e^(0.109T). Applying this calibration to the Mg/Ca profiles provides a range of temperatures with a difference in average temperatures of ~4.4°C between LGM and MIS 5E profiles below 2000 meters depth. Notably, the Lear calibration yields an average temperature for the MIS 5E vertical (5.40°C) profile that is substantially warmer than each of the other profiles, and an LGM average temperature

(1.0°C) that is well above freezing. Utilizing the calibration proposed by Martin et al. [2002] does not appreciably alter these results.

If I compare the difference in temperatures calculated from the Lear et al. [2002] between each core in the collection individually at successive marine isotope stages, some immediate trends emerge. The transition from MIS 5E to 5D is accompanied by a more than 2.0°C cooling in deep ocean temperature localized below 2000 meters depth. Although there is some spread in the differences between the 5D and 5A profiles, on average there is only a small difference in temperature (~0.3°C). The difference in temperature between MIS 5A and MIS 4 is larger, averaging 0.6°C, with the bulk of this temperature difference confined to the mid-depth region between 2200 and 2900 meters depth. The difference between MIS 4 and the LGM, on average 2.0°C over the length of the profile, mostly stems from changes in the Mg/Ca profile above 2200 meters. The difference between the LGM and core top data shows a roughly constant offset of 1.4°C.

By taking the average of the differences in temperature between marine isotope stages over the length of each profile, I can calculate the difference in sea level implied by the Lear et al. temperature calibration of the Mg/Ca data and the $\delta^{18}O$ data using the scaling relationship of $\delta^{18}O_{sw}$/sea level of 1.1 per mil for 120 meters of sea level. The estimates of sea level change calculated this way are within 15 meters of those estimated from the sea level curve described by Cutler et al. [2003] for the 5E-5D, 5D-5B/A, and 5B-5A/4 transitions. The sea level change implied by the average change in temperature across the MIS 4-LGM transition is the opposite sign of that estimated by the Cutler et al. [2003] sea level curve, while the implied sea level change between the LGM and present

is more than 25 meters larger than any of the coral-based sea level reconstructions [*R G Fairbanks*, 1989].

If I instead limit the selection of cores to those below 2400 meters, the difference in the average temperatures changes slightly for each of the profiles, but does not alter the sea level estimates significantly (>5m), with the exception of the transitions in and out of MIS 4. In particular, the MIS 5A/5B-MIS 4 estimate of sea level change is reduced by 25 meters, and the sense of the sea level change from MIS 4 to LGM changes sign. In any case, applying the Lear et al.[2002] calibration to my Mg/Ca data appears to violate the existing independent constraints on sea level and deep ocean temperature change, particularly for the LGM.

While the published calibrations evidently do not appear to accurately describe the local Mg/Ca-temperature relationship for this core collection, constraints for temperature and salinity can still be developed using these vertical profiles. For example, comparing the Mg/Ca profiles for MIS 5D and 4 time periods with those of the Core Top and LGM profiles provides information about the temperatures of those time periods without requiring any sort of calibration. At MIS 5D, the Mg/Ca profile is nearly identical in structure and magnitude to the core top profile, while the stable isotope profile offset by an average of 0.7 per mil. Using the scaling relationship of 1.1 per mil/120 meters of sea level [*J F Adkins et al.*, 2002] suggests that the sea level at MIS 5D must have been at least 70 meters lower than it currently is today. Taking a similar approach for MIS 4 by comparing its Mg/Ca data to that of the LGM profile implies that the MIS 4 and LGM temperatures were nearly identical in the deep ocean. Using the

same $\delta^{18}O_{sw}$-sea level scaling relationship as before suggests there must have been at least 40 meters of sea level change to account for the >0.4 per mil increase in $\delta^{18}O$ between MIS 4 and MIS 2. Both of these calculations potentially overestimate changes in sea level, as the $\delta^{18}O$ of the source water could have changed in both intervals. Still, the overlap between the MIS 5D/Core Top and MIS 4/LGM Mg/Ca profiles provide a strong constraint on the temperature of the Southern Atlantic for MIS 5D and MIS 4; regardless of calibration these temperatures must have been similar to that of the late Holocene and LGM, respectively.

A final approach for the deconvolution of temperature and ice volume is to use the scaling relationship of 1.1 per mil/120 meters of sea level [*J F Adkins et al.*, 2002] and the sea level curve from Cutler et al. [2003] to correct the $\delta^{18}O$ vertical profiles for changes in ice volume (Figure 2.2). The resulting difference in $\delta^{18}O$ in the profiles shows a large (~0.6 per mil) difference in $\delta^{18}O_{corr}$ between MIS 5E and 5D, depending on the choice of sea level value for MIS 5D. A smaller change in $\delta^{18}O_{corr}$ of ~0.25 per mil occurs across the MIS 5A-MIS 4 transition, again dependent on the choice of sea level. The difference between the LGM and core top profiles after this correction is 0.7 per mil. Converting the difference in $\delta^{18}O$ to temperature according to the $\delta^{18}O$ -temperature relationship of -4.0 °C/per mil yields a cooling of ~2.5°C across the MIS 5E-5D transition and of ~1.1°C across the MIS 5A-MIS 4 transition. The change in $\delta^{18}O$ between the LGM and core tops implies a warming of ~2.8°C.

2.4 Discussion

The structure of the stable oxygen isotope and Mg/Ca profiles vary in a consistent manner as glacial conditions build. The changes in these profiles give rise to several main observations regarding the structure of the Southeastern Atlantic over the last glacial cycle, which can be summarized as follows:

1) The MIS 5E/5D transition shows a large difference in absolute value for both Mg/Ca and $\delta^{18}O$ that reflects a large-scale cooling over this transition below 1800 meters. The structure for Mg/Ca and $\delta^{18}O$ at MIS 5D shows a gradient in both tracers across mid-depths that is not present in the MIS 5E profile (Figure 2.3 E)
2) The MIS 5D/5A profiles are nearly identical in both $\delta^{18}O$ and Mg/Ca values, and have a nearly identical structure (Figure 2.3 D).
3) The transition between MIS 5A and MIS 4 shows the development of a stronger gradient in Mg/Ca between 2000 and 2700 meters driven by changes in the structure of the vertical profile below 2000 meters depth. The equivalent comparison of the two stages for $\delta^{18}O$ shows the gradient in $\delta^{18}O$ is present but reduced over those depths during MIS 4 in comparison to MIS 5A (Figure 2.3 C).
4) The MIS 4/LGM transition shows sharp gradient between shallow and mid-depth waters to 2000 meters. The values of Mg/Ca below 2000 meters at the LGM are nearly identical to those at MIS 4 (Figure 2.3 B).

These observations are qualitative descriptions of the changes in water mass geometry. The previously published calibrations of Mg/Ca to temperature [*C H Lear et al.*, 2002; *P A Martin et al.*, 2002] represent one obvious means of transforming the results into a more qualitative interpretation. However, these previous calibrations are incompatible with the various constraints presented here, as they yield temperatures for the core top and LGM profiles that are much warmer than implied by local CTD casts in the modern ocean (Fig. 1) and by porewater data from the LGM [*J F Adkins et al.*, 2002]. Also, when combined with the measured $\delta^{18}O$ values for these profiles, the Lear et al. [2002] calibration of Mg/Ca overestimates the known amount of sea level change between the LGM and present by at least 25 meters and would seemingly require sea level to have reached a minimum during MIS 4. Similarly, a two-step temperature calibration of Mg/Ca using fixed sea-level values for MIS 5E, the LGM, and the Holocene and the $\delta^{18}O$ values for the vertical profiles requires that sea level reach a minimum during MIS 4. Thus, the sea level changes implied by applying any of the existing Mg/Ca calibrations are incompatible with the current consensus from coral observations on how sea level must have evolved.

The errors in the sea level reconstructions in the attempts above are likely due to some combination of the problems that have bedeviled the use of benthic Mg/Ca as a paleothermometer, most notably the difficulty in creating an accurate low-temperature calibration of Mg/Ca [*S P Bryan and T M Marchitto*, 2008] and the effect of low carbonate ion on Mg incorporation [*H Elderfield et al.*, 2006; *J Yu and H Elderfield*, 2008]. Nevertheless, the compilation of vertical profiles of paired Mg/Ca and $\delta^{18}O$ have

two unique aspects that provide new constraints. For example, the overlap between the Mg/Ca profiles for MIS 5D and the Core Top profiles implies that these two time periods experienced near-identical temperature conditions over the length of the profile, even without a local calibration of Mg/Ca and temperature in place; the overlap in Mg/Ca between MIS 4 and the LGM suggests the same average temperature prevailed for MIS 4 and the LGM. Given the strong constraints on the temperature of the ocean during the Holocene and at the LGM, the large differences in $\delta^{18}O$ between the MIS 5D/Core Top and MIS 4/LGM profiles signal some combination of changes in ice volume and the $\delta^{18}O$ of the source waters. Additionally, these paired measurements allow for a closer examination of the depth distribution of each tracer. Both sets of tracer should respond to changes in the density structure of the deep ocean, and as such allow for inferences about the distribution of water masses at various key time points in the evolution of glacial conditions; the analysis of changes in stratification do not, in and of themselves, require a specific calibration of Mg/Ca to temperature.

Starting with the first of these points, the comparison of Mg/Ca profiles for this collection implies that sea level decreased on the order of 70 meters between MIS 5E and 5D, and 40 meters between MIS 4 and the LGM. The MIS 5D estimate is significantly greater sea level change than is estimated from limited coral observations, which tend to estimate the sea level lowering across the MIS 5E/5D transition as 25 meters [*K Cutler et al.*, 2003]. A much larger change is not outside the realm of possibility, as few records exist to confirm or deny this estimate. Alternatively, if the $\delta^{18}O$ difference between modern and MIS 5D resulted partially from water mass $\delta^{18}O_{sw}$ changes (as opposed to

ocean volume changes exclusively), then this would imply much saltier water than present during MIS 5D. Likewise, there are few records to either confirm or refute the estimate of 40 meters of change between MIS 4 and the LGM, though in this case the published coral records agree with this estimate.

The changes in the profiles of $\delta^{18}O$ and Mg/Ca between the substages have substantial implications for how glacial conditions evolved. Starting at the peak of the last interglacial, the large change in both Mg/Ca and $\delta^{18}O$ between MIS 5E and 5D is consistent with several observations that have implied a large cooling of deep ocean temperature across the MIS 5E/5D transition [*J Chappell and N J Shackleton*, 1986; *K Cutler et al.*, 2003; *J F Adkins*, 2013]. This observation also fits with the implied temperature change from Kr and Xe records, which suggests a cooling of 2°C – 2.5°C across the MIS 5E/5D transition [*M A Headley*, 2008].

The structure of the MIS 5D $\delta^{18}O$ and Mg/Ca profiles show the development of a gradient between low Mg/Ca (high $\delta^{18}O$) waters below 2700 meters and high Mg/Ca (low $\delta^{18}O$) waters at 2000 meters. This structure is not present in the MIS 5E profiles of $\delta^{18}O$ and Mg/Ca, which, while more scattered, appear to reflect the vertical structure of the core top profiles of those elements. This is consistent with the idea that colder southern sourced waters were confined to depths below at least 3600 meters during MIS 5E, and that they expanded to at least 3000 meters depth by the close of MIS 5D. It is also worth noting that the vertical structure of $\delta^{18}O$ and Mg/Ca both show a nearly identical structure above 2000 meters, suggesting that the majority of the cooling across MIS 5E/5D was confined below 2000 meters.

The comparison of the MIS 5D and 5A profiles is complicated by the fact the MIS 5A profile actually corresponds to the MIS 5A/5B transition (see Chapter 1). The vertical structure and absolute values for the MIS 5D and MIS 5A profiles are nearly identical, which suggests that the MIS 5A/5B transitional structure of the deep ocean was probably close to that of MIS 5D.

The transition between the MIS 5A and MIS 4 profiles shows several notable characteristics. First the development of a sharp mid-depth front between 2000 and 2700 meters in Mg/Ca suggests that MIS 4 saw a further increase in the influence of southern-sourced waters, promoting a sharpened gradient in Mg/Ca, likely as a result of a combination of changing temperature and carbonate ion concentration. Surprisingly, the gradient between 2000 and 2700 meters in $\delta^{18}O$ for MIS 4 is relatively small compared with the MIS 5A profile. The lack of a large $\delta^{18}O$ gradient across these depths could be a result of the cooling of the shallower waters around 2000 meters, which is consistent with a negative offset in Mg/Ca seen in the upper part of the profile, or an increase in the salinity of the deep ocean at depth, or some combination thereof.

The Mg/Ca profile at the close of the LGM shows a sharp discontinuity above 2200 meters. Below 2200 meters the LGM values of Mg/Ca are nearly identical to those for MIS 4, while shallower cores show an additional reduction in Mg/Ca from the MIS 4 profile. The LGM $\delta^{18}O$ structure shows a similar picture, with a stronger gradient between 2200 and 1600 meters as compared to MIS 4. Depending on the estimates of sea level change between MIS 4 and the LGM, a good portion of the change in $\delta^{18}O$ between the MIS 4 and LGM profiles can be attributed to sea-level change. It is also interesting to

note that the $\delta^{18}O$ profile for the LGM matches the vertical structure and magnitude observed in $\delta^{18}O$ in the LGM Western Atlantic along the Brazil Margin [*W B Curry and D W Oppo*, 2005]. This is commonly thought of as evidence that the boundary between southern- and northern-sourced water masses shoaled to 2000 meters, an interpretation supported by the gradient in Mg/Ca shown here and by radiocarbon reconstructions of these profiles [*J. Munson, pers. communication*].

Taken together these observations paint a picture of how Atlantic glacial conditions likely evolved over the last 125 kyr. From a comparison between the MIS 5E and core top profiles I can assume that the vertical structure of the mid-depth and deep ocean during the last interglacial was close to modern, as has been surmised from other records [*J-C Duplessy and N J Shackleton*, 1985; *J Duplessy et al.*, 2007; *H Evans et al.*, 2007]. The structure of the MIS 5D profiles of $\delta^{18}O$ and Mg/Ca suggest that the boundary between Southern Component Water (SCW) and Northern Component Water (NCW) shoaled, and that the deep ocean experienced substantial cooling across this transition. This matches previous observations from the Southern Ocean, which show an expansion of SCW to at least 3000 meters across this transition [*A Govin et al.*, 2009]. The conditions observed at MIS 5A remained similar to those at MIS 5D, with Southern sourced waters confined below 3000 meters depth. Subsequent cooling at the MIS 5A/4 transition mainly occurred at mid-depths, with the gradient between SCW and NCW shoaling and sharpening, matching previous evidence from stable isotope [*A Govin et al.*, 2009] and sortable silt [*E G Molyneux et al.*, 2007; *G Martínez-Méndez et al.*, 2008; *D J Thornalley et al.*, 2013] records. The boundary between NCW and SCW shoaled even

further between MIS 4 and the LGM, eventually mimicking the structure observed in depth transect records for the LGM in the Atlantic [*W B Curry and D W Oppo*, 2005], as well as the Indian [*N Kallel et al.*, 1988], Pacific [*J Herguera et al.*, 1992] and Southern Oceans [*U S Ninnemann and C D Charles*, 2002]. The comparison of the MIS 4 and LGM profiles also shows that there was likely little cooling occurring below 2200 meters, and perhaps across the length of the profile using the sea level estimate for the MIS 4-2 transition from Cutler et al. [2003].

While a full mechanistic explanation of the evolution of glacial conditions remains out of reach, it is possible to speculate on the means by which these changes could have been achieved. At the MIS 5E/5D transition, for instance, I suggest both a large-scale ocean cooling and an increase in the influence of SCW is evident in the profiles. The enhanced cooling of high latitudes consistent with a whole ocean cooling could subsequently promote the expansion of sea ice-cover, which could in turn enhance deep convection of SCW [*H H Hellmer*, 2004; *R Ferrari et al.*, 2014]. Evidence for an increase in sea ice formation around Antarctica during MIS 5D has been observed in several sediment cores [*C Bianchi and R Gersonde*, 2002]. The observed reduction in CO_2 at the MIS5E/5D transition [*J-R Petit et al.*, 1999] could then be explained by some combination of whole-ocean cooling and the expansion of sea ice.

An alternative explanation for the observed $\delta^{18}O$ profile changes across the MIS 5E/5D transition is that a reduction in Northern Hemisphere summertime insolation cooled NCW, which likely in turn would have altered the manner of production of SCW. Several studies have suggested that cooling NCW would have a knock-on effect of

creating saltier SCW by reducing the amount of 'pre-freshening' of SCW occurring around the Weddell Sea [*M Miller et al.*, 2012; *J F Adkins*, 2013]. This would in turn cause the boundary between NCW and SCW to shoal and to sharpen, as the boundary between the water masses moves upward, away from the rough topography at mid-ocean ridges. This mechanism could also explain a portion of the large changes in sea level implied by the paired Mg/Ca and $\delta^{18}O$ profiles for the MIS 5E/5D transition, as saltier SCW from a reduction in 'pre-freshening' would result in an overestimate of the MIS 5D sea level change.

In contrast to the MIS 5E/5D transition, the MIS 5A/4 transition shows cooling mainly localized at mid-depths in the profile. However, this cooling also is compatible with the mechanism proposed in the preceding paragraph; the observed cooler NCW would create saltier SCW, forcing the boundary between the water masses to shoal. There is in fact evidence for the sharpening of the gradient in the structure of the Mg/Ca profile across this transition, as would be implied by the shift of the water mass boundary away from rough topography and by the increase in density contrast between the two water masses. The lack of a similar sharp transition in $\delta^{18}O$ could be due to some combination of the enhanced salinity and higher $\delta^{18}O$ signature of SCW compensating for the enhanced cooling of NCW shallower in the profile. The increase in stratification of the deep ocean at this transition would then provide a mechanism for the nearly 40 p.p.m.v. decrease in pCO_2 that is commonly observed in ice cores over this transition.

2.5 Conclusion

The problems associated with Mg/Ca paleothermometry for *C. wuellerstorfi* preclude its use in divining absolute changes in sea level or temperature over the last glacial/interglacial cycle. However, the temperature dependence of Mg/Ca measurements can be paired with observations of $\delta^{18}O$ in the vertical to understand the timing of changes in the structure of the deep ocean. By doing so I observe that a large whole ocean cooling event occurred at the MIS 5E/5D boundary, and was accompanied by an increase in the relative proportion of SCW present below 3000 meters in the Southeastern Atlantic. Furthermore, the vertical profiles show that across the 5A/4 boundary the ocean cooled at mid-depths, and potentially grew saltier in the deep ocean. This change is consistent with mechanisms proposed by Adkins [2013] that would increase stratification in the deep ocean, trapping CO_2 and potentially creating the ~40 p.p.m.v. reduction of CO_2 observed in ice cores. Further work is needed, particularly from shallower cores in the same collection, to establish the vertical structure of the proxies examined above in intermediate waters.

Chapter 2, in part, will be submitted for publication Paleoceanography. Foreman, A.D., Charles, C.D., Rae, J. W., Adkins, J.F., and Slowey, N. C. The dissertation author was the primary investigator and author of this paper.

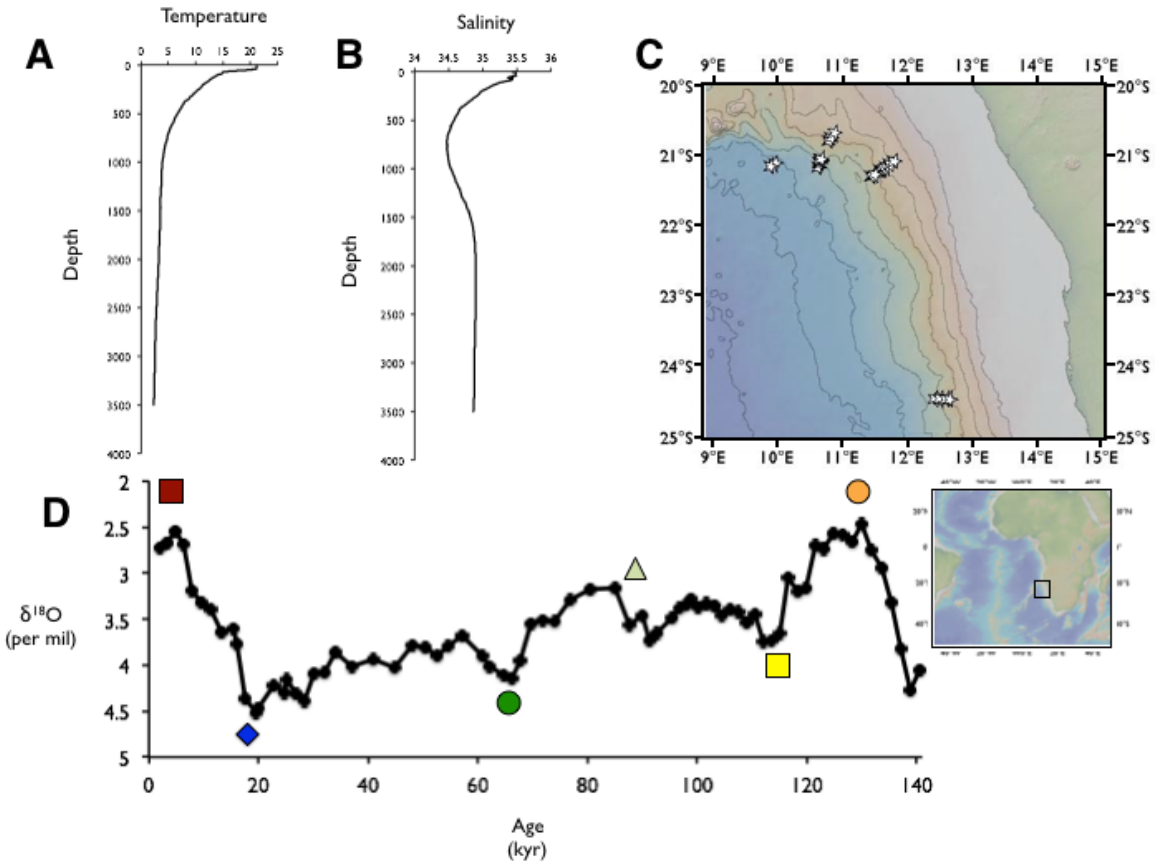

Figure 2.1 (A) Temperature and (B) Salinity profiles measured at 21°S and 10°E, near (C) the collection area for the cores. (D) The stratigraphy for core MV09-PC21 and the resulting color labeled Marine Isotope Stages are standard across each of the profiles: MIS 5E (Orange), 5D (Yellow), 5A/5B (Light Green), 4 (Dark Green), 2 (Blue), and 1 (Red).

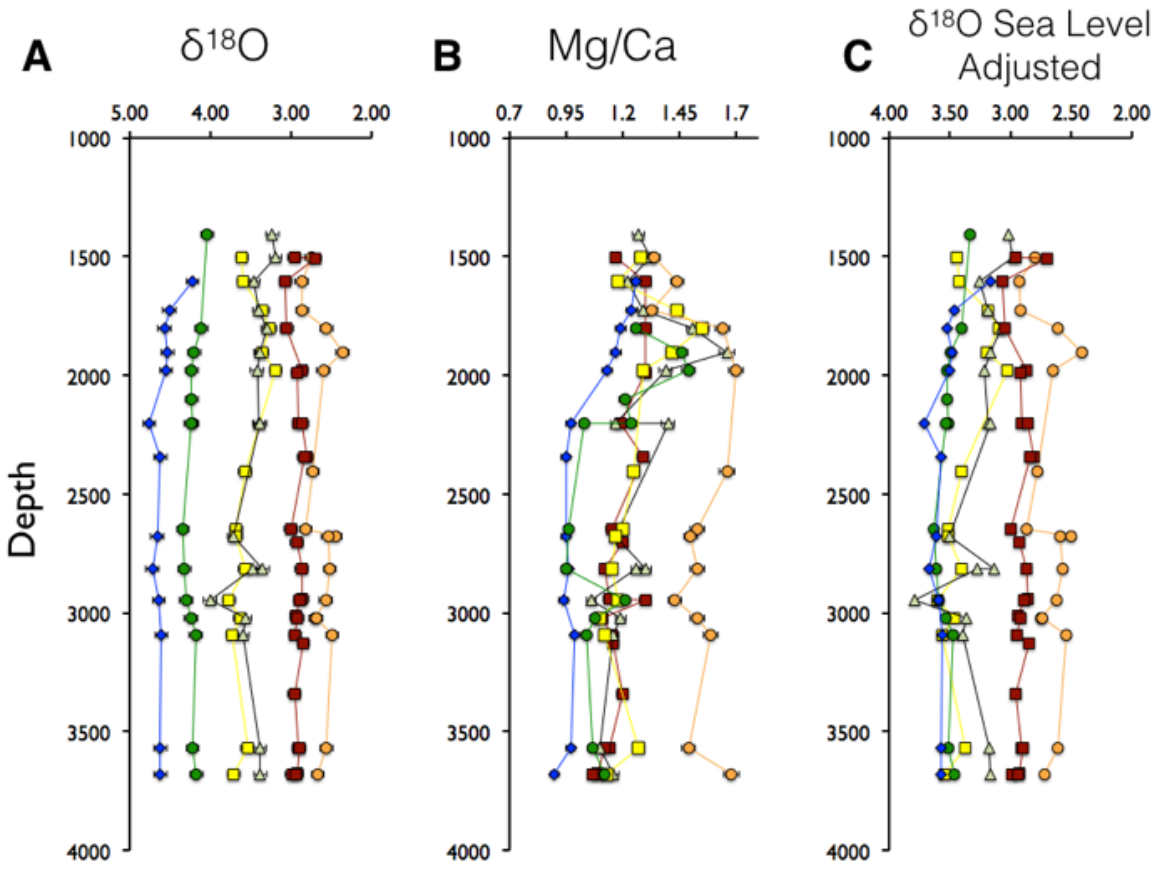

Figure 2.2 (A) $\delta^{18}O$ and (B) Mg/Ca profiles for the six Marine Isotope Stages: MIS 5E (Orange), 5D (Yellow), 5A (Light Green), 4 (Dark Green), 2 (Blue), and 1 (Red) The $\delta^{18}O$ values were corrected using porewater $\delta^{18}O$ /Sea level relationships and the Cutler (2003) sea level values to provide (C) 'Sea Level Corrected' value for $\delta^{18}O$.

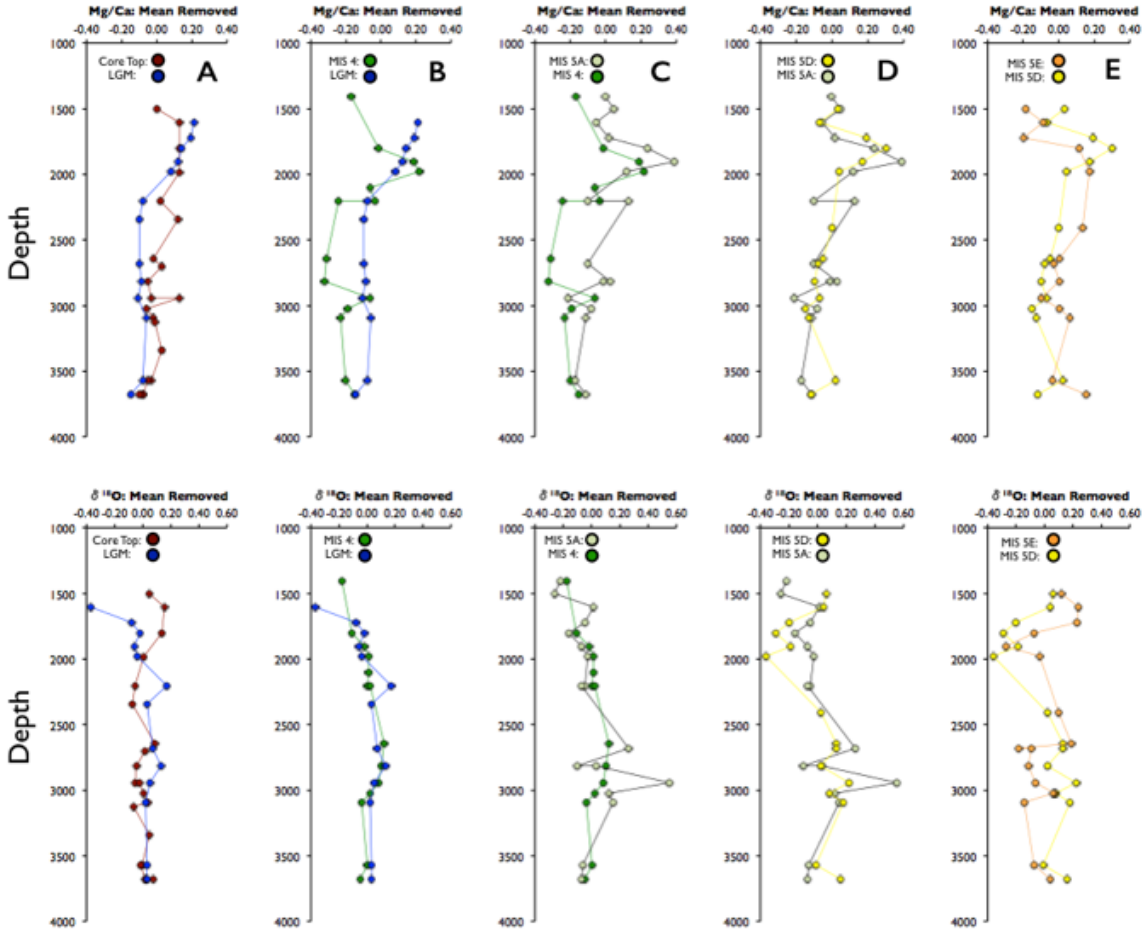

Figure 2.3 Comparison of the structure of the water column for Mg/Ca (Top) and $\delta^{18}O$ (Bottom) between various Marine Isotope Stages: (A) Core Top (Red)/LGM (Blue), (B) MIS 4 (Dark Green)/LGM (Blue), (C) MIS 5A (Light Green)/4 (Dark Green), (D) MIS 5D (Yellow)/5A (Light Green), and (E) MIS 5E (Orange)/5D (Yellow). Mean values of Mg/Ca and $\delta^{18}O$ were subtracted from every data point, and the remainder plotted against depth. Evidence from Mg/Ca in (C, top panel) suggests that there were large changes in the mid-depth structure in temperature across the MIS 5E/5D and MIS 5A/4 boundaries.

2.6 References

Adkins, J. F. (2013), The role of deep ocean circulation in setting glacial climates, *Paleoceanography*, *28*(3), 539-561.

Adkins, J. F., K. McIntyre, and D. P. Schrag (2002), The salinity, temperature, and δ18O of the glacial deep ocean, *Science*, *298*(5599), 1769-1773.

Barker, S., M. Greaves, and H. Elderfield (2003), A study of cleaning procedures used for foraminiferal Mg/Ca paleothermometry, *Geochemistry, Geophysics, Geosystems*, *4*(9).

Barker, S., I. Cacho, H. Benway, and K. Tachikawa (2005), Planktonic foraminiferal Mg/Ca as a proxy for past oceanic temperatures: a methodological overview and data compilation for the Last Glacial Maximum, *Quaternary Science Reviews*, *24*(7), 821-834.

Bianchi, C., and R. Gersonde (2002), The Southern Ocean surface between Marine Isotope Stages 6 and 5d: Shape and timing of climate changes, *Palaeogeography, Palaeoclimatology, Palaeoecology*, *187*(1), 151-177.

Bryan, S. P., and T. M. Marchitto (2008), Mg/Ca–temperature proxy in benthic foraminifera: New calibrations from the Florida Straits and a hypothesis regarding Mg/Li, *Paleoceanography*, *23*(2).

Chappell, J., and N. J. Shackleton (1986), Oxygen isotopes and sea level, *Nature*, *324*(6093), 137-140.

Craig, H., and L. I. Gordon (1965), Deuterium and oxygen 18 variations in the ocean and the marine atmosphere.

Curry, W. B., and D. W. Oppo (2005), Glacial water mass geometry and the distribution of δ13C of ΣCO2 in the western Atlantic Ocean, *Paleoceanography*, *20*(1).

Cutler, K., R. Edwards, F. Taylor, H. Cheng, J. Adkins, C. Gallup, P. Cutler, G. Burr, and A. Bloom (2003), Rapid sea-level fall and deep-ocean temperature change since the last interglacial period, *Earth and Planetary Science Letters*, *206*(3), 253-271.

Duplessy, J., D. Roche, and M. Kageyama (2007), The deep ocean during the last interglacial period, *Science*, *316*(5821), 89-91.

Duplessy, J.-C., and N. J. Shackleton (1985), Response of global deep-water circulation to Earth's climatic change 135,000-107,000 years ago, *Nature*, *316*, 500-507.

Dutton, A., and K. Lambeck (2012), Ice volume and sea level during the last interglacial, *Science*, *337*(6091), 216-219.

Elderfield, H., M. Cooper, and G. Ganssen (2000), Sr/Ca in multiple species of planktonic foraminifera: Implications for reconstructions of seawater Sr/Ca, *Geochemistry, Geophysics, Geosystems*, *1*(11).

Elderfield, H., J. Yu, P. Anand, T. Kiefer, and B. Nyland (2006), Calibrations for benthic foraminiferal Mg/Ca paleothermometry and the carbonate ion hypothesis, *Earth and Planetary Science Letters*, *250*(3), 633-649.

Evans, H., I. R. Hall, G. Bianchi, and D. W. Oppo (2007), Intermediate water links to Deep Western Boundary Current variability in the subtropical NW Atlantic during marine isotope stages 5 and 4, *Paleoceanography*, *22*(3).

Fairbanks, R. G. (1989), A 17,000-year glacio-eustatic sea level record: influence of glacial melting rates on the Younger Dryas event and deep-ocean circulation, *Nature*, *342*(6250), 637-642.

Ferrari, R., M. F. Jansen, J. F. Adkins, A. Burke, A. L. Stewart, and A. F. Thompson (2014), Antarctic sea ice control on ocean circulation in present and glacial climates, *Proceedings of the National Academy of Sciences*, *111*(24), 8753-8758.

Foster, G. (2008), Seawater pH, pCO 2 and [CO 2− 3] variations in the Caribbean Sea over the last 130 kyr: a boron isotope and B/Ca study of planktic foraminifera, *Earth and Planetary Science Letters*, *271*(1), 254-266.

Govin, A., E. Michel, L. Labeyrie, C. Waelbroeck, F. Dewilde, and E. Jansen (2009), Evidence for northward expansion of Antarctic Bottom Water mass in the Southern Ocean during the last glacial inception, *Paleoceanography*, *24*(1).

Headley, M. A. (2008), Krypton and xenon in air trapped in polar ice cores: Paleo-atmospheric measurements for estimating past mean ocean temperature and summer snowmelt frequency, Ph.D thesis.

Hellmer, H. H. (2004), Impact of Antarctic ice shelf basal melting on sea ice and deep ocean properties, *Geophysical Research Letters*, *31*(10).

Herguera, J., E. Jansen, and W. Berger (1992), Evidence for a bathyal front at 2000-M depth in the glacial Pacific, based on a depth transect on Ontong Java Plateau, *Paleoceanography*, *7*(3), 273-288.

Kallel, N., L. D. Labeyrie, A. Juillet-Leclerc, and J.-C. Duplessy (1988), A deep hydrological front between intermediate and deep-wafpr, masses in the glacial Indian Ocean, *Nature*, *333*(6174), 651-655.

Labeyrie, L., C. Waelbroeck, E. Cortijo, E. Michel, and J.-C. Duplessy (2005), Changes in deep water hydrology during the Last Deglaciation, *Comptes Rendus Geoscience*, *337*(10), 919-927.

Lea, D. W., T. A. Mashiotta, and H. J. Spero (1999), Controls on magnesium and strontium uptake in planktonic foraminifera determined by live culturing, *Geochimica et Cosmochimica Acta*, *63*(16), 2369-2379.

Lea, D. W., D. K. Pak, and H. J. Spero (2000), Climate impact of late Quaternary equatorial Pacific sea surface temperature variations, *Science*, *289*(5485), 1719-1724.

Lear, C. H., Y. Rosenthal, and N. Slowey (2002), Benthic foraminiferal Mg/Ca-paleothermometry: A revised core-top calibration, *Geochimica et Cosmochimica Acta*, *66*(19), 3375-3387.

Lisiecki, L. E., and M. E. Raymo (2005), A Pliocene-Pleistocene stack of 57 globally distributed benthic δ18O records, *Paleoceanography*, *20*(1).

Lynch-Stieglitz, J., J. F. Adkins, W. B. Curry, T. Dokken, I. R. Hall, J. C. Herguera, J. J.-M. Hirschi, E. V. Ivanova, C. Kissel, and O. Marchal (2007), Atlantic meridional

overturning circulation during the Last Glacial Maximum, *science*, *316*(5821), 66-69.

Martin, P. A., D. W. Lea, Y. Rosenthal, N. J. Shackleton, M. Sarnthein, and T. Papenfuss (2002), Quaternary deep sea temperature histories derived from benthic foraminiferal Mg/Ca, *Earth and Planetary Science Letters*, *198*(1), 193-209.

Martínez-Méndez, G., R. Zahn, I. R. Hall, L. D. Pena, and I. Cacho (2008), 345,000-year-long multi-proxy records off South Africa document variable contributions of Northern versus Southern Component Water to the Deep South Atlantic, *Earth and Planetary Science Letters*, *267*(1), 309-321.

Miller, M., J. Adkins, D. Menemenlis, and M. Schodlok (2012), The role of ocean cooling in setting glacial southern source bottom water salinity, *Paleoceanography*, *27*(3).

Molyneux, E. G., I. R. Hall, R. Zahn, and P. Diz (2007), Deep water variability on the southern Agulhas Plateau: Interhemispheric links over the past 170 ka, *Paleoceanography*, *22*(4).

Ninnemann, U. S., and C. D. Charles (2002), Changes in the mode of Southern Ocean circulation over the last glacial cycle revealed by foraminiferal stable isotopic variability, *Earth and Planetary Science Letters*, *201*(2), 383-396.

Petit, J.-R., J. Jouzel, D. Raynaud, N. I. Barkov, J.-M. Barnola, I. Basile, M. Bender, J. Chappellaz, M. Davis, and G. Delaygue (1999), Climate and atmospheric history of the past 420,000 years from the Vostok ice core, Antarctica, *Nature*, *399*(6735), 429-436.

Rae, J. W., G. L. Foster, D. N. Schmidt, and T. Elliott (2011), Boron isotopes and B/Ca in benthic foraminifera: Proxies for the deep ocean carbonate system, *Earth and Planetary Science Letters*, *302*(3), 403-413.

Schlitzer, R. (2000), Electronic atlas of WOCE hydrographic and tracer data now available, *Eos, Transactions American Geophysical Union*, *81*(5), 45-45.

Schrag, D. P., J. F. Adkins, K. McIntyre, J. L. Alexander, D. A. Hodell, C. D. Charles, and J. F. McManus (2002), The oxygen isotopic composition of seawater during the Last Glacial Maximum, *Quaternary Science Reviews*, *21*(1), 331-342.

Skinner, L., and N. Shackleton (2005), An Atlantic lead over Pacific deep-water change across Termination I: implications for the application of the marine isotope stage stratigraphy, *Quaternary Science Reviews*, *24*(5), 571-580.

Thornalley, D. J., S. Barker, J. Becker, I. R. Hall, and G. Knorr (2013), Abrupt changes in deep Atlantic circulation during the transition to full glacial conditions, *Paleoceanography*, *28*(2), 253-262.

Toggweiler, J. (1999), Variation of atmospheric CO2 by ventilation of the ocean's deepest water, *Paleoceanography*, *14*(5), 571-588.

Toggweiler, J., and B. Samuels (1995), Effect of sea ice on the salinity of Antarctic bottom waters, *Journal of Physical Oceanography*, *25*(9), 1980-1997.

Waelbroeck, C., N. Frank, J. Jouzel, F. Parrenin, V. Masson-Delmotte, and D. Genty (2008), Transferring radiometric dating of the last interglacial sea level high stand to marine and ice core records, *Earth and Planetary Science Letters*, *265*(1), 183-194.

Waelbroeck, C., L. Skinner, L. Labeyrie, J. C. Duplessy, E. Michel, N. Vazquez Riveiros, J. M. Gherardi, and F. Dewilde (2011), The timing of deglacial circulation changes in the Atlantic, *Paleoceanography*, *26*(3).

Weiss, R., H. Östlund, and H. Craig (1979), Geochemical studies of the Weddell Sea, *Deep Sea Research Part A. Oceanographic Research Papers*, *26*(10), 1093-1120.

Wit, J. C., L. De Nooijer, M. Wolthers, and G.-J. Reichart (2013), A novel salinity proxy based on Na incorporation into foraminiferal calcite, *Biogeosciences*, *10*(10), 6375-6387.

Yu, J., and H. Elderfield (2008), Mg/Ca in the benthic foraminifera Cibicidoides wuellerstorfi and Cibicidoides mundulus: Temperature versus carbonate ion saturation, *Earth and Planetary Science Letters*, *276*(1), 129-139.

Chapter 3. Co-evolution of conservative and non-conservative tracers over the last glacial/interglacial cycle: implications for remineralization, air-sea gas exchange, and carbon storage

Abstract

Conservative tracers suggest the development of deep ocean conditions during cold episodes that were stratified by salt, as opposed to temperature. Yet the consequences of such a change in stratification for the cycling of carbon and nutrients remains to be established. One avenue to address this problem is the parallel development of multiple conservative and nonconservative tracer observations from a single set of samples. Here I have made co-occurring measurements of 7 different non-conservative tracers ($\delta^{13}C$, U/Ca, Mn/Ca, Nd/Ca, B/Ca, Sr/Ca, and Na/Ca) in tandem with measurements of the conservative tracer $\delta^{18}O$. These observations provide a way to infer the relative significance of remineralization, air-sea gas exchange, and other nonconservative properties. Taken together, the vertical profile measurements are all consistent with the phenomenon of nutrient deepening in the South Atlantic during the cold episodes of the full glacial cycle. I finish the chapter by speculating about the controls governing the less well-characterized proxies, in particular Na/Ca and Sr/Ca, which are highly correlated and potentially related to carbonate ion concentrations.

3.1 Introduction

Understanding the relationship between ocean circulation and glacial/interglacial cycles has long been a topic of considerable interest to the paleoceanographic community. In the modern Atlantic Ocean, surface and intermediate waters lose buoyancy in the North Atlantic and flow south as North Atlantic Deep Water (NADW). This southward-flowing water extends to 40°S and is bracketed in the Southern Hemisphere above and below by Antarctic Intermediate Water (AAIW) and Antarctic Bottom Water (AABW). During the Last Glacial Maximum (LGM), however, there is considerable evidence from conservative water mass tracers (e.g. $\delta^{18}O$ and $\Delta^{14}C$) that a completely different pattern of circulation existed in which southern-sourced deep water extended northward to 60°N and in which NADW shoaled roughly 2 km [*W B Curry and D W Oppo*, 2005; *J Lynch-Stieglitz et al.*, 2007; *S Barker et al.*, 2009; *L Skinner et al.*, 2010; *D Lund et al.*, 2011; *A Burke and L F Robinson*, 2012]. Other lines of evidence reinforce the idea that the deep ocean experienced dramatically different conditions at the LGM, most notably that the deep ocean was both saltier and near to freezing [*J F Adkins et al.*, 2002; *D P Schrag et al.*, 2002].

This altered density structure of the deep ocean at the LGM should be evident in measurements of non-conservative tracers sensitive to changes in both circulation and nutrient distribution. Many studies have shown this to be the case, most notably in records of benthic $\delta^{13}C$ from the deep ocean, which are commonly interpreted as reflecting both the shoaling of the boundary between northern- and southern-sourced water masses and a related transfer of carbon to the deep ocean [*W B Curry et al.*, 1988; *J*

Duplessy et al., 1988; *N Kallel et al.*, 1988; *J Herguera et al.*, 1992; *M Sarnthein et al.*, 1994; *L D Keigwin*, 1998; *U S Ninnemann and C D Charles*, 2002; *W B Curry and D W Oppo*, 2005].

Efforts to further constrain circulation using $\delta^{13}C$ have been hampered by the fact that the distribution of $\delta^{13}C$ can be altered significantly by remineralization of sinking biogenic particles and by air-sea gas exchange, which can both alter the apparent strength of changes in circulation or mixing (Figure 3.1). Other tracers, especially trace element proxies, suffer from similar non-conservative effects due to particle scavenging and subsequent redistribution. As a result, the uncertainty of the magnitude of tracer redistribution from remineralization relative to advection and vertical mixing has strongly limited the observations that can be made regarding the evolution of the circulation glacial deep ocean. Equally problematic, the lack of knowledge regarding the magnitude of tracer redistribution from remineralization limits the ability of these proxies to be simulated during ice ages, hindering the development of realistic ocean carbon cycle models for glacial/interglacial simulations.

One way to address this problem is by comparing the evolution of conservative and non-conservative tracers measured from the same set of samples in a depth transect. By doing so, it is possible to disentangle the relative influence of particle flux and other non-conservative effects on the distribution of commonly used paleoproxies. Of the suite of conservative paleoceanographic tracers, the stable oxygen isotopic ratio ($\delta^{18}O$) of benthic foraminiferal calcite is most suited for this task over a full glacial/interglacial

cycle, as it is the product of the temperature and $\delta^{18}O$ of seawater (which is directly related to salinity), and hence, density.

Here I present paired observations for 7 different non-conservative tracers ($\delta^{13}C$, U/Ca, Mn/Ca, Nd/Ca, B/Ca, Sr/Ca, and Na/Ca) at 6 different time points throughout the evolution of the last glacial/interglacial cycle. These measurements were made using multiple cores from a tightly constrained geographical area, and together make up vertical profiles that comprise depths spanning between 1500-3600 meters along the Southeastern Atlantic margin.

I derive a pair of key observations from these vertical profiles. First, the data for these profiles were collected in tandem with $\delta^{18}O$ measurements from the same set of samples (presented in Chapter 2), and allow for an explicit comparison of the behavior of conservative and nonconservative tracers over a full glacial cycle, which in turn provides a means to discern the influence of proxy redistribution via particle transport. The close geographical distribution of these cores provides an ideal control for this comparison, as it means the cores were likely exposed to nearly identical conditions of particle rain. Second, these profiles allow for the inference of the likely primary influences on less well-documented proxies (e.g. Nd/Ca, Na/Ca, and Sr/Ca) by comparing their behavior with more well-characterized proxies (e.g. $\delta^{13}C$ and B/Ca). In doing so it is possible to gain insight into proxy systematics that has implications for future reconstructions of variables sensitive to carbon cycling.

3.2 Proxy Systematics

It has long been recognized that benthic foraminiferal tests bear the imprint of the deep-water chemistry in which they calcify, and many proxies have been developed which provide constraints on changes in deep-water chemical and physical characteristics by measuring the chemical composition of these tests. To understand the implications of these proxies as they change over the glacial cycle, however, it is necessary to understand the various non-conservative controls on the tracers being used. Below I briefly summarize the known controls on the proxies developed in this chapter.

3.2.1 U/Ca

Uranium (U) behaves conservatively in oxygenated seawater as a soluble uranium U (VI) carbonate complex with a relatively long (>400 kyr) residence time [*G Klinkhammer and M Palmer*, 1991; *R Dunk et al.*, 2002]. Under suboxic conditions, soluble U(VI) is reduced to insoluble U(IV) and is removed via precipitation in sediment porewaters. U added to sediment in this manner is referred to as authigenic uranium, and is limited by the depth of penetration of the redox boundary in the sediment. This redox boundary is governed by bottom water oxygen concentrations and by the amount of organic carbon being delivered to the sediment, making authigenic uranium a powerful tool for investigating changes in bottom water oxygenation and organic matter accumulation [*N Kumar et al.*, 1995; *Y Rosenthal et al.*, 1995; *Z Chase et al.*, 2001; *J McManus et al.*, 2005; *A Martínez‐Garcia et al.*, 2009; *S L Jaccard et al.*, 2016].

Several studies have shown that foraminiferal tests buried under reducing conditions accumulate secondary U coatings from the sediment [*G M Henderson and R K O'nions*, 1995; *D W Lea et al.*, 2005], and that concentration of U in these coatings

eclipses lattice-bound U concentrations by a factor of ~20 [*M L Delaney and E A Boyle*, 1983; *A D Russell et al.*, 1994; *J Yu et al.*, 2008; *M Raitzsch et al.*, 2011]. Building on this observation, recent research by Boiteau et al [2012] has shown that the U/Ca mmol/mol concentrations of these coatings are highly correlated with bulk authigenic U, and that changes in these concentrations can be attributed to changes in authigenic uranium accumulation. As such, measurements of U/Ca in foraminifera appear to provide a means of evaluating sedimentary redox conditions during periods of variable bottom water conditions.

3.2.2 Mn/Ca

Similar to uranium, the concentration of manganese (Mn) in sediments is governed by redox control of its speciation. Unlike U, however, Mn accumulates in sediments under oxygenated environments and is not accumulated under reducing conditions. This occurs because Mn (III) and Mn (IV) form relatively insoluble oxyhydroxides in the presence of oxygen, while the reduced phase, Mn(II), is much more soluble [*S Calvert and T Pedersen*, 1996]. An increase/decrease in accumulation of Mn in bulk sediments during periods of high/low deep water oxygenation has been observed by several studies [*B P Finney et al.*, 1988; *D J Burdige*, 1993; *A Mangini et al.*, 2001; *S L Jaccard et al.*, 2016]. Concentrations of Mn measured from the Mn-oxide coatings of foraminiferal tests follow the same pattern [*R Boiteau et al.*, 2012], and can be used in combination with U/Ca to investigate changes in sedimentary redox state.

3.2.3 B/Ca

Boron (B) incorporation by benthic foraminifera has been empirically linked to the degree of carbonate ion saturation of the water in which the organisms are calcifying by several core-top studies [*J Yu and H Elderfield*, 2007; *J Yu et al.*, 2010; *J W Rae et al.*, 2011]. The reasons for the link between B and carbonate ion saturation state are not well understood, and further research remains to eliminate the possibility that B/Ca measurements may be more sensitive to changes in carbonate ion at lower degrees of carbonate ion saturation.

3.2.4 Sr/Ca

Considerations of the effect of sea level and the characteristics of shallow water carbonate deposition suggest that there should be a significant change in seawater Sr/Ca over an ice age cycle [*H M Stoll and D P Schrag*, 1998; *H M Stoll et al.*, 1999]. Actual benthic foraminiferal strontium (Sr) concentration data tend to show significantly more variability over glacial/interglacial cycles than expected from the sea level/carbonate connection alone [*H M Stoll et al.*, 1999; *H Elderfield et al.*, 2000; *D Hodell et al.*, 2001]. A number of reasons have been put forward to explain this difference, including secondary influences on foraminiferal Sr/Ca from temperature, salinity, pH, dissolution, and shell size [*J Yu et al.*, 2014]. Recently, Yu et al. [2014] were able to test the influence of these factors on benthic Sr/Ca by comparing core top measurements of benthic Sr/Ca to the overlying deep water. The Sr/Ca measurements for these core tops do not show a correlation with temperature, salinity, pH, or post-mortal dissolution. Instead, they demonstrate a strong correlation between Sr/Ca concentration and deep-water carbonate ion saturation. Down-core measurements of Sr/Ca from the same study show a strong

correlation with co-occurring measurements of B/Ca, further supporting the notion that carbonate ion saturation is strongly influencing foraminiferal Sr/Ca. If true, this might explain the strong correlation observed between foraminiferal Sr/Ca and deep South Atlantic % $CaCO_3$ [*D Hodell et al.*, 2001].

3.2.5 Nd/Ca

Dissolved neodymium (Nd) concentrations in the oceans generally show a linear increase with depth. This has commonly been explained as a result of reversible scavenging, in which Nd is adsorbed onto particles before being released due to particle dissolution/remineralization [*M Siddall et al.*, 2008]. Though there has been considerable effort to document Nd isotopic composition over the Pleistocene ice ages as a means for understanding water mass mixing in the deep ocean [*R L Rutberg et al.*, 2000; *A M Piotrowski et al.*, 2008; *L D Pena and S L Goldstein*, 2014], little research exists on how foraminifera acquire a Nd/Ca signal. Evidence suggests that planktonic foraminifera record the Nd concentrations of their position in the water column [*M Martínez-Boti et al.*, 2009]. It therefore seems plausible that benthic Nd/Ca signals reflect the Nd/Ca concentrations of the overlying bottom water.

3.3 Methods

The cores presented here were collected aboard the R/V Melville in March 2003. All but 3 of the cores were collected along two depth transects within an area defined by 19° 43.3′S and 21° 33.1′S and 9° 54.1′E and 12° 48.1′E, and range in depth from 1405 to 3678 meters. The remaining cores were taken further south along a transect at 24° 28.0′S, 12° 26.0′E and range in depth from 2200 to 2600 m.

The stratigraphy for the cores used in the vertical profiles presented in this chapter is discussed in significantly greater detail in Chapter 1. Briefly, measurements for core top profiles were collected within the top 3 centimeters of each of the cores. A combination of radiocarbon measurements and downcore XRF elemental ratio measurements were used to develop a common tie point for the close of the Last Glacial Maximum (LGM). For older vertical profiles where radiocarbon cannot provide an age constraint, the benthic $\delta^{18}O$ record of MV09-PC21 (2680m depth) was tied to the LR04 stack [*L E Lisiecki and M E Raymo*, 2005] to develop a chronology for core MV09-PC21. Down core measurements of various elemental ratios (Fe/Ca and Si/Ti) for each of the other cores in the collection were then tied to the MV09-PC21 record between Marine Isotope Stage (MIS) 5E and the LGM. This approach led to good agreement between several different, semi-independent variables in down-core records (see Chapter 1). I was able to collect vertical profiles for marine isotope stages 5E, 5D, 4, 2 (LGM), and 1 (Core Tops) (Figure 3.2). I collected a sixth profile that fell on the transition between MIS 5B and 5A, but which presented a clear stratigraphic target from the XRF data.

Analysis of trace elemental ratios followed Rae et al [2011], which combined the techniques used by Foster [2008] with oxidative cleaning methods developed by Barker et al [2003]. *Cibicidoides wuellerstorfi* specimens >200μm were selected for a single morphotype (according to guidelines established by Rae et al. [2011]), before being crushed between clean glass slides and transferred to acid-cleaned centrifuge tubes. The samples were subjected to repeated ultrasonication and rinses with MilliQ >18.2 MΩ-cm water to remove clays. The samples were then treated with a 1% hydrogen peroxide

solution buffered with 0.1M ammonium hydroxide at 70°C to oxidize organic matter. Following oxidation, samples were treated with a weak acid leach (0.0005M nitric acid) for 30 seconds to remove any adsorbed contaminants, and then dissolved in 250µl of 0.075 M nitric acid. No reductive cleaning step was used, as reductive cleaning has been shown to alter the Mg/Ca ratio in cleaned biogenic carbonate [*S Barker et al.*, 2003; *J Yu and H Elderfield*, 2008]. Samples were centrifuged immediately after dissolution, and transferred to Teflon vials for storage, leaving a residual (~10µl) amount in the centrifuge tube to exclude any remaining dissolved contaminants. All nitric acid used in these procedures was trace metal clean (SEASTAR brand, ultra pure), and work was carried out in a dedicated flow hood within an over-pressured clean lab using water generated by a boron-free MilliQ package. Aliquots of the dissolved samples were analyzed for trace elements (Li, B, Na, Mg, Al, Ca, Mn, Sr, Cd, Ba, Nd, U) on an Agilent ICP-MS, matching sample and standard concentration at 1 mmol/l.

There is a strong linear correlation in the measurements of Na/Ca and Sr/Ca for each of the depth profiles. 4 points fell well off of the linear relationship between these elements, presumably due to contamination, and are not shown here. Measurements with significantly elevated values of Al/Ca were also excluded from these figures.

3.4 Results

In this section I present co-occurring measurements of $\delta^{13}C$, Nd/Ca, U/Ca, Mn/Ca, B/Ca, Sr/Ca, Na/Ca, for 6 vertical profiles (MIS 5E, MIS 5D, MIS 5A, MIS 4, LGM, and core tops) across the evolution of the glacial interglacial cycle. Measurements of $\delta^{13}C$ for these time slices show an enhanced gradient in $\delta^{13}C$ between the mid-depth

and deep ocean over the course of the glacial cycle, with large changes in this gradient occurring over the MIS 5E/5D and MIS 5A/4 transitions. The gradient in $\delta^{13}C$ is at a maximum during MIS 4, and remains in place through the LGM (Figure 3.4). Modern core top $\delta^{13}C$ shows a significantly reduced gradient in $\delta^{13}C$ compared to the LGM and reflects the properties of the major water masses that bathe the collection area (Figure 3.3). The modern vertical distribution of variables related to the proxies presented in this chapter (e.g. carbonate ion undersaturation and B/Ca or oxygen concentrations and U/Ca) are also presented in Figure 3.3.

The changes in the absolute strength of the vertical gradient of Nd/Ca are close to those of $\delta^{13}C$ during the buildup of glacial conditions (Figure 3.4). Nd/Ca concentrations for MIS 5E, MIS 5D, MIS 5A, and the core top profiles do not vary strongly in the vertical, while the Nd/Ca gradient is largest during MIS 4 and at the LGM. There is a substantial correlation between $\delta^{13}C$ and Nd/Ca for the vertical profiles, especially during glacial periods (Figure 3.6).

In general, the profile measurements show low concentrations of U/Ca during interglacial periods and high concentrations of U/Ca during glacial periods (Figure 3.4). U/Ca concentrations are very low during MIS 5E and in the core top profile compared with the other time slices. Values of U/Ca are elevated during MIS 5D, especially as compared with MIS 5E. The MIS 4 profile shows the highest U/Ca concentrations of any of the time slices, while concentrations of U/Ca for the LGM roughly mirror those at MIS 5D.

Mn/Ca measurements largely show the opposite behavior compared to that of U/Ca; namely, concentrations of Mn/Ca are elevated during interglacial periods, particularly at depth (Figure 3.4). Mn/Ca values during MIS 5D are slightly reduced in Mn/Ca compared with MIS 5E, with the exception of the two deepest values. Mn/Ca concentrations decrease between MIS 5D and 5A, and again between MIS 5A and 4, before reaching an absolute minimum at the LGM. Core top measurements of Mn/Ca are elevated compared to the LGM vertical profile, but lower than both the MIS 5D and MIS 5E vertical profiles.

In contrast to the $\delta^{13}C$ and Nd/Ca profiles, the B/Ca vertical profiles (Figure 3.5) do not seem to show a change in vertical structure in the buildup to glacial conditions (Figure 3.7). Instead, each profile seems to have roughly the same slope, particularly for MIS 5D, MIS 4, and the LGM. The exception to this observation is the profile for MIS 5E, which is elevated compared to the other profiles below 2500 meters depth.

Measurements of Sr/Ca and Na/Ca are highly correlated (Figure 3.8), and, similar to the co-occurring B/Ca measurements, show a constant slope across the evolution of the glacial profile (Figure 3.5). The measurements making up the MIS 5E profiles of Sr/Ca and Na/Ca also are both elevated below 2500 meters. Interestingly, the shallowest two values of Sr/Ca and Na/Ca the MIS 4 profile are reduced as compared with the cores immediately below them. This may also be the case for B/Ca, although the scatter in the B/Ca profile makes it difficult to be certain.

3.5 Discussion

As discussed below in greater detail and in Chapter 4 of this thesis, the difference in behavior between the vertical profiles of $\delta^{13}C$ and physical water mass tracers is consistent with the idea of nutrient deepening [*E A Boyle*, 1988]. There are, however, multiple ways that this nutrient deepening could come about. The trapping of carbon and nutrients at depth could either arise through a change in the strength or geometry of overturning circulation, or through an enhancement of the biological pump and a change in export production, or through some combination of the two. By developing multiple tracers from the same set of samples that are controlled by different non-conservative processes, I show below that it is possible to make inferences regarding both the mechanisms of how nutrient deepening may have come about, and about the controls on other less well-studied non-conservative proxies.

The notable changes in the vertical structure of the various sedimentary paleo-proxies across the last glacial cycle are summarized as follows:

1) The vertical gradient in $\delta^{13}C$ builds steadily across the evolution of the glacial cycle, with the strongest gradients observed at MIS 4 and at the LGM.
2) This behavior is mirrored by changes in foraminiferal Nd/Ca, with maximum gradients in the Nd/Ca ratio observed at MIS 4 and the LGM.
3) Foraminiferal U/Ca values are diminished during interglacial periods and elevated during glacial periods, without displaying a significant vertical gradient, although U/Ca values generally appear to be at a minimum in the deepest part of the profiles.

4) Foraminiferal measurements of Mn/Ca behave in the opposite manner of U/Ca, with higher concentrations of Mn/Ca generally appearing during interglacial periods and lower concentrations appearing during glacial periods.
5) Foraminiferal B/Ca measurements, while scattered in the profiles, generally do not show a change in vertical structure across the full glacial/interglacial cycle; the lone exception to this generalization occurred during the MIS 5E/5D transition where the deepest part of the profile suggests decreased boron concentrations, and therefore implies a decrease in carbonate ion concentration between MIS 5E and 5D.
6) Foraminiferal Sr/Ca and Na/Ca appear to be highly correlated and, similar to B/Ca, their vertical gradients do not change much over the course of the ice age cycle.

The observation of the evolution of the $\delta^{13}C$ gradient is interesting in light of the measurements of conservative tracers (i.e. $\delta^{18}O$, Mg/Ca) made on the same set of samples (Chapter 2). The conservative tracers, which should respond only to changes in the density structure of the interior of the ocean, show a stepwise shoaling of the boundary between southern-sourced and northern-sourced water at the MIS 5E/5D and MIS 5A/4 transitions. The LGM vertical profile shows a further shoaling of the southern-source/northern-source boundary to ~2000 meters, and, combined with $\Delta^{14}C$ measurements from the same set of cores, suggests a radiocarbon-rich, warmer water mass overlying a radiocarbon-poor, cooler water mass. This is in line with the existing

observations of the structure of the Western Atlantic at the LGM along the Brazil Margin [*W B Curry and D W Oppo*, 2005].

If the influence of remineralization on the $\delta^{13}C$ profiles was negligible relative to circulatiom, the vertical structure of the $\delta^{13}C$ profiles should reflect those of the $\delta^{18}O$ and Mg/Ca profiles. Instead there are marked differences between the $\delta^{13}C$ and $\delta^{18}O$ profiles over the course of the glacial/interglacial cycle. In particular the $\delta^{13}C$ values continue to decrease with depth below the boundary between water masses suggested by the conservative tracer profiles. This behavior is an expression of the "nutrient deepening" hypothesis proposed by Boyle [1988], which suggests that an increase in the amount of carbon being respired in the deep ocean would prompt an decrease in atmospheric CO_2 due to both the increased volume available for carbon storage and the subsequent increase in alkalinity from $CaCO_3$ dissolution. This issue is discussed in greater detail in Chapter 4 by examining the gradients in $\delta^{13}C$ and $\delta^{18}O$ between mid-depth (MV09-PC21) and deep (MV09-PC23) cores from this core collection.

The parallel development of multiple proxies from the same set of samples provides a starting point from which to evaluate the relative impacts of the various possible influences on the distribution of $\delta^{13}C$ within the vertical profiles. For example, there is a strong correlation between the distribution of Nd/Ca and $\delta^{13}C$, particularly during MIS 4 and at the LGM. Given that dissolved Nd concentrations are thought to be altered by a combination of circulation and reversible scavenging [*M Siddall et al.*, 2008; *T Arsouze et al.*, 2009], this correlation suggests that the influence of organic particle remineralization is the dominant influence on the vertical structure of $\delta^{13}C$, as expected.

It is also significant that the vertical gradient in both $\delta^{13}C$ and Nd/Ca was strongest during MIS 4, and weakened slightly between MIS 4 and the LGM. This may indicate that the difference in atmospheric pCO_2 between these periods ultimately did not strictly follow from an increase in the strength of the soft-tissue pump. It also suggests that the carbon cycle was likely not at steady state during the close of the last ice age, since the strength of the vertical gradient is lowest during MIS 4. Finally, the correlation between Nd/Ca and $\delta^{13}C$ also suggests a connection with local particle flux: the Nd/Ca concentrations, which reflect a local balance of advection and remineralization, have no *a. priori* reason to match the $\delta^{13}C$ gradients if they were set remotely by, for example, iron-fertilized increases in the Subantarctic [*M P Hain et al.*, 2010; *S Jaccard et al.*, 2013]. Instead the similarity in the gradients between Nd/Ca and $\delta^{13}C$ would require either sort of basin-wide change in export production (in order to alter remineralization), or else a change in the local concentrations of dissolved Nd that was synchronous with dust input and export production in the Subantarctic. Of these possibilities, it seems more likely that the increased vertical gradient in Nd/Ca was the product of some combination of more sluggish circulation and increased remineralization at depth.

In any case, the transfer of carbon from the atmosphere to the deep ocean via nutrient deepening implied by the $\delta^{13}C$ profiles should be accompanied by lowered dissolved oxygen (O_2) concentrations [*E A Boyle*, 1988], if the deep ocean grow more stratified and mixing became more sluggish. Given that the concentrations of U in foraminiferal coatings have been shown to reflect bottom water oxygenation [*R Boiteau et al.*, 2012], one would expect the resulting changes in redox conditions to be reflected

in the distribution of U/Ca. This is generally the case in these profiles, as the interglacial/interstadial periods all show relatively low concentrations of U compared to glacial/stadial periods.

In particular, the U/Ca concentrations for MIS 5E and MIS 5A both suggest that the cores experienced redox conditions at these times that were similar to modern. In contrast, the highest concentrations of U/Ca are observed during MIS 4 and the LGM, suggesting a significant change in the redox conditions of the sediment. This is in line with observations of both bulk authigenic and foraminiferal uranium accumulation from the glacial Atlantic [*A Mangini et al.*, 2001; *A Martínez‐Garcia et al.*, 2009; *R Boiteau et al.*, 2012], Pacific [*S L Jaccard et al.*, 2009; *L Bradtmiller et al.*, 2010], Southeastern Arabian [*J Pattan and N J G Pearce*, 2009] and Southern Oceans [*J Gottschalk et al.*, 2016; *S L Jaccard et al.*, 2016]. This observation also fits with locally observed changes in Benguela benthic foraminifera population assemblages, which shift during the cold periods toward taxa that that favor significantly oxygen-depleted environments [*C McKay et al.*, 2016].

Without a record of export production it is difficult to know definitively whether the observed differences between interglacial and glacial periods are from increased rain of organic matter or changes in the overlying bottom water O_2 content. It seems likely that the record of foraminiferal U/Ca (and therefore authigenic U) is being driven by changes in bottom water oxygenation, as the increase in deep ocean Uranium would imply a significant increase in open-ocean productivity during glacial periods, and changes in sedimentation and mass accumulation rate in the deeper cores do not support

this assumption [*K Crabill*, 2017]. At the very least, the evolution of U/Ca concentrations in these measurements is consistent with the hypothesis that the remineralization of DIC was shifted deeper in the water column during glacial periods, as suggested by $\delta^{13}C$ measurements and by previous studies of the deep Pacific Ocean [*S L Jaccard et al.*, 2009; *L Bradtmiller et al.*, 2010].

The decrease in deep ocean oxygen is also supported by a decrease in Mn/Ca at depth over the course of the evolution of glacial conditions. Mn and U generally behave in opposite ways in the deep ocean, because of the formation of Mn oxides in oxygenated conditions [*S Calvert and T Pedersen*, 1996; *S L Jaccard et al.*, 2009; *R Boiteau et al.*, 2012]. The data shown in Figure 3.4 supports the idea that the deep ocean grew progressively less oxygenated following the transition from interglacial to glacial periods.

Interestingly, Mn measurements for the shallower cores are generally low throughout the glacial/interglacial cycle, especially compared with deeper cores. This is likely a result of larger amounts of organic material delivered to the shallower cores throughout the glacial/interglacial cycle, as is currently the case [*Munson, unpublished*]. A larger flux of organic material might produce enough of a reduction in porewater oxygen to prevent the formation of Mn coatings on the foraminifera. In situations where Mn and U are both low in the shallower cores (e.g. interglacial periods), conditions of oxygenation might exist in which the gradient in oxygen in the porewater is low enough to prevent the formation of Mn oxides, but high enough to prevent significant U enrichment. Alternatively it is possible that some diagenetic process is affecting one of the elements but not the other. Given that foraminiferal calcite Mn has begun to be

utilized to normalize U concentrations when reconstructing redox conditions [*J Gottschalk et al.*, 2016], the lack of consistent behavior in shallower cores is significant in that it suggests that Mn as a tracer of deep water oxygen may only be applicable in cores with relatively low amounts of organic rain.

One factor that can be ruled out in both the U and Mn records is post-depositional diagenetic redistribution of these trace metals. Oxidative 'burn down' can occur when precipitated metals are diagenetically dissolved/enriched during renewed exposure to O_2 in porewaters [*J Crusius and J Thomson*, 2000; *A Mangini et al.*, 2001], and the effect is most prominent in sediment columns and sequences characterized by low accumulation rate (<2 cm/kyr). Burn down seems not to have impacted the cores presented here during these time periods [*K Crabill*, 2017], probably because sedimentation rates for these cores generally stay above 5 cm/kyr for the deepest cores and above 8 cm/kyr for the shallower cores.

In addition to altering deep-water oxygen, the transfer of carbon to the deep ocean should have consequences for carbonate ion concentration ($[CO_3^{2-}]$). As proposed by Boyle [1988], the shift of DIC to the deep would initially decrease $[CO_3^{2-}]$ without strongly influencing alkalinity, which would in turn prompt the dissolution of calcium carbonate. Dissolution would continue to occur until carbonate ion concentrations in the deep increased enough to restore the balance between alkalinity input and burial. This process effectively decouples $[CO_3^{2-}]$ and $\delta^{13}C$, as carbonate compensation should have little effect on the $\delta^{13}C$ of DIC in seawater.

As such, the comparison of the profiles of tracers sensitive to carbonate ion concentration (B/Ca, Sr/Ca) with profiles of $\delta^{13}C$ provides further insight to the nutrient deepening that evidently occurred during the cold episodes. B/Ca and Sr/Ca both maintain nearly constant gradients over the course of the glacial evolution, most notably across the MIS 5A/4 transition, and at the LGM, when gradients in $\delta^{13}C$ are at their maximum. Given that the time scale for carbonate ion is ~5-7 kyr [*W S Broecker and T-H Peng*, 1982] and that these profiles were selected to achieve 'quasi-steady state' for each marine isotope stage, it is possible that the lack of change in the B/Ca and Sr/Ca profiles are a result of carbonate compensation associated with nutrient deepening. This inference is consistent with the vertical gradients in $\%CaCO_3$ from the same set of cores, which stay nearly constant for the same time periods observed here [*K Crabill*, 2017].

Interestingly, the Sr/Ca profiles show a strong correlation with Na/Ca profiles of co-occurring samples. The reasons for this correlation are not clear, despite being noted in previous analyses of planktonic foraminifera [*M L Delaney et al.*, 1985]. Little research exists describing the mechanisms by which Na is incorporated into foraminiferal calcite or coatings. It has been hypothesized that Na/Ca concentrations in benthic foraminifera are linked to changes in salinity [*J C Wit et al.*, 2013], though not for the benthic species used here. There is also not a large change in salinity across the depths of the cores used in the core top profile, which would then require Na/Ca to be particularly sensitive to changes in salinity.

There are several other possible variables that might influence Na incorporation in benthic foraminifera, particularly in light of the fact that the Na/Ca measurements

correspond so closely with Sr/Ca. The most obvious of these might be changes in carbonate ion concentration (or some other variable related to the carbon cycle). It is also possible that Na/Ca could be sensitive to pressure, in which case the tight relationship between Sr/Ca and Na/Ca would be in part due to the relationship between pressure and carbonate saturation state, and in part due to the fact that carbonate ion stayed relatively constant for the profiles that I measured.

In any case, the carbonate ion proxy data presented here is an interesting complement to the time series produced by Yu et al., 2016, which suggest that the deepest parts of the South Atlantic experienced a significant drop in carbonate ion between MIS 5A/4. However, Yu et al. [2016] report only small (~10 μmol/mol) changes in B/Ca been observed for the mid-depth core RC13-228 (22°S, 3.2 km) and the deep core RC13-229 (26°S, 4.2 km) for the time periods that correlate with the profiles at MIS 5A/5B and at MIS 4, consistent with the relatively small changes seen in the B/Ca and Sr/Ca profiles. It is likely that, given the profiles presented here for MIS 5A actually represent some point on the transition between MIS 5B/5A, the change in carbonate ion for MIS 5A/4 is greater than I observe, and could align with that reported by Yu et al. [2016]. This consideration would not affect Yu et al.'s main conclusion that there was a decoupling of $\delta^{13}C$ and B/Ca at mid-depths in the Southeastern Atlantic, since this observation is generally borne out in my measurements as well.

It is also worth pointing out that the bulk of the change in the South Atlantic B/Ca observed by Yu et al. [2016] comes from changes in core TN057-21, located in the deepest part of the South Atlantic (41°S, 5km depth). Yu et al. [2016] suggest that the

changes in this core stem from an increased influence of southern-sourced water, and that the boundary between northern-sourced and southern-sourced water shoaled to at least 3000 meters across the MIS 5A/4 boundary, consistent with observations from physical water mass tracers (Chapter 2) for the same cores. Given the $\delta^{13}C$ profiles, however, it seems likely that the B/Ca and Sr/Ca profiles are reflecting a combination of deep ocean circulation change and changes in the strength and depth of remineralization of carbon.

3.6 Conclusion

The profiles of $\delta^{13}C$ over the last glacial cycle described above suggest that more carbon was stored in the deep ocean during the cold episodes of last ice age cycle, as part of a nutrient deepening phenomenon. Three key points emerge from the analysis of co-occurring non-conservative proxy measurements. First, the profiles of Nd/Ca suggest both that the role of remineralization in governing tracer distribution grew significantly during glacial periods. By extension this observation implies that air-sea gas exchange did not significantly impact the distribution of $\delta^{13}C$ in the accompanying profiles. Second, profiles of U/Ca and Mn/Ca both suggest that the deep ocean was characterized by lower concentrations of dissolved oxygen during glacial periods consistent with a stratified (and presumably more sluggish) deep ocean. Finally, decoupling of the tracers sensitive to carbonate ion concentrations (B/Ca, Sr/Ca) from the profiles of $\delta^{13}C$ suggests that process of carbonate compensation resulted in a relatively invariant structure of the carbonate-sensitive tracers across many of the transitions of the ice age cycle. Instead, the only changes in carbonate ion concentrations evident in these profiles were limited to an apparent elevation in deep ocean carbonate ion during the last interglacial period.

An enticing observation from this chapter is that measurements of Na/Ca, which is not a well-characterized proxy, show strong correlation Sr/Ca measurements, perhaps suggesting perhaps that Na/Ca might closely track carbonate ion concentrations. This would be of considerable interest for future work, as Na/Ca is significantly easier to measure than B/Ca, the current tracer most commonly used to infer changes in carbonate ion concentrations. Moreover, this correlation underlines the importance of the parallel development of multiple proxies for the same samples. Future work in this area should focus on the development of multiple tracer fields that can allow for the diagnosis of both particle redistribution and changes in boundary conditions.

Chapter 3, in part, will be submitted for publication Paleoceanography. Foreman, A.D., Charles, C.D., Rae, J. W., Adkins, J.F., and Slowey, N. C. The dissertation author was the primary investigator and author of this paper.

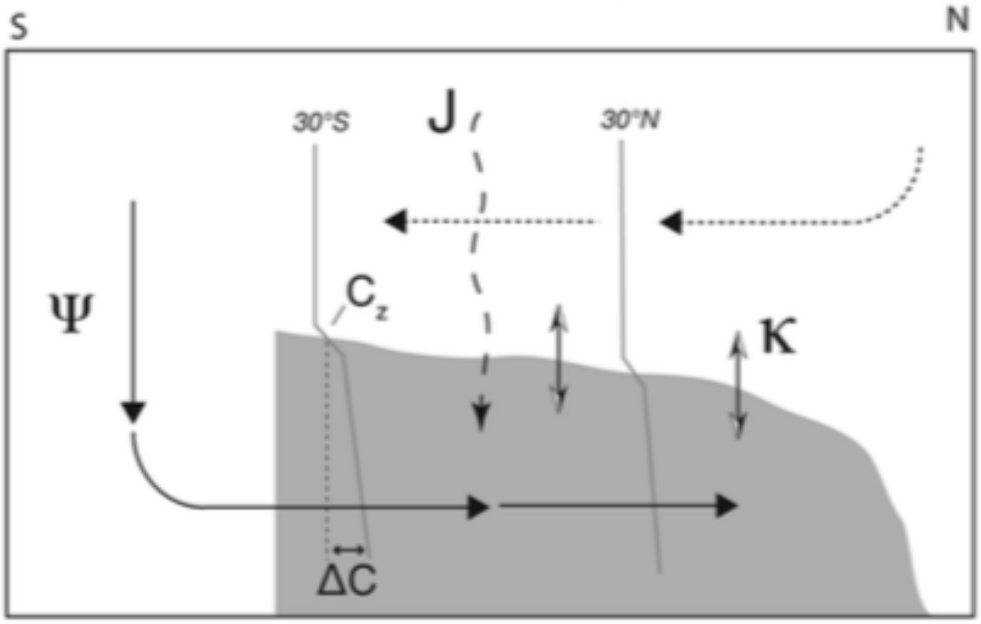

Figure 3.1 Two dimensional representation of the processes involved in transport and mixing in the deep Atlantic taken from Lund et al. [2011]. Conservative tracers such as $\delta^{18}O$ are only affected by transport (ψ) and vertical mixing (κ), which means the balance between these terms would set both the vertical tracer gradient (C_z) and the difference between the tracer surface and the seafloor (ΔC). In contrast, nonconservative tracers (e.g. $\delta^{13}C$) are affected by the additon of non-conservative processes (J) such as remineralization, which would alter the tracer distribution in the vertical.

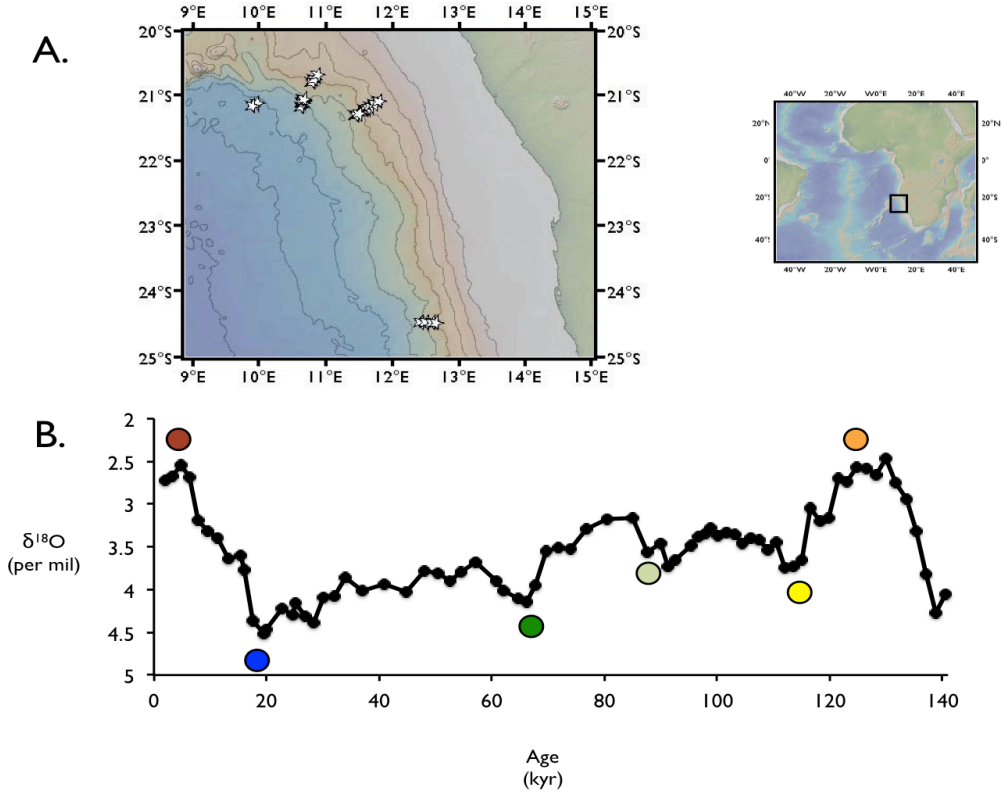

Figure 3.2 (A) Collection area for the set of cores used to develop these profiles and (B) Oxygen isotope stratigraphy for core MV09-PC21. The colored circles in (B) denote the Marine Isotope Stages shown for the vertical profiles in this chapter: MIS 5E (Orange), 5D (Yellow), 5A/5B (Light Green), 4 (Dark Green), 2 (Blue), and 1 (Red).

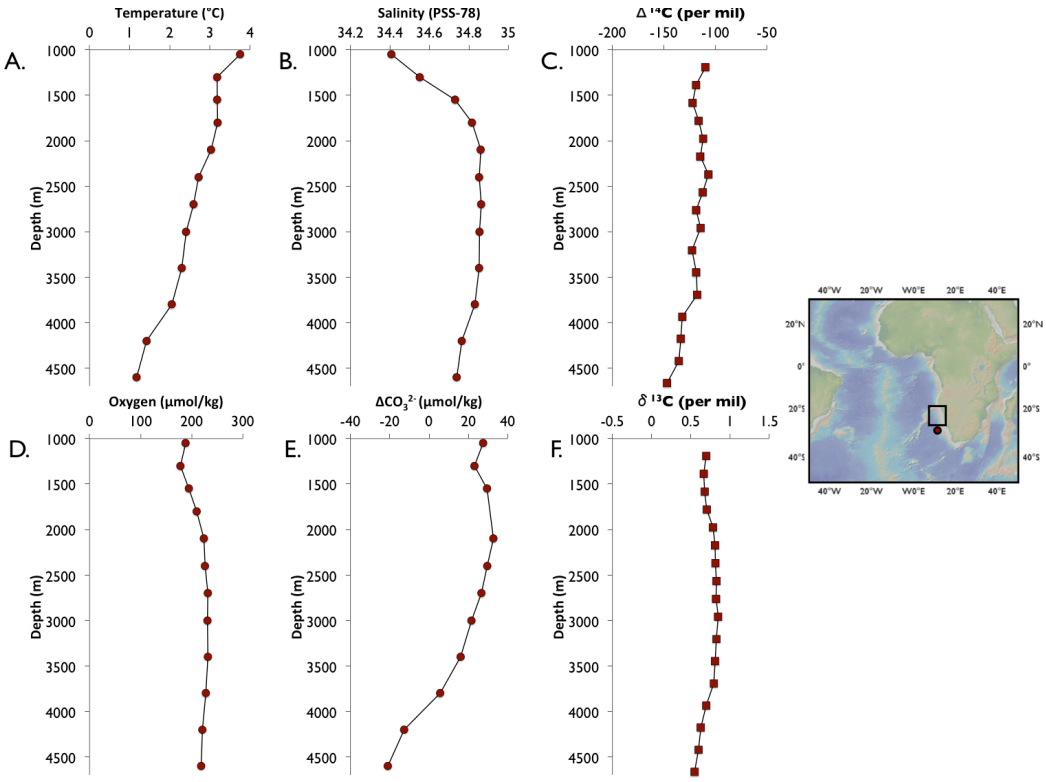

Figure 3.3 (A) Temperature, (B) Salinity, (C) $\Delta^{14}C$ (D) Dissolved Oxygen (E) Difference between in situ carbonate ion concentration and saturation, and (F) $\delta^{13}C$ profiles measured during WOCE A10 cruise at 30°S 9°E, south of the core collection area.

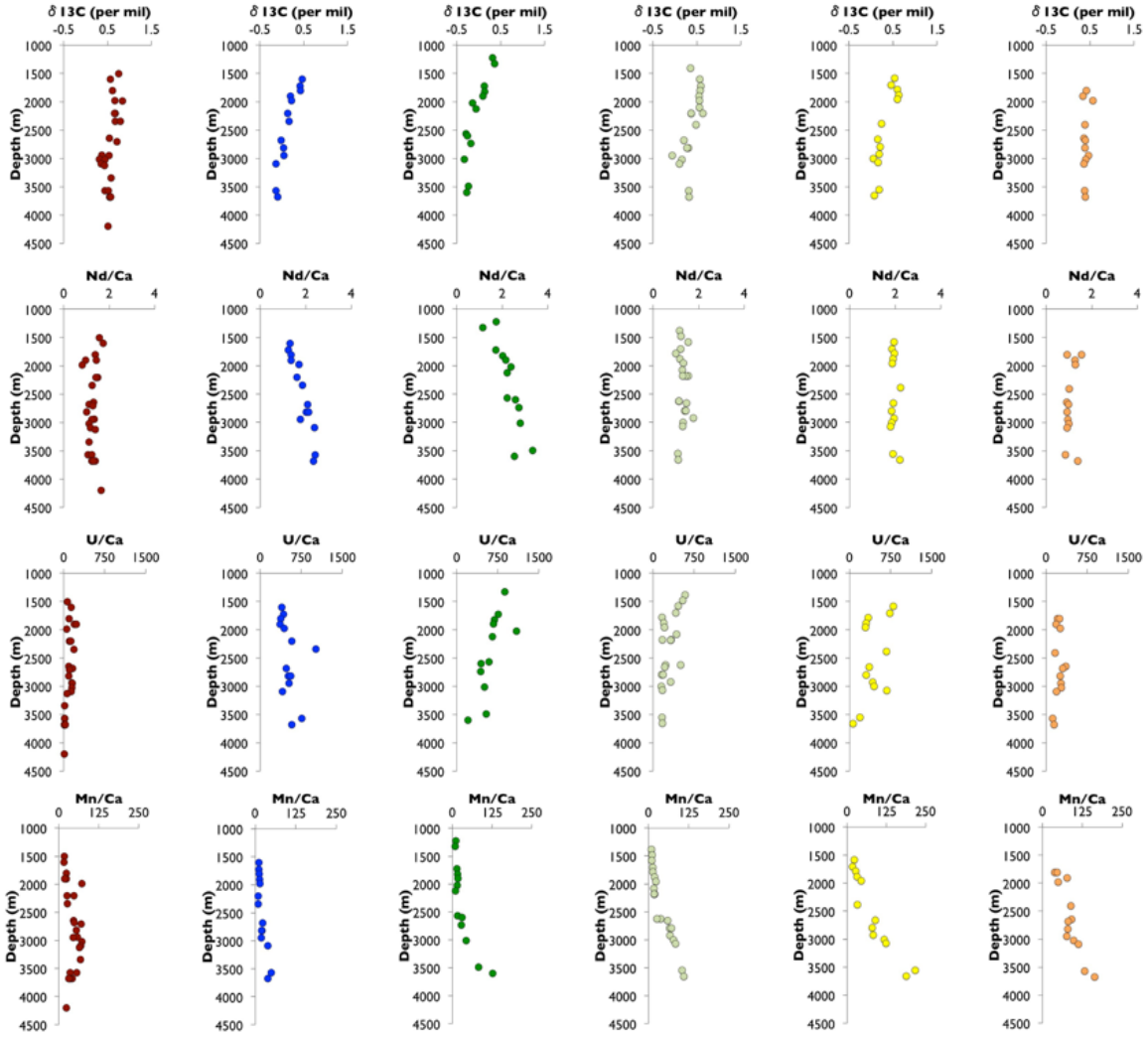

Figure 3.4 Profiles of (A) $\delta^{13}C$ (B) Nd/Ca (C) U/Ca (D) Mn/Ca for MIS 5E (Orange), 5D (Yellow), 5A/5B (light green), 4 (Dark Green), 2 (Blue), and 1 (Red). Glacial periods show elevated gradients in $\delta^{13}C$ at the same time as increased Nd, particularly in the deep ocean. Glacial periods also show elevated values of U/Ca and reduced values of Mn/Ca, consistent with observations by Boiteau et al [2012]. These observations imply that the movement of nutrients to the deep ocean occurred during the buildup of glacial conditions, as suggested by Boyle [1988].

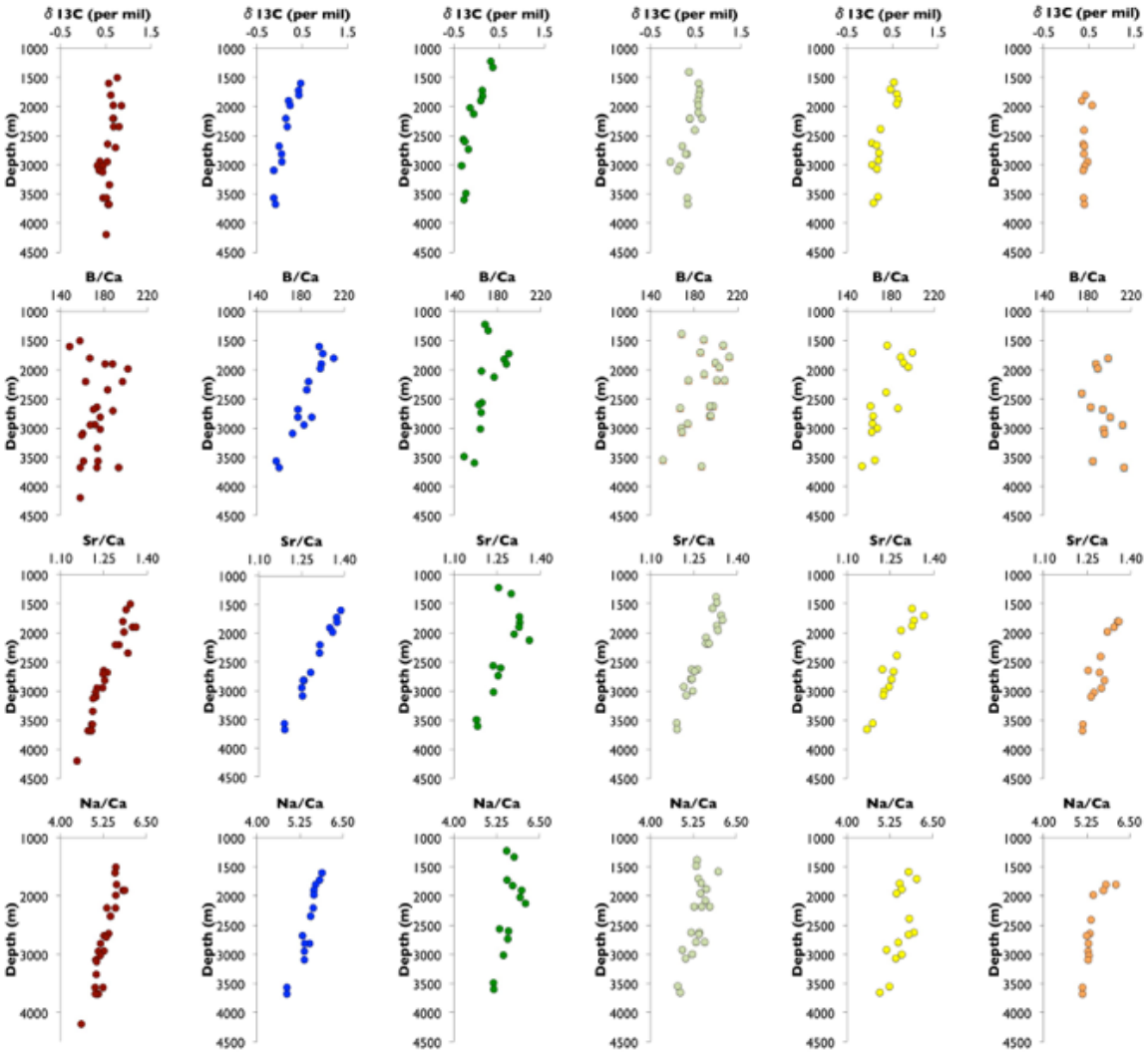

Figure 3.5 Profiles of (A) $\delta^{13}C$ (B) B/Ca (C) Sr/Ca (D) Na/Ca for MIS 5E (Orange), 5D (Yellow), 5A/5B (light green), 4 (Dark Green), 2 (Blue), and 1 (Red). The $\delta^{13}C$ gradient between mid depth and the deep ocean becomes progressively steeper during the cold episodes, while gradients in B/Ca, Sr/Ca and Na/Ca remain the same throughout the ice age cycle. The difference in behavior of the $\delta^{13}C$ and B/Ca profiles suggests that the cores are reflecting changes in carbonate ion concentrations tied to carbonate compensation.

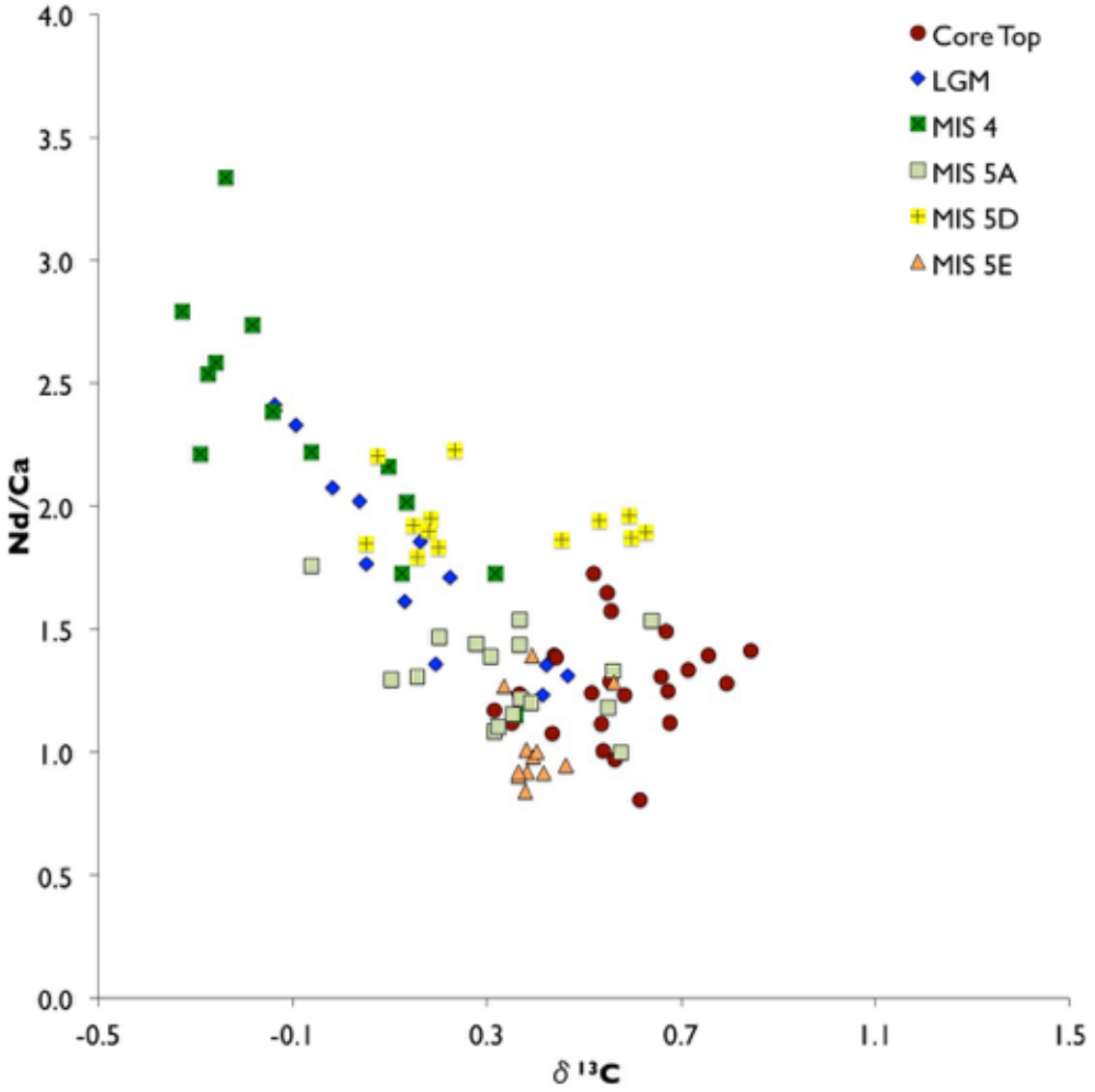

Figure 3.6 Paired Nd/Ca and $\delta^{13}C$ measurements from each of the vertical profiles. There is a strong relationship between Nd/Ca and $\delta^{13}C$ for the MIS 4 and MIS 2 profiles in particular, implying strong Nd addition from particles during these time periods.

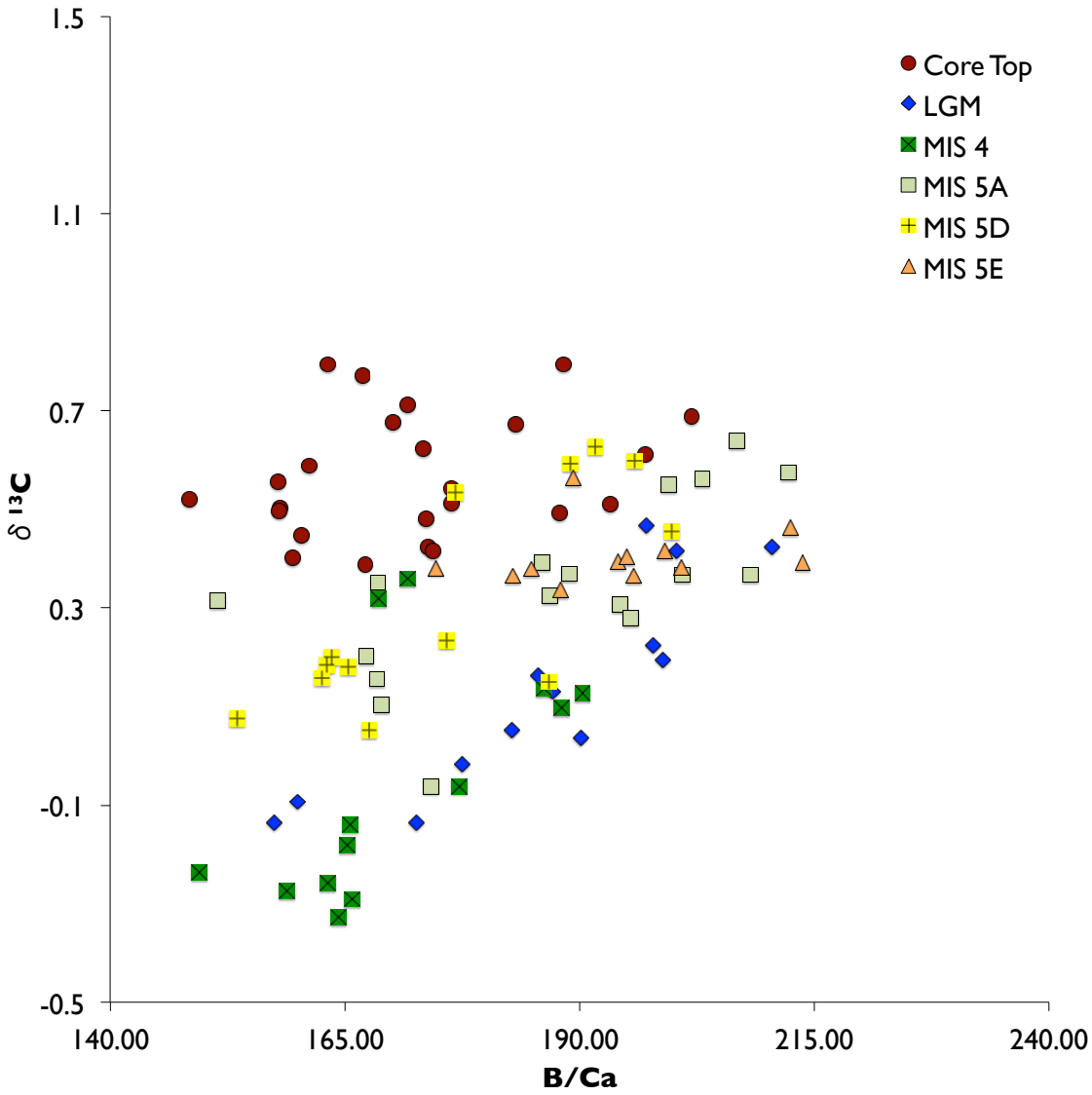

Figure 3.7 Paired B/Ca and $\delta^{13}C$ measurements from each of the vertical profiles. B/Ca profiles for each of the time periods have nearly the same slope in the vertical profiles, likely as a result of carbonate compensation.

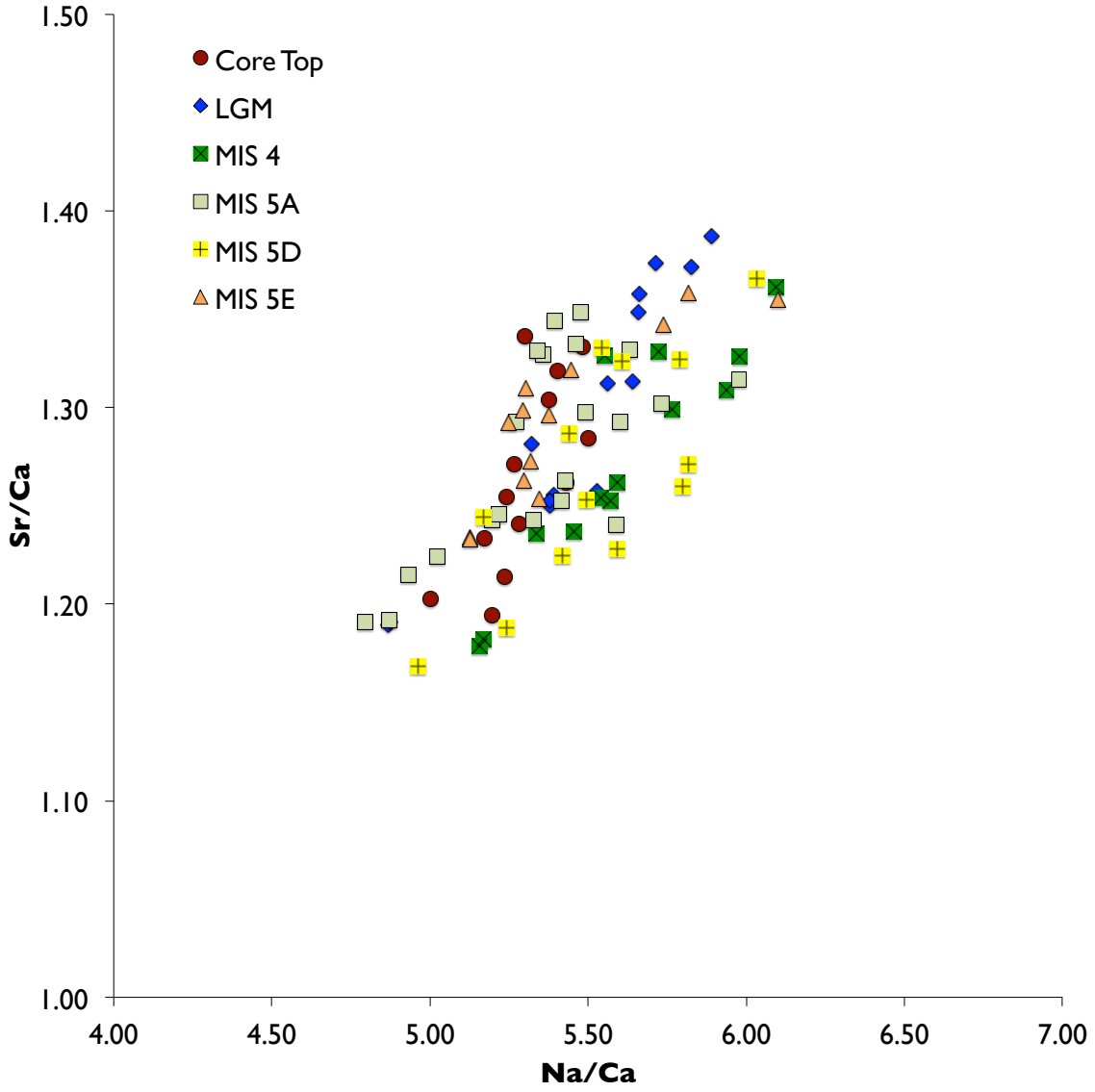

Figure 3.8 Paired Sr/Ca and Na/Ca measurements from each of the vertical profiles. The tight correlation between the Na/Ca and Sr/Ca measurements suggest that two proxies are responding to a common variable.

3.7 References

Adkins, J. F., K. McIntyre, and D. P. Schrag (2002), The salinity, temperature, and δ18O of the glacial deep ocean, *Science*, *298*(5599), 1769-1773.

Arsouze, T., J. Dutay, F. Lacan, and C. Jeandel (2009), Reconstructing the Nd oceanic cycle using a coupled dynamical-biogeochemical model, *Biogeosciences*, *6*(12), 2829-2846.

Barker, S., M. Greaves, and H. Elderfield (2003), A study of cleaning procedures used for foraminiferal Mg/Ca paleothermometry, *Geochemistry, Geophysics, Geosystems*, *4*(9).

Barker, S., P. Diz, M. J. Vautravers, J. Pike, G. Knorr, I. R. Hall, and W. S. Broecker (2009), Interhemispheric Atlantic seesaw response during the last deglaciation, *Nature*, *457*(7233), 1097-1102.

Boiteau, R., M. Greaves, and H. Elderfield (2012), Authigenic uranium in foraminiferal coatings: A proxy for ocean redox chemistry, *Paleoceanography*, *27*(3).

Boyle, E. A. (1988), Vertical oceanic nutrient fractionation and glacial/interglacial CO2 cycles, *Nature*, *331*(6151), 55-56.

Bradtmiller, L., R. Anderson, J. Sachs, and M. Fleisher (2010), A deeper respired carbon pool in the glacial equatorial Pacific Ocean, *Earth and Planetary Science Letters*, *299*(3), 417-425.

Broecker, W. S., and T.-H. Peng (1982), *Tracers in the Sea*.

Burdige, D. J. (1993), The biogeochemistry of manganese and iron reduction in marine sediments, *Earth-Science Reviews*, *35*(3), 249-284.

Burke, A., and L. F. Robinson (2012), The Southern Ocean's role in carbon exchange during the last deglaciation, *Science*, *335*(6068), 557-561.

Calvert, S., and T. Pedersen (1996), Sedimentary geochemistry of manganese; implications for the environment of formation of manganiferous black shales, *Economic Geology*, *91*(1), 36-47.

Chase, Z., R. F. Anderson, and M. Q. Fleisher (2001), Evidence from authigenic uranium for increased productivity of the glacial Subantarctic Ocean, *Paleoceanography*, *16*(5), 468-478.

Crabill, K. (2017), Late Quaternary carbonate deposition and oceanographic processes in the Southeast Atlantic Ocean, Texas A&M University.

Crusius, J., and J. Thomson (2000), Comparative behavior of authigenic Re, U, and Mo during reoxidation and subsequent long-term burial in marine sediments, *Geochimica et Cosmochimica Acta*, *64*(13), 2233-2242.

Curry, W. B., and D. W. Oppo (2005), Glacial water mass geometry and the distribution of δ13C of ΣCO2 in the western Atlantic Ocean, *Paleoceanography*, *20*(1).

Curry, W. B., J.-C. Duplessy, L. Labeyrie, and N. J. Shackleton (1988), Changes in the distribution of δ13C of deep water ΣCO2 between the last glaciation and the Holocene, *Paleoceanography*, *3*(3), 317-341.

Delaney, M. L., and E. A. Boyle (1983), Uranium and thorium isotope concentrations in foraminiferal calcite, *Earth and Planetary Science Letters*, *62*(2), 258-262.

Delaney, M. L., A. W. Bé, and E. A. Boyle (1985), Li, Sr, Mg, and Na in foraminiferal calcite shells from laboratory culture, sediment traps, and sediment cores, *Geochimica et Cosmochimica Acta*, *49*(6), 1327-1341.

Dunk, R., R. Mills, and W. Jenkins (2002), A reevaluation of the oceanic uranium budget for the Holocene, *Chemical Geology*, *190*(1), 45-67.

Duplessy, J., N. Shackleton, R. Fairbanks, L. Labeyrie, D. Oppo, and N. Kallel (1988), Deepwater source variations during the last climatic cycle and their impact on the global deepwater circulation, *Paleoceanography*, *3*(3), 343-360.

Elderfield, H., M. Cooper, and G. Ganssen (2000), Sr/Ca in multiple species of planktonic foraminifera: Implications for reconstructions of seawater Sr/Ca, *Geochemistry, Geophysics, Geosystems*, *1*(11).

Finney, B. P., M. W. Lyle, and G. R. Heath (1988), Sedimentation at MANOP Site H (eastern equatorial Pacific) over the past 400,000 years: climatically induced redox variations and their effects on transition metal cycling, *Paleoceanography*, *3*(2), 169-189.

Foster, G. (2008), Seawater pH, pCO 2 and [CO 2− 3] variations in the Caribbean Sea over the last 130 kyr: a boron isotope and B/Ca study of planktic foraminifera, *Earth and Planetary Science Letters*, *271*(1), 254-266.

Gottschalk, J., L. C. Skinner, J. Lippold, H. Vogel, N. Frank, S. L. Jaccard, and C. Waelbroeck (2016), Biological and physical controls in the Southern Ocean on past millennial-scale atmospheric CO2 changes, *Nature communications*, *7*.

Hain, M. P., D. M. Sigman, and G. H. Haug (2010), Carbon dioxide effects of Antarctic stratification, North Atlantic Intermediate Water formation, and subantarctic nutrient drawdown during the last ice age: Diagnosis and synthesis in a geochemical box model, *Global Biogeochemical Cycles*, *24*(4).

Henderson, G. M., and R. K. O'nions (1995), 234U238U ratios in quaternary planktonic foraminifera, *Geochimica et cosmochimica acta*, *59*(22), 4685-4694.

Herguera, J., E. Jansen, and W. Berger (1992), Evidence for a bathyal front at 2000-M depth in the glacial Pacific, based on a depth transect on Ontong Java Plateau, *Paleoceanography*, *7*(3), 273-288.

Hodell, D., C. Charles, and F. Sierro (2001), Late Pleistocene evolution of the ocean's carbonate system, *Earth and Planetary Science Letters*, *192*(2), 109-124.

Jaccard, S., C. T. Hayes, A. Martínez-García, D. Hodell, R. F. Anderson, D. Sigman, and G. Haug (2013), Two modes of change in Southern Ocean productivity over the past million years, *Science*, *339*(6126), 1419-1423.

Jaccard, S. L., E. D. Galbraith, A. Martínez-García, and R. F. Anderson (2016), Covariation of deep Southern Ocean oxygenation and atmospheric CO2 through the last ice age, *Nature*, *530*(7589), 207-210.

Jaccard, S. L., E. D. Galbraith, D. M. Sigman, G. H. Haug, R. Francois, T. F. Pedersen, P. Dulski, and H. R. Thierstein (2009), Subarctic Pacific evidence for a glacial deepening of the oceanic respired carbon pool, *Earth and Planetary Science Letters*, *277*(1), 156-165.

Kallel, N., L. D. Labeyrie, A. Juillet-Leclerc, and J.-C. Duplessy (1988), A deep hydrological front between intermediate and deep-wafpr, masses in the glacial Indian Ocean, *Nature*, *333*(6174), 651-655.

Keigwin, L. D. (1998), Glacial-age hydrography of the far northwest Pacific Ocean, *Paleoceanography*, *13*(4), 323-339.

Klinkhammer, G., and M. Palmer (1991), Uranium in the oceans: where it goes and why, *Geochimica et Cosmochimica Acta*, *55*(7), 1799-1806.

Kumar, N., R. Anderson, R. Mortlock, and P. Froelich (1995), Increased biological productivity and export production in the glacial Southern Ocean, *Nature*, *378*(6558), 675.

Lea, D. W., D. K. Pak, and G. Paradis (2005), Influence of volcanic shards on foraminiferal Mg/Ca in a core from the Galápagos region, *Geochemistry, Geophysics, Geosystems*, *6*(11).

Lisiecki, L. E., and M. E. Raymo (2005), A Pliocene-Pleistocene stack of 57 globally distributed benthic δ18O records, *Paleoceanography*, *20*(1).

Lund, D., J. Adkins, and R. Ferrari (2011), Abyssal Atlantic circulation during the Last Glacial Maximum: Constraining the ratio between transport and vertical mixing, *Paleoceanography*, *26*(1).

Lynch-Stieglitz, J., J. F. Adkins, W. B. Curry, T. Dokken, I. R. Hall, J. C. Herguera, J. J.-M. Hirschi, E. V. Ivanova, C. Kissel, and O. Marchal (2007), Atlantic meridional

overturning circulation during the Last Glacial Maximum, *science*, *316*(5821), 66-69.

Mangini, A., M. Jung, and S. Laukenmann (2001), What do we learn from peaks of uranium and of manganese in deep sea sediments?, *Marine Geology*, *177*(1), 63-78.

Martínez-Boti, M., D. Vance, and P. Mortyn (2009), Nd/Ca ratios in plankton-towed and core top foraminifera: Confirmation of the water column acquisition of Nd, *Geochemistry, Geophysics, Geosystems*, *10*(8).

Martínez-Garcia, A., A. Rosell-Melé, W. Geibert, R. Gersonde, P. Masqué, V. Gaspari, and C. Barbante (2009), Links between iron supply, marine productivity, sea surface temperature, and CO2 over the last 1.1 Ma, *Paleoceanography*, *24*(1).

McKay, C., H. Filipsson, O. Romero, J. B. Stuut, and S. Björck (2016), The interplay between the surface and bottom water environment within the Benguela Upwelling System over the last 70 ka, *Paleoceanography*, *31*(2), 266-285.

McManus, J., W. M. Berelson, G. P. Klinkhammer, D. E. Hammond, and C. Holm (2005), Authigenic uranium: relationship to oxygen penetration depth and organic carbon rain, *Geochimica et Cosmochimica Acta*, *69*(1), 95-108.

Ninnemann, U. S., and C. D. Charles (2002), Changes in the mode of Southern Ocean circulation over the last glacial cycle revealed by foraminiferal stable isotopic variability, *Earth and Planetary Science Letters*, *201*(2), 383-396.

Pattan, J., and N. J. G. Pearce (2009), Bottom water oxygenation history in southeastern Arabian Sea during the past 140ka: results from redox-sensitive elements, *Palaeogeography, Palaeoclimatology, Palaeoecology*, *280*(3), 396-405.

Pena, L. D., and S. L. Goldstein (2014), Thermohaline circulation crisis and impacts during the mid-Pleistocene transition, *Science*, *345*(6194), 318-322.

Piotrowski, A. M., S. L. Goldstein, R. H. Sidney, R. G. Fairbanks, and D. R. Zylberberg (2008), Oscillating glacial northern and southern deep water formation from

combined neodymium and carbon isotopes, *Earth and Planetary Science Letters*, *272*(1), 394-405.

Rae, J. W., G. L. Foster, D. N. Schmidt, and T. Elliott (2011), Boron isotopes and B/Ca in benthic foraminifera: Proxies for the deep ocean carbonate system, *Earth and Planetary Science Letters*, *302*(3), 403-413.

Raitzsch, M., H. Kuhnert, E. C. Hathorne, J. Groeneveld, and T. Bickert (2011), U/Ca in benthic foraminifers: A proxy for the deep-sea carbonate saturation, *Geochemistry, Geophysics, Geosystems*, *12*(6).

Rosenthal, Y., P. Lam, E. A. Boyle, and J. Thomson (1995), Authigenic cadmium enrichments in suboxic sediments: Precipitation and postdepositional mobility, *Earth and Planetary Science Letters*, *132*(1-4), 99-111.

Russell, A. D., S. Emerson, B. K. Nelson, J. Erez, and D. W. Lea (1994), Uranium in foraminiferal calcite as a recorder of seawater uranium concentrations, *Geochimica et Cosmochimica Acta*, *58*(2), 671-681.

Rutberg, R. L., S. R. Hemming, and S. L. Goldstein (2000), Reduced North Atlantic Deep Water flux to the glacial Southern Ocean inferred from neodymium isotope ratios, *Nature*, *405*(6789), 935.

Sarnthein, M., K. Winn, S. J. Jung, J. C. Duplessy, L. Labeyrie, H. Erlenkeuser, and G. Ganssen (1994), Changes in east Atlantic deepwater circulation over the last 30,000 years: Eight time slice reconstructions, *Paleoceanography*, *9*(2), 209-267.

Schrag, D. P., J. F. Adkins, K. McIntyre, J. L. Alexander, D. A. Hodell, C. D. Charles, and J. F. McManus (2002), The oxygen isotopic composition of seawater during the Last Glacial Maximum, *Quaternary Science Reviews*, *21*(1), 331-342.

Siddall, M., S. Khatiwala, T. van de Flierdt, K. Jones, S. L. Goldstein, S. Hemming, and R. F. Anderson (2008), Towards explaining the Nd paradox using reversible scavenging in an ocean general circulation model, *Earth and Planetary Science Letters*, *274*(3), 448-461.

Skinner, L., S. Fallon, C. Waelbroeck, E. Michel, and S. Barker (2010), Ventilation of the deep Southern Ocean and deglacial CO2 rise, *Science*, *328*(5982), 1147-1151.

Stoll, H. M., and D. P. Schrag (1998), Effects of Quaternary sea level cycles on strontium in seawater, *Geochimica et Cosmochimica Acta*, *62*(7), 1107-1118.

Stoll, H. M., D. P. Schrag, and S. C. Clemens (1999), Are seawater Sr/Ca variations preserved in Quaternary foraminifera?, *Geochimica et Cosmochimica Acta*, *63*(21), 3535-3547.

Wit, J. C., L. De Nooijer, M. Wolthers, and G.-J. Reichart (2013), A novel salinity proxy based on Na incorporation into foraminiferal calcite, *Biogeosciences*, *10*(10), 6375-6387.

Yu, J., and H. Elderfield (2007), Benthic foraminiferal B/Ca ratios reflect deep water carbonate saturation state, *Earth and Planetary Science Letters*, *258*(1), 73-86.

Yu, J., and H. Elderfield (2008), Mg/Ca in the benthic foraminifera Cibicidoides wuellerstorfi and Cibicidoides mundulus: Temperature versus carbonate ion saturation, *Earth and Planetary Science Letters*, *276*(1), 129-139.

Yu, J., H. Elderfield, Z. Jin, and L. Booth (2008), A strong temperature effect on U/Ca in planktonic foraminiferal carbonates, *Geochimica et Cosmochimica Acta*, *72*(20), 4988-5000.

Yu, J., G. L. Foster, H. Elderfield, W. S. Broecker, and E. Clark (2010), An evaluation of benthic foraminiferal B/Ca and δ 11 B for deep ocean carbonate ion and pH reconstructions, *Earth and Planetary Science Letters*, *293*(1), 114-120.

Yu, J., H. Elderfield, Z. Jin, P. Tomascak, and E. J. Rohling (2014), Controls on Sr/Ca in benthic foraminifera and implications for seawater Sr/Ca during the late Pleistocene, *Quaternary Science Reviews*, *98*, 1-6.

Yu, J., L. Menviel, Z. Jin, D. Thornalley, S. Barker, G. Marino, E. Rohling, Y. Cai, F. Zhang, and X. Wang (2016), Sequestration of carbon in the deep Atlantic during the last glaciation, *Nature Geoscience*, *9*(4), 319-324.

Chapter 4. Changes in the stable isotope composition of atmospheric CO_2 linked to Southeastern Atlantic carbon isotope gradient and enhanced carbon storage via deep ocean stratification.

Abstract

A significant body of evidence exists showing that cycles of CO_2 are an integral part of the evolution of glacial/interglacial periods. Yet the mechanisms that govern the partitioning of carbon in the earth's ocean-atmosphere-land system on these time scales are not completely understood. Here I utilize newly developed records of the $\delta^{13}C$ of atmospheric CO_2 in tandem with my own records of deep ocean $\delta^{13}C$ to document the amount of excess carbon stored in the deep South Atlantic Ocean during cold episodes. The calculation of carbon storage is based on the divergence in benthic foraminiferal $\delta^{13}C$ between two closely spaced sediment cores that have identical oxygen isotopic histories. The magnitude and timing of this $\delta^{13}C$ divergence record match other independent attempts to calculate vertical $\delta^{13}C$ gradients in the Subantarctic South Atlantic and can be tied directly to the ice core atmospheric CO_2 records. The various comparisons suggest that enhanced carbon storage at depth in the ocean is indeed responsible for much of the atmospheric $\delta^{13}C$ CO_2 and, by extension, the atmospheric concentration of CO_2. The similarity of my record of $\delta^{13}C$ divergence and a record of circumpolar deep water temperature suggests that carbon trapping in the deep South Atlantic ocean was associated with colder, saltier water, consistent with the mechanisms proposed in Chapters 2 and 3 of this thesis.

4.1 Introduction

Polar ice core research over the past few decades has shown that atmospheric carbon dioxide (CO_2) concentrations have varied between 180-280 ppm over the last 800,000 years [*D Lüthi et al.*, 2008], and that these fluctuations are strongly correlated with Earth's climate. In particular, cold glacial periods experience 80-100 ppm lower atmospheric CO_2 concentrations than warmer interglacial periods, indicating a large-scale transfer of carbon within the land-ocean-atmosphere system. Reconstructions of terrestrial carbon reservoirs during the Last Glacial Maximum (LGM) show a ~500Gt reduction in carbon compared to the Late Holocene [*M I Bird et al.*, 1994; *P Ciais et al.*, 2012], which translates to an increase of 15 ppm in atmospheric CO_2 after taking carbonate compensation into account [*D M Sigman and E A Boyle*, 2000]. Given the relative size and rate of overturning of the oceanic reservoir of carbon, the changes in atmospheric CO_2 on these time scales have usually been attributed to changes in circulation and carbon storage in the deep ocean. However, there have been recent suggestions that the variable volcanic inputs of CO_2 to the atmosphere over glacial cycles may also play a role in setting atmospheric CO_2 concentrations [*P Huybers and C Langmuir*, 2009; *W S Broecker et al.*, 2015].

Understanding the mechanisms involved in the large observed changes in atmospheric CO_2 has been the subject of considerable focus in the paleoceanographic community. One of the main tools used to study past changes in circulation is the stable carbon isotopic composition of dissolved inorganic carbon ($\delta^{13}C_{DIC}$). The carbon isotopic distribution in the ocean/atmosphere system is primarily sensitive to photosynthetic

fractionation, which initially led many to use the $\delta^{13}C$ of foraminifera as a direct proxy for oceanic nutrient concentrations [*E Boyle and L Keigwin*, 1985; *L D Labeyrie and J C Duplessy*, 1985; *J Duplessy et al.*, 1988]. However, the recognition that air-sea gas exchange can exert a significant effect on deep ocean $\delta^{13}C_{DIC}$ [*W S Broecker and T-H Peng*, 1982; *W Broeker and E Maier-Reimer*, 1992; *C D Charles et al.*, 1993] requires that any interpretation of the marine $\delta^{13}C$ signal must consider the significance of non-biological processes. The interpretation of the time series of marine $\delta^{13}C$ must also take into account the timing and magnitude of the transfer of terrestrial carbon into the ocean, which has been estimated to play a relatively significant role in altering whole-ocean $\delta^{13}C_{DIC}$ [*J Duplessy et al.*, 1988; *P Köhler et al.*, 2010; *P Ciais et al.*, 2012; *C D Peterson et al.*, 2014].

Given that each of these processes fractionates stable carbon isotopes differently, measurements of $\delta^{13}C$ of atmospheric CO_2 should be able to be combined with measurements of marine $\delta^{13}C_{DIC}$ to discern the relative importance of the various processes described above. For example, the movement of carbon to the deep ocean from the atmosphere (through any mechanism such as iron fertilization or enhanced stratification) would lead to a decrease in atmospheric CO_2, a decrease in deep ocean $\delta^{13}C$ and an increase in the $\delta^{13}C$ of atmospheric CO_2. In contrast, cooling of surface waters should lead to a decrease in atmospheric CO_2, an increase in deep ocean $\delta^{13}C$, and a decrease in $\delta^{13}C$ of atmospheric CO_2. Thus the combination of deep sea and atmospheric records of $\delta^{13}C$ could potentially provide insight into the relative importance of these processes that can alter carbon isotopes in different manners.

Until recently, the lack of a complete $\delta^{13}C$ atmospheric record has prevented these types of paired observations from being made for large transitions in the atmospheric CO_2 record. However, newly published results [*J Elsig et al.*, 2009; *J Schmitt et al.*, 2012; *R Schneider et al.*, 2013; *S Eggleston et al.*, 2016] constitute the first continuous data set of atmospheric $\delta^{13}C$ CO_2 over a full glacial/interglacial cycle; they can now be combined with analogous observations from the deep sedimentary archives to provide significant insight into the relative importance of the various possible pathways for global carbon cycling.

Here I present new stable isotopic and trace metal evidence from a set of sediment cores that form a tightly controlled depth transect in the Southeastern Atlantic. These cores have been shown to have experienced similar depositional and lithological conditions throughout the collection (Chapter 1), and can be logically combined to provide robust insight as to how gradients in the deep ocean $\delta^{13}C$ (and thus carbon storage) evolved over time. In particular I use neighboring mid-depth and deep cores to create a time series of the vertical gradient in $\delta^{13}C$ ($\Delta\delta^{13}C_{DIC}$) for this area. The close geographic proximity of these cores makes it possible to circumvent many of the potential problems associated with using sedimentary time series of $\delta^{13}C$ [*A Mackensen et al.*, 2001]. I show that this record can be explicitly tied to the ice core record of $\delta^{13}C_{atm}$ and that the combined set of observations of deep ocean $\delta^{13}C$, $\delta^{18}O$, Mg/Ca, and radiocarbon from the core collection implies that the variations in $\delta^{13}C_{atm}$ are primarily a result of nutrient deepening [*E A Boyle*, 1988b]. I also show that the evolution of the gradient in $\delta^{13}C$ between the two cores matches a previously published $\delta^{13}C_{surface\text{-}deep}$

record from the Agulhas plateau [*M Ziegler et al.*, 2013]. The close match between these two records, despite the differences in location and in the manner in which the $\delta^{13}C$ gradient was calculated reinforces my confidence in the validity of these determinations. I finish by showing that the record of deep ocean $\delta^{13}C$ presented here closely matches a deep ocean temperature record of Circumpolar Deep Water, and suggest that the observed nutrient deepening and resulting change in atmospheric $\delta^{13}C$ was potentially associated with changes in the density structure of the deep and mid-depth ocean.

4.2 Oceanographic Setting

4.2.1 Core collection and subsampling

The cores presented here were collected aboard the R/V Melville in March 2003. All but 3 of the cores were collected along two depth transects within an area defined by 19° 43.3′S and 21° 33.1′S and 9° 54.1′E and 12° 48.1′E, and range in depth from 1405 to 3678 meters. The remaining cores were taken further south along a transect at 24° 28.0′S, 12° 26.0′E and range in depth from 2200 to 2600 m.

The stratigraphy for the cores used in the vertical profiles presented in this chapter is discussed in significantly greater detail in Chapter 1. Briefly, downcore XRF elemental ratio measurements were used to develop a common tie point for the close of the Last Glacial Maximum (LGM). Radiocarbon measurements on planktonic samples indicated that stratigraphic consistency was achieved to within 500 years at the close of the LGM for the collection of cores used in these vertical profiles.

The time series of carbon and oxygen stable isotopes discussed below were created using foraminifera sub-sampled from cores MV09-PC21 (2680m; 21°3.8’S;

10°40.9’ E) and MV09-PC-23 (1977m; 20°47.9’ S; 10° 48.5’ E) at 5 cm intervals. Samples for these time series were excised from the cores using 2 cm diameter round plugs, dried in a 50°C oven, and wet sieved through 63μm mesh before foraminiferal specimens were picked out.

4.2.2 Water Mass Distribution

The vertical profile approach requires proxy observations from the core tops to reflect the modern overlying water column. The different northern- and southern- sourced water masses are stacked vertically for the collection area, and can be distinguished by their varying nutrient contents and densities. Antarctic Intermediate Water (AAIW) and Upper Circumpolar Deep Water (UCDW) make up part of the water column between 500-1500 meters depth, and overlie constituents of North Atlantic Deep Water. In particular, Labrador Sea Water (LSW) occupies the 1700-2000 meter depth range [*R Schlitzer*, 2000]. Deeper in the water column, North Atlantic Deep Water (NADW) borders the southern-sourced Lower Circumpolar Deep Water (LCDW) at roughly 3600 meters depth (Figure 4.1).

The $\delta^{13}C$ of the dissolved inorganic carbon $\delta^{13}C_{DIC}$ mirrors this water mass distribution in the modern southeastern Atlantic (Figure 1.1). There is a minimum in the $\delta^{13}C_{DIC}$ in the oxygen minimum zone underlying the surface layer of the ocean. This minimum extends until roughly 1500 m depth, at which point $\delta^{13}C$ values begin to increase as the influence of northern sourced waters grows. Values of $\delta^{13}C$ remain high until roughly 3600 meters, at which point $\delta^{13}C_{DIC}$ begins to decrease to values consistent with the low $\delta^{13}C$ values of LCDW.

Several studies have suggested that the $\delta^{13}C$ of benthic foraminifera over time may not reflect the bottom water $\delta^{13}C_{DIC}$ because the decomposition of organic matter might create a micro-environment with a highly localized carbon isotopic composition [*A Mackensen et al.*, 1993; *A Mackensen et al.*, 2001]. It seems unlikely, however, that the cores analyzed here experienced greatly different changes in organic matter rain rates or productivity, given their close geographical distribution. In particular, the cores MV09-PC21 and MV09-PC-23 used for the time series are separated by less than a degree of latitude (Figure 4.1), and have near identical sedimentation rates and bulk lithologies.

4.3 Methods

Stable carbon and oxygen isotope measurements for the LGM vertical profile were made on splits from crushed *Cibicidoides wuellerstorfi* specimens. These splits were taken after the ultrasonication step, to ensure the removal of clays. Stable isotope values for $\delta^{13}C$ and $\delta^{18}O$ were measured on a Thermo Finnigan MAT 253 mass spectrometer equipped with a Kiel IV carbonate device. Analytical precision, estimated from measurements of NBS 19 standards, was 0.07 per mil and 0.04 per mil for $\delta^{18}O$ and $\delta^{13}C$ respectively. Co-occurring trace element measurements for the LGM vertical profile were made following the procedures outlined in Chapter 2 and 3 of this thesis.

Stable carbon and oxygen isotope measurements for the two time series developed from cores MV09-PC21 and MV09-PC-23 were made on the tests of *Cibicidoides wuellerstorfi,* Three *Cibicidoides wuellerstorfi* specimens were picked from the >200um size fraction at 5 cm intervals and subsequently analyzed for $\delta^{13}C$ and $\delta^{18}O$.

Stable isotope values were measured on a Finnigan MAT 253 mass spectrometer equipped with a Kiel IV carbonate device. Analytical precision, estimated from measurements of NBS 19 standards, was 0.07 per mil and 0.04 per mil for $\delta^{18}O$ and $\delta^{13}C$ respectively.

Radiocarbon measurements were made by Jenna Munson [*Unpublished*] at the Center for Accelerator Mass Spectrometry at Lawrence Livermore National Laboratory on *Globigerina bulloides* and mixed benthic samples. Foraminiferal tests were sonicated in a .0001N HCl solution; planktonics were sonicated briefly to avoid having the shells explode, whereas benthics were sonicated for 1 minute. The HCl was then pipetted off and the samples were dried, weighed, and graphitized. Sample sizes varied between 0.4 and 8 mg. The $\delta^{13}C$ of the samples used for radiocarbon analysis was not measured, but Munson et al. [*unpublished*] assigned a $^{13}C/^{12}C$ ratio of 1.0‰ for planktonic samples, and 0‰ for the benthic samples to correct for the mass-dependent fractionation. To convert the benthic foraminiferal ages to $\Delta^{14}C$, the values were decay corrected to 1950 using the coexisting planktonic foraminiferal $\Delta^{14}C$ as an estimate of calendar age, and then calculated as $\Delta^{14}C$ using the equations in Stuiver and Polach [1977].

4.4 Results

4.4.1 Conservative and nonconservative tracer profiles at the LGM

I analyzed benthic foraminifera from 13 piston cores spanning modern depths between 1483 and 3678 meters for oxygen stable isotopes and Mg/Ca to create vertical profiles of these tracers at the LGM (Figure 4.2). For $\delta^{18}O$, the shallowest point in the water column profile is roughly 0.3 per mil lower than the rest of the profile, and below

this point values of $\delta^{18}O$ grow higher until 2200 meters depth. $\delta^{18}O$ values from cores deeper than 2200 meters remain roughly constant around 4.65 per mil over the length of the profile. Co-occurring measurements of Mg/Ca show a broadly similar structure as the $\delta^{18}O$ profile (Figure 4.2). Mg/Ca values decrease linearly by 0.3 mmol/mol between 1483m-2200m depths. Below 2200 meters the profile of Mg/Ca stays nearly constant, averaging 0.94 mmol/mol.

Radiocarbon measurements on paired benthic and planktonic foraminifera made by Jenna Munson [*pers. communication*] on cores from the same location suggest that the water column was dominated below a modern water depth of 1977 meters by a single older water mass. Benthic-Planktonic age differences below this depth are in line with the benthic-planktonic age at 3650 m depth of ~1000 years reported by Skinner et al.[2010] in the South Atlantic. Higher up in the water column the benthic-planktonic measurements suggest a transition between 1977m-1804m to a uniformly younger water mass (~500 years) between 1300-1800 meters water depth (Figure 4.2).

In contrast with the vertical distribution of the tracers described above, carbon isotope measurements made concurrently with the stable oxygen isotope measurements show a drastically different distribution of $\delta^{13}C$ within the LGM deep ocean (Figure 4.2). While a sharp gradient exists across the upper section of the profile (1500-2000 meters), values for $\delta^{13}C$ continue to decrease by nearly 0.35 per mil between 2000-3600 meters.

4.4.2 Evolution of Stable Isotope Time Series

The construction of a time series of stable carbon and oxygen isotopes provides a means by which to understand the timing and magnitude of the divergence in behavior

between $\delta^{13}C$ and $\delta^{18}O$. The profiles of $\delta^{18}O$ for both the shallower MV09-PC23 and MV09-PC21 vary almost identically over the duration of the glacial/interglacial cycle. In both cores the $\delta^{18}O$ values fall between an interglacial value of 2.5 per mil and a glacial value of 4.5 per mil, and the $\delta^{18}O$ values of the cores show almost no divergence between the two time series throughout the record. This suggests the gradient in $\delta^{18}O$ between 1977 and 2680 m depth was negligible over most of the last interglacial cycle in this location (Figure 4.3).

In contrast, the $\delta^{13}C$ record for these two cores shows periods of marked divergence, in line with what is implied by the depth profiles at the close of the LGM. At MIS 5E, the records show almost identical values for $\delta^{13}C$. By MIS 5D, however, a strong gradient in $\delta^{13}C$ (~0.5 per mil) has developed, which then collapses completely by MIS 5C. This gradient reappears during MIS 5b before collapsing very briefly during MIS 5A. By MIS 4 the gradient is again at a maximum, before collapsing again at the very beginning of MIS 3.The record of $\delta^{13}C$ difference ($\Delta\delta^{13}C$) between the cores continues to show variations of as much as 0.65 per mil during MIS 3. Eventually this difference reaches an LGM value of 0.7 per mil, before collapsing during the deglaciation (Figure 4.4).

To understand the implications and the scale of the $\Delta\delta^{13}C$ record generated here, I compare the time series of $\Delta\delta^{13}C$ to a record of planktonic-benthic $\Delta\delta^{13}C$ (hereafter referred to as $\Delta\delta^{13}C_{\text{therm-deep}}$) generated by Ziegler et al [2013] from the Subantarctic Southern Ocean (Figure 4.1 and Figure 4.4). The record created by Ziegler et al. [2013]

was created by measuring the gradient between $\delta^{13}C$ of the deep-dwelling planktonic foraminfer *G. truncatulinoides* and the $\delta^{13}C$ of the benthic foraminfer *C. wuellerstorfi* from a core retrieved at 3000 meters depth on the Agulhas Plateau, near the Subtropical Front. Ziegler et al suggest that their record of $\Delta\delta^{13}C$ is driven by a combination of changes in the $\delta^{13}C$ of Subantarctic Mode Water (SAMW) in the thermocline and Circumpolar Deep Water (CPDW) at depth. Interestingly, despite the differences in sedimentation rate and sampling resolution, the $\Delta\delta^{13}C$ record developed from the deep South Atlantic near the Walvis ridge captures the same broad-scale features as the Ziegler et al [2013] record, albeit with lower variability. In particular, the magnitude of the large-scale $\Delta\delta^{13}C$ transitions is remarkably similar, with large gradients evolving in both records across the transitions associated with the evolution of MIS 5e/5D, MIS 5a/4, and the MIS 3/LGM.

This comparison can be extended to the ice core record of atmospheric CO_2, because the planktonic record of $\delta^{13}C$ of *G. truncatulinoides* from Ziegler et al. [2013] corresponds in both timing and magnitude with the $\delta^{13}C$ record of CO_2 over the last 140 kyr (Figure 4.5) [*J Elsig et al.*, 2009; *J Schmitt et al.*, 2012; *R Schneider et al.*, 2013; *S Eggleston et al.*, 2016]. The match between the $\delta^{13}C$ record of *G. truncatulinoides* and the $\delta^{13}C$ of atmospheric CO_2 suggests that this particular planktonic foraminiferal $\delta^{13}C$ record directly reflects the carbon isotopic composition of the atmosphere, without intervening effects such as gas exchange or carbon export from the overlying surface ocean (Figure 4.5).

This observation has some interesting implications. By itself, the ice core $\delta^{13}C$ of CO_2 record must be the aggregate of whole ocean/atmosphere transfers of terrestrial carbon, the effective strength of the marine biological pump of carbon to the deep ocean, and air-sea gas exchange:

(1) $\delta^{13}C_{atm} = \delta_{whole\ o\text{-}a} + \delta_{bio\ pump} - \delta_{gas\ exchange}$

The planktonic record of $\delta^{13}C$ should reflect similar changes as the ice core $\delta^{13}C$ of CO_2, except for those driven by air-sea gas exchange:

(2) $\delta^{13}C_{planktonic} = \delta_{whole\ o\text{-}a} + \delta_{bio\ pump} + \delta_{gas\ exchange}$

The benthic record of $\delta^{13}C$ should reflect the same changes as the ice core $\delta^{13}C$ of CO_2 due to the transfer of terrestrial carbon, but opposite changes in $\delta^{13}C$ due to alterations in the strength of the biological pump and air-sea gas exchange:

(3) $\delta^{13}C_{benthic} = \delta_{whole\ o\text{-}a} - \delta_{bio\ pump} + \delta_{gas\ exchange}$

Equations (1) and (2) suggest that any deviation of $\delta^{13}C$ from the near-replicate of the ice core record in the marine realm (i.e. the *G. truncatulinoides* foraminiferal record) must reflect changes due to gas exchange. In this case, the deviation is close to zero over the buildup of glacial conditions:

(4) $\Delta\ \delta^{13}C_{atm\text{-}planktonic} = 2 * \delta_{gas\ exchange} = 0$

From (2) and (3) we see that changes in the gradient of $\delta^{13}C$ in the vertical reflect changes in the strength of the biological pump:

(5) $\Delta\ \delta^{13}C_{plank\text{-}benthic} = 2 * \delta_{bio\ pump}$

Lastly, (5) implies that the record of benthic $\delta^{13}C$ developed by Ziegler et al [2013] is reflecting changes from inputs of terrestrial carbon:

(6) $\delta^{13}C_{benthic[Ziegler]} = \delta_{whole\ o\text{-}a}$

It is possible to obtain a rough estimate of the amount of carbon transferred to the deep ocean across the major transitions in the glacial cycle using the change in the vertical gradient in $\delta^{13}C$. To do so, I first scale the change in the vertical gradient in $\delta^{13}C$ to a change in total carbon, using a photosynthetic fractionation factor of -20 per mil [*W S Broecker and T-H Peng*, 1982] and an average deep ocean value for TCO_2 of 2250. For simplicity I assume that the change in $\delta^{13}C$ in the deep ocean is limited to the depths of my cores and does not continue to grow significantly beyond the deepest extent of the core collection.

Following the logic laid out by Boyle [1988a], a change in $\delta^{13}C$ of 0.75 in the deep ocean would initially result in a respective change in TCO_2 and alkalinity of ~85 μmol/kg and ~17.25 μmol/kg, assuming that the sinking biogenic matter was remineralized according to the Redfield ratio. Subsequent carbonate compensation would alter the change in TCO_2 and alkalinity of the deep ocean, eventually resulting in a change of ~151 μmol/kg of TCO_2 and ~151.5 μmol/kg of alkalinity. Once this altered deep water is upwelled to the surface, the removal of biogenic debris would in turn change the surface TCO_2 and alkalinity by ~67 μmol/kg and 133.5 μmol/kg. Using the thermodynamic equations for pCO_2 as a function of TCO_2 and alkalinity, I find that these changes would correspond to a lowering of pCO_2 on the order of 50 ppm for the given 0.75‰ change in $\delta^{13}C$. While this number is far from exact due to assumptions regarding both TCO_2 and the extent to which the gradient may have grown at depth, it does suggest that the observed changes in $\delta^{13}C$ from nutrient deepening would constitute a significant component of the total glacial-interglacial atmospheric CO_2 change (of ~90 ppm).

Ziegler et al. [2013] relate the changing vertical $\delta^{13}C$ gradients in their record to atmospheric dust. However, the $\delta^{13}C$ gradients for the two records also bear a strong resemblance to a time series of Mg/Ca recorded by the benthic foraminfer *U. peregrina* from ODP site 1123 at 3290 meters depth in the Southwestern Pacific (Figure 4.6)[*H Elderfield et al.*, 2010]. This site is bathed in Circumpolar Deep Water (CPDW) in the modern ocean, and Elderfield et al. [2010] suggest that changes in Mg/Ca in their record reflect changes in the temperature of CPDW over the last 140 kyr. A comparison between this record and my record of $\Delta\delta^{13}C$ change shows that large increases in $\Delta\delta^{13}C$ were

coincident with large-scale cooling of CPDW, particularly at the MIS 5A/4 transition. Similarly, collapses in the gradient of $\delta^{13}C$ in my record match periods of presumed warming in the deep Southwestern Pacific (Figure 4.6). This time series comparison therefore extends the results from the LGM time horizon, which showed an enhanced vertical $\delta^{13}C$ gradient associated with colder, older water below 2000 meters. The Elderfield et al. [2010] time series shows that the magnitude of the $\delta^{13}C$ gradient for my record scales directly with temperature throughout the last full ice age cycle.

4.5 Discussion

Below I discuss the implications of the above sedimentary time series for the timing of carbon transfer to the deep ocean over the last glacial/interglacial cycle, and examine whether these observations can shed light on the mechanisms that may have driven these changes. I begin by exploring the state of the ocean at the Last Glacial Maximum as suggested by the LGM sedimentary depth transect. Of particular interest is the fact that the vertical profiles for the quasi-conservative tracers $\delta^{18}O$, Mg/Ca, and radiocarbon show divergent behavior compared to the co-occurring profiles of $\delta^{13}C$ below 2000 meters depth during this time. To understand how these conditions may have evolved, I next examine the time series of oxygen and carbon stable isotopes from 1977 meters and 2670 meters depth. These sedimentary records show that the gradient in $\delta^{13}C$ at mid/deep depths grew and collapsed repeatedly during the evolution of the last glacial/interglacial cycle, most notably reaching relative maxima across the MIS 5E/5D and MIS 5A/4 transitions and as the deep ocean entered maximal glacial conditions. In

contrast, the gradient in $\delta^{18}O$ between these depths was either significantly reduced or non-existent during the same time periods.

I finish by considering the co-evolution of the $\Delta\delta^{13}C$ gradient of my time series, the atmospheric $\delta^{13}C$ CO_2 record, the $\Delta\delta^{13}C_{surface\text{-}deep}$ from the Agulhas Plateau, and the Mg/Ca record from the deep Southwestern Pacific. The invariance of the $\delta^{13}C$ of atmospheric CO_2 and the *G. truncatulinoides* records, along with the simultaneous changes in the records of $\delta^{13}C$ from my sediment cores (mid-depth/deep records) and the Agulhas Plateau cores (thermocline/deep records), suggests that a common process was governing the storage of carbon in the deep ocean over these time periods, and that this signal was not being altered by air-sea gas exchange. Instead the evolution of this carbon storage corresponds with periods of cooling observed in the deep Southwestern Pacific, suggesting that the cooling of CPDW was related to an increase in carbon storage in the deep ocean. Together this set of relationships allows me to evaluate the possible mechanisms that could be driving these changes.

4.5.1 Evolution of carbon storage in the deep South Atlantic over the last 140 kyr

The mid-depth tracer gradient in $\delta^{18}O$ and radiocarbon at the LGM implies that the Southeastern Atlantic had a vertical structure similar to what has been reported in the Atlantic [*W B Curry and D W Oppo*, 2005], Pacific [*J Herguera et al.*, 1992; *L D Keigwin*, 1998], Indian [*N Kallel et al.*, 1988], and Southern Oceans [*U S Ninnemann and C D Charles*, 2002]. The profiles of $\delta^{18}O$, $\delta^{13}C$, Mg/Ca, and Benthic-Planktonic $\Delta^{14}C$ radiocarbon show a divide centered at 2000 meters, with a radiocarbon-rich, nutrient-poor, warmer water mass overlying a radiocarbon-poor, nutrient-rich, colder water mass.

This is in line with reconstructions of the structure of the Southwestern Atlantic along the Brazil margin, which show gradients in $\delta^{18}O$ and $\delta^{13}C$ [*W B Curry and D W Oppo*, 2005] and Cd/Ca [*T M Marchitto and W S Broecker*, 2006] at similar depths.

Below ~2000 meters depth the behavior of the paleoproxies begins to diverge. The $\delta^{18}O$, Mg/Ca, and radiocarbon measurements remain constant, likely indicating the same water mass occupies these depths. In contrast, the $\delta^{13}C$ profile continues to decrease over the length of the profile. Given that physical ($\delta^{18}O$, Mg/Ca) and ventilation ($D^{14}C$) tracers indicate a uniform water mass below 2 km, it seems most likely that this is an expression of nutrient deepening, a theory first posited by Boyle [1988b] that suggests a transfer of nutrients to the deep ocean would prompt an increase in DIC and an eventual increase in alkalinity that would lower atmospheric pCO_2. Subsequent studies have used nutrient deepening to explain the distribution of $\delta^{13}C$ in the Atlantic [*D A Hodell et al.*, 2003] and the Pacific [*S L Jaccard et al.*, 2009] over glacial cycles.

The time series presented here indicate that nutrient deepening occurred at other points over the evolution of glacial conditions. The evolution of both the $\delta^{18}O$ profiles (Chapter 2) and the $\delta^{18}O$ time series across the last interglacial cycle suggests that there was not a large gradient in $\delta^{18}O$ between 2000-2600 m depth throughout most of the glacial cycle. In contrast, both the $\delta^{13}C$ profiles and the $\Delta\delta^{13}C$ time series provide evidence for a gradient in $\delta^{13}C$ present during periods of decreased CO_2. MIS 5D, for instance, saw the buildup of a gradient in $\Delta\delta^{13}C$ between these depths, concurrent with a 40 ppm decrease in CO_2 [*D Lüthi et al.*, 2008] and a likely decrease in ocean temperature

evident in both the Mg/Ca profiles (Chapter 2) and suggested by other sources [*K Cutler et al.*, 2003; *M A Headley*, 2008; *J F Adkins*]. Similarly, MIS 4 saw a maximum in the gradient of $\delta^{13}C$ in both the time series and the stable isotope profiles that coincides with a minimum in CO_2.

The similarity between my $\Delta\delta^{13}C$ record and the $\Delta\delta^{13}C_{surface\text{-}deep}$ record generated by Ziegler et al [2013] implies that a common process was driving the evolution of the $\delta^{13}C$ gradient near the Walvis Ridge and along the Agulhas plateau. This is particularly interesting in light of the observation that the changes in the planktonic record of $\delta^{13}C$ from the Agulhas plateau are almost identical in magnitude and timing to the observed changes in the atmospheric CO_2 record of $\delta^{13}C$ (Figure 4.5). This close tie between the planktonic record and the $\delta^{13}C$ of atmospheric CO_2 makes sense, as *G. truncatulinoides* is likely calcifying in SAMW, which communicates with the atmosphere near the subtropical front before being subducted northward towards the subtropical gyre [*L D Talley*, 2011]. The match between the planktonic record from Ziegler, the atmospheric record of $\delta^{13}C$ of CO_2, and the observed $\Delta\delta^{13}C$ record combine to suggest that the signal of $\Delta\delta^{13}C$ from the core collection represents a transfer of carbon to the deep ocean with minimal alteration from air-sea gas exchange effects.

4.5.2 Mechanisms of Change

There are several possibilities for how the transfer of carbon to the deep ocean could have been accomplished. One of the most commonly cited mechanisms for transferring carbon to the deep interior of the ocean is by increasing the efficiency of the biological pump via dust-derived iron fertilization [*J H Martin*, 1990]. This seems

unlikely to be driving the $\delta^{13}C$ gradients documented here for several reasons. First, the record of $\Delta\delta^{13}C$ derived from these cores (as well as the record of $\delta^{13}C$ from Ziegler et al. [2013]) fluctuates remarkably closely with the *U. peregrina* Mg/Ca record of CDW temperature at ODP site 1123 in the Pacific [*H Elderfield et al.*, 2010]. If iron fertilization were driving the changes in $\Delta\delta^{13}C$, there is no *a priori* reason that the gradient in $\delta^{13}C$ across depth should scale with the bottom water temperature (Figure 4.6). Second, the similarity between my record of $\Delta\delta^{13}C$ and that of Ziegler [2013] suggests that if the observed changes in $\Delta\delta^{13}C$ were driven by iron fertilization, the fluctuations in dust inputs were necessarily basin-wide for the Southeastern Atlantic. This too seems unlikely, as the two core sites are separated by 20° of latitude and experience different depositional regimes. Finally, as discussed in more detail in Chapter 3, the strong relationship between Nd/Ca and $\delta^{13}C$ in the vertical profiles suggests that a similar process governed $\delta^{13}C$ distribution and Nd concentrations in these cores. As Nd/Ca likely responds to local particle flux, the correlation between Nd/Ca and $\delta^{13}C$ implies that the remineralization of particles and the development of steeper gradients of carbon in the deep ocean were not set exclusively in the Subantarctic.

Given the correlation with CDW Mg/Ca from a site in the Pacific, it seems more likely that changes in the circulation of the ocean prompted an increase in the $\delta^{13}C$ gradient. One possible explanation for this correlation was recently proposed by Adkins [2013], who pointed out that cooling of NADW, itself a precursor to CDW, would reduce the "prefreshening" of AABW, creating a denser, saltier water mass. As this deep, saltier water mass filled the deep Atlantic, the boundary between the water masses would have

shoaled away from rough topography in the deep ocean, more efficiently trapping carbon [*D Lund et al.*, 2011]. The shoaling of this boundary would have also increased the volume of poorly ventilated water by a factor of 4 by the LGM, increasing the ability of the deep ocean to store carbon at depth [*L Skinner et al.*, 2010]. As carbon was stored in the deep ocean, cooling could have potentially allowed for sea ice expansion, which has been dynamically linked to the expansion of deep waters of Antarctic origin and the creation of the shallow overturning cell seen at the LGM [*R Ferrari et al.*, 2014]. An expansion of sea ice would have also reduced the communication with the atmosphere, further reducing CO_2 outgassing [*B B Stephens and R F Keeling*, 2000] while also altering the available preformed nutrient content of the water.

The proposed cooling of NADW, and subsequently CDW, could explain the correlation between the record of CDW temperature from the Pacific and the stable carbon isotopic gradients in the Atlantic. As CDW cools, it promotes the formation of cold, salty deep water, which in turn is able to trap more respired carbon. As such, the gradient of $\delta^{13}C$ in the deep ocean would be expected to increase, as observed. In this scenario the link between the Ziegler record of $\delta^{13}C$ of SAMW and the $\delta^{13}C$ atmospheric record would be through the shallow overturning occurring the Sub-Antarctic Zone (SAZ), while changes at depth would be occurring as the deeper water mass expanded during glacial periods, trapping carbon and providing a link between the maxima in the $\delta^{13}C$ gradient observed in the core collection and the maxima in the $\delta^{13}C$ atmospheric CO_2 record.

The trapping of respired carbon in this "nutrient deepening" scheme would also be expected to lower dissolved oxygen in the bottom waters in these areas. The increase in U/Ca and decrease in Mn/Ca ratios seen in the vertical profiles (Chapter 3) during MIS 4 and the LGM suggests that the profiles were in fact exposed to low oxygen conditions. Authigenic uranium has often been used as a proxy for bottom water oxygen conditions [*J McManus et al.*, 2005], and recent evidence links changes in foraminiferal U/Ca to changes bulk sediment authigenic uranium [*R Boiteau et al.*, 2012]. Likewise, the low values for Mn/Ca during glacial times suggests that there was little accumulation of Mn oxide coatings, and that bottom water concentrations of oxygen may have remained low during these times.

While there are substantial uncertainties involved in estimating the magnitude of the various effects of iron fertilization and stratification, a number of efforts to model the carbon cycle incorporating $\delta^{13}C_{DIC}$ and $\delta^{13}C$ CO_2 have suggested that impacts on atmospheric $\delta^{13}C$ from changes in stratification are likely larger than those from iron fertilization [*P Köhler et al.*, 2010; *T Tschumi et al.*, 2010; *N Bouttes et al.*, 2011; *L Menviel et al.*, 2015]. In particular, Bouttes et al. [2011] suggest that brine-induced stratification plays a dominant role in altering atmospheric CO_2, $\Delta\delta^{13}C$ in the ocean, and $\delta^{13}C$ of CO_2 as compared to both iron fertilization and reduced diffusion across water mass boundaries. This indicates that there is a basis for the hypothesis explained above; namely, that cooling of NADW led to cooler CDW, which in turn promoted the expansion of a deep, cold, salty water mass capable of trapping large amounts of carbon.

4.6 Conclusion

Here I argue that the difference in physical water mass tracers and $\delta^{13}C$ in the vertical profiles at the close of the LGM and in the $\Delta\delta^{13}C$ time series over the last 140kyr represents the expression of nutrient deepening [*E A Boyle*, 1988b]. It is particularly interesting that the intervals of maximum gradient in $\Delta\delta^{13}C$ coincide with the maxima in atmospheric $\delta^{13}C$ of CO_2. The $\delta^{13}C$ gradient described here could be achieved either by an enhancement of the biological pump through iron fertilization, or a change in the ventilation of the deep water mass. Given both the correlation between my record of $\Delta\delta^{13}C$, the record created by Ziegler et al [2013], and the deep ocean temperature record of ODP site 1123 in the Pacific, I argue that this nutrient deepening effect was not primarily the result of changes in export production at the surface. Instead, the trapping of carbon likely arose from changes in the age and ventilation of the water mass. I speculate that this occurred as a result of changes in deep ocean temperature of CDW, which altered the conditions under which southern-sourced water was formed and allowed for the creation of a southern-sourced cold, salty deep water mass. Co-occurring measurements of the suite of trace elements measured in Chapter 3 (B/Ca, Sr/Ca, Mg/Ca, Nd/Ca) for the two time series would clarify how temperature, oxygen, and carbonate ion may have changed over this period, and perhaps provide more insight into the possible mechanisms involved.

Further work in this area could provide clarity regarding the role that dust supply plays in regulating global climate. For instance, records of atmospheric dust deposition form the Southern Atlantic [*A Martínez-Garcia et al.*, 2011] suggest that the amount of dust deposition over the last 140 kyr only began to increase significantly after MIS 5A.

However, the record of $\Delta\delta^{13}C$ record presented here demonstrates that a large gradient in $\delta^{13}C$ developed across the MIS 5E/5D transition. It would therefore be of great interest to develop high-resolution multi-proxy records during periods of low dust depostion (such as MIS 5D) to better understand the drivers of the deep ocean $\Delta\delta^{13}C$ gradient.

Chapter 4, in part, will be submitted for publication Paleoceanography. Foreman, A.D., Charles, C.D., Rae, J. W., Adkins, J.F., and Slowey, N. C. The dissertation author was the primary investigator and author of this paper.

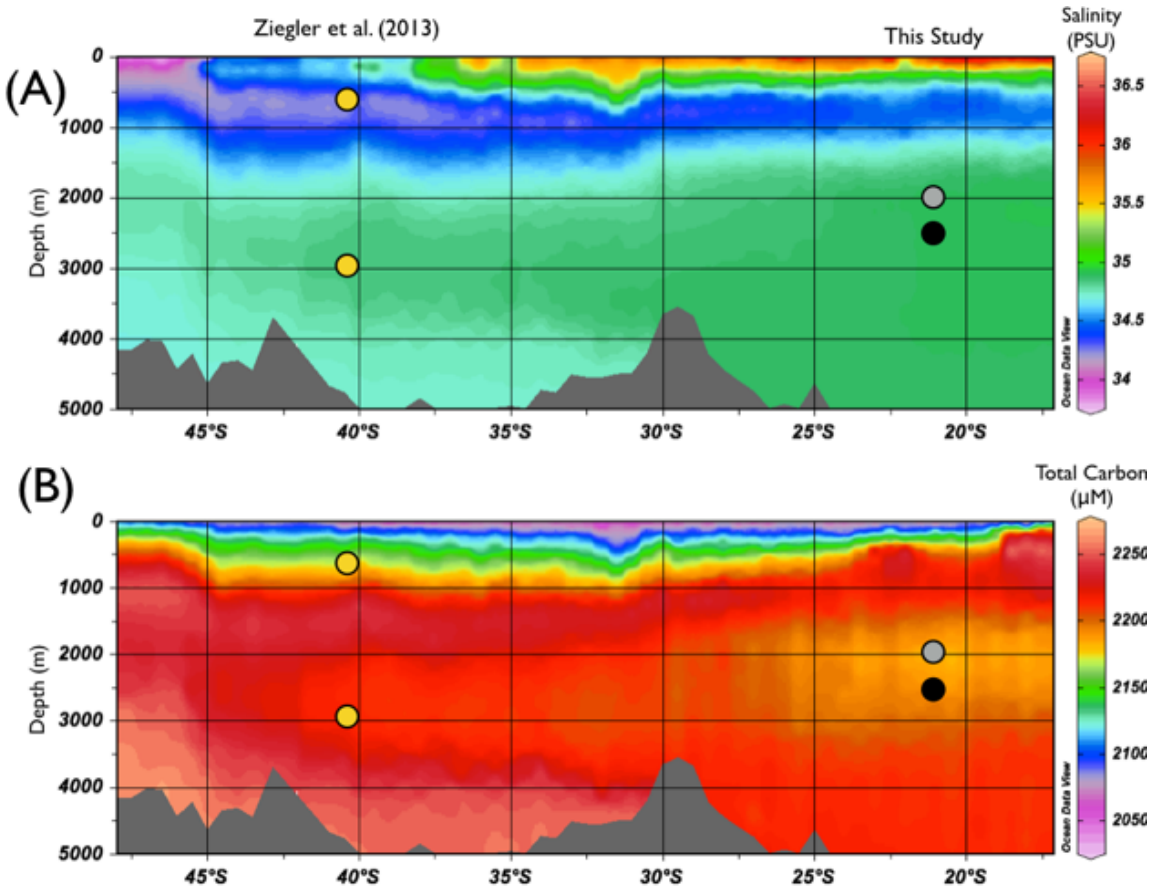

Figure 4.1 Sampling locations for this study (Grey and Black) and the Ziegler et al. [2013] study (Yellow) mapped on to salinity (A) and Total Carbon (B) data from the CLIVAR A13.5 cruise (http://cdiac.ornl.gov/ftp/oceans/CLIVAR/A13.5_2010.data/). The Ziegler record of $\Delta\delta^{13}C$ was created by taking the difference between the planktonic species *G. truncatulinoides* (top, yellow) and the benthic species *C. wuellerstorfi* (bottom, yellow). In contrast, the record of $\Delta\delta^{13}$ presented in Figure 4.4 was created by examining the difference in the $\delta^{13}C$ of two different *C. wuellerstorfi* records from neighboring cores (grey circle, 1977m depth; black circle, 2680m depth)

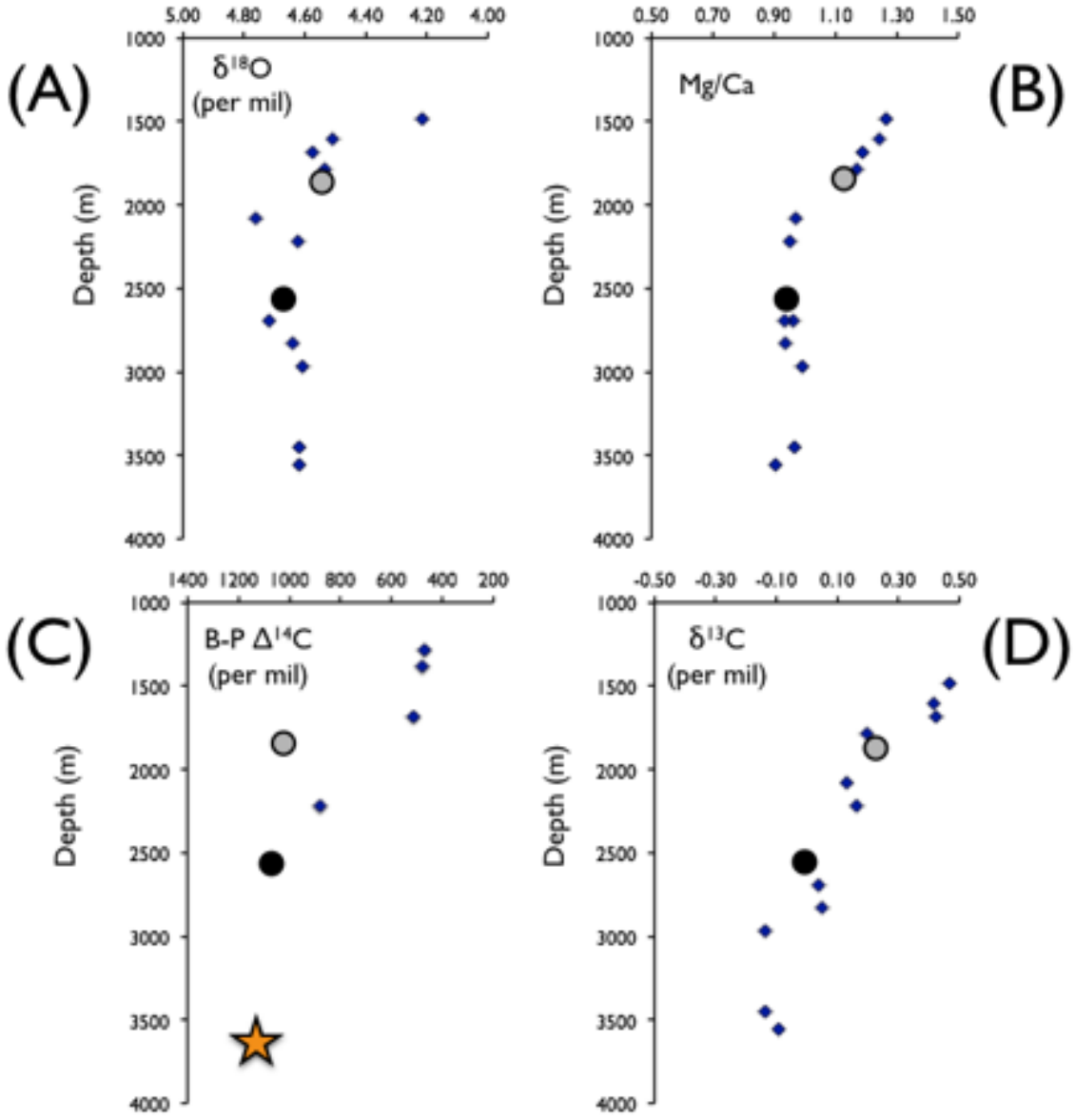

Figure 4.2 The vertical profiles reconstructed for the distribution of (A) $\delta^{18}O$, (B) Mg/Ca, (C) Benthic-Planktonic $\Delta^{14}C$, and (D) $\delta^{13}C$ at the close of the Last Glacial Maximum. The sediment cores from this core collection that were used to reconstruct the benthic-benthic $\Delta\ \delta^{13}C$ gradient shown in Figure 4.4 are highlighted by grey (MV09-PC23) and black (MV09-PC21) circles. The radiocarbon measurements in (C) are made on samples from the same set of cores as measurements for (A), (B), and (D) [*Jenna Munson, pers. communication*], with the exception of the deepest core (orange star), which was taken from a measurement on core MD07-3076 made by Skinner et al. [2010]. The 'physical' tracers and radiocarbon all show almost no gradient below 2000 meters depth. In contrast, $\delta^{13}C$ continues to decrease moving down the water column. This decrease is most likely the expression of nutrient deepening [*E A Boyle*, 1988b].

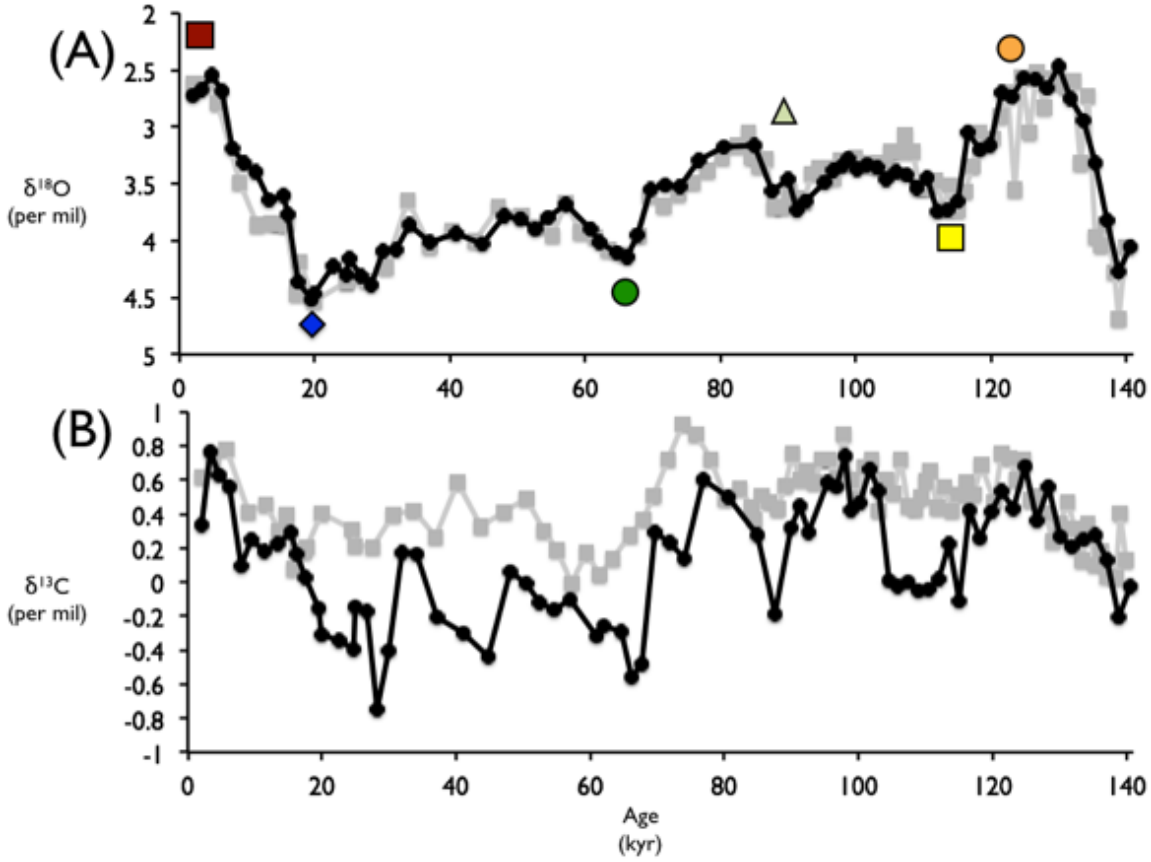

Figure 4.3 Measurements of (A) $\delta^{18}O$ and (B) $\delta^{13}C$ for sediment cores MV09-PC21 (black circles, 2680 meters depth) and MV09-PC23 (grey squares, 1977 meters depth). The colored symbols in (A) show the 6 points that were reconstructed in time slices in Chapters 2 and 3. The time series in (A) and (B) demonstrate that the gradient in $\delta^{18}O$ between 1977 and 2680 meters was negligible over the last glacial cycle, while gradients in $\delta^{13}C$ evolved at MIS 5D, 4, and the LGM.

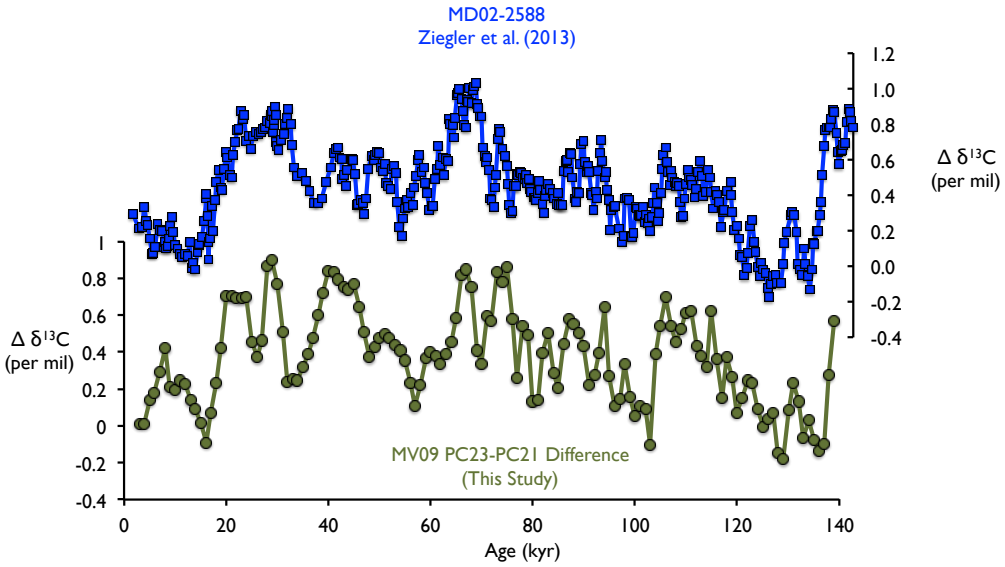

Figure 4.4 Measurements of the planktonic-benthic $\Delta\delta^{13}C$ made by Ziegler et al [2013] from a core near the Agulhas Plateau (top, blue squares) and measurements of the benthic-benthic $\Delta\delta^{13}C$ gradient between 1977m (MV09-PC23) and 2680m (MV09-PC21) derived from cores in this core collection (bottom, green circles). Periods of high gradient in both records correspond to glacial periods. The timing and magnitude of changes in the gradient in $\delta^{13}C$ for both time series implies that a common process is governing changes in the $\delta^{13}C$ of the cores in this study (located at 21°S near the Walvis Ridge) and core MD02-2588 (located at 41°S) on the Agulhas Plateau.

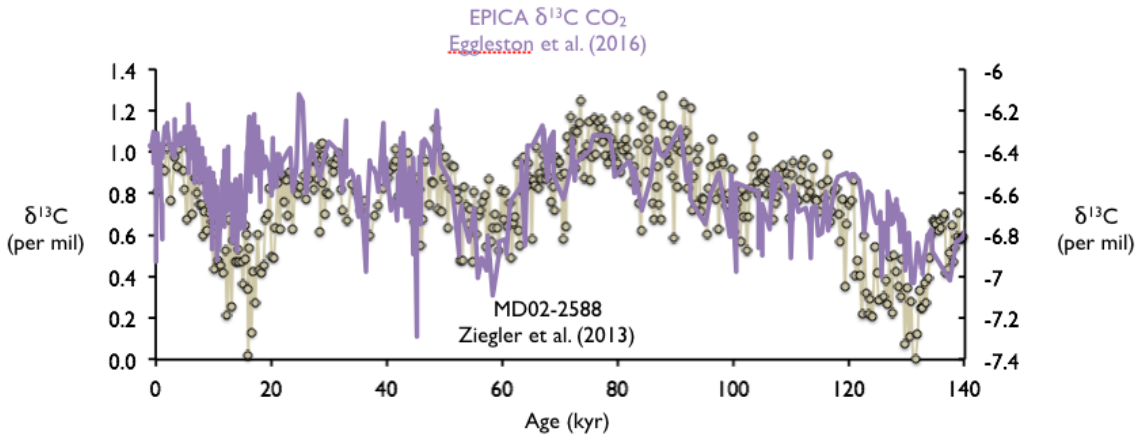

Figure 4.5 Measurements of the $\delta^{13}C$ of the thermocline-dwelling planktonic species *G. truncatulinoides* by Ziegler et al [2013] (tan circles) and of the $\delta^{13}C$ of pCO_2 from ice cores by Eggleston et al. [2016] (light purple). The *G. truncatulinoides* record matches the timing and magnitude of changes in the $\delta^{13}C$ of pCO_2, implying that the record of $\delta^{13}C$ from *G. truncatulinoides* is recording the $\delta^{13}C$ of the atmosphere without additional alteration by air-sea gas exchange.

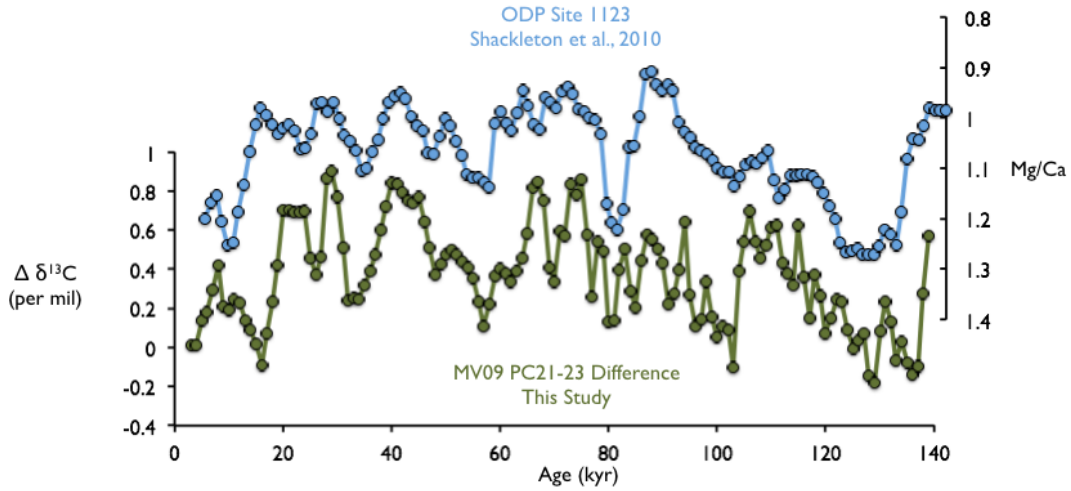

Figure 4.6 Measurements of the Mg/Ca ratios of *U. peregrina* from ODP site 1123 by Elderfield et al. [2010] (top, blue circles) and measurements of the benthic-benthic $\Delta\delta^{13}C$ gradient between 1977m (MV09-PC23) and 2680m (MV09-PC21) derived from cores in this core collection (bottom, green circles). Transitions in Mg/Ca (y-axis reversed) in the Pacific at ODP site 1123 closely match changes in $\Delta\delta^{13}C$ in the interior of the ocean, suggesting that transitions to colder temperatures in Circumpolar Deep Water were accompanied by an increase in the gradient of $\delta^{13}C$ in the ocean interior in the Southern Atlantic.

4.7 References

Adkins, J. F. (2013), The role of deep ocean circulation in setting glacial climates, *Paleoceanography*, *28*(3), 539-561.

Bird, M. I., J. Lloyd, and G. D. Farquhar (1994), Terrestrial carbon storage at the LGM, *Nature*, *371*(6498), 566-566.

Boiteau, R., M. Greaves, and H. Elderfield (2012), Authigenic uranium in foraminiferal coatings: A proxy for ocean redox chemistry, *Paleoceanography*, *27*(3).

Bouttes, N., D. Paillard, D. M. Roche, V. Brovkin, and L. Bopp (2011), Last Glacial Maximum CO2 and δ 13C successfully reconciled, *Geophysical Research Letters*, *38*(2).

Boyle, E., and L. Keigwin (1985), Comparison of Atlantic and Pacific paleochemical records for the last 215,000 years: Changes in deep ocean circulation and chemical inventories, *Earth and Planetary Science Letters*, *76*(1-2), 135-150.

Boyle, E. A. (1988a), The role of vertical chemical fractionation in controlling late Quaternary atmospheric carbon dioxide, *Journal of Geophysical Research: Oceans*, *93*(C12), 15701-15714.

Boyle, E. A. (1988b), Vertical oceanic nutrient fractionation and glacial/interglacial CO2 cycles, *Nature*, *331*(6151), 55-56.

Broecker, W. S., and T.-H. Peng (1982), *Tracers in the Sea*.

Broecker, W. S., J. Yu, and A. E. Putnam (2015), Two contributors to the glacial CO 2 decline, *Earth and Planetary Science Letters*, *429*, 191-196.

Broeker, W., and E. Maier-Reimer (1992), The influence of air and sea exchange on the carbon isotope distribution in the sea, *Global Biogeochemical Cycles*, *6*, 315-320.

Charles, C. D., J. D. Wright, and R. G. Fairbanks (1993), Thermodynamic influences on the marine carbon isotope record, *Paleoceanography*, *8*(6), 691-697.

Ciais, P., A. Tagliabue, M. Cuntz, L. Bopp, M. Scholze, G. Hoffmann, A. Lourantou, S. P. Harrison, I. Prentice, and D. Kelley (2012), Large inert carbon pool in the terrestrial biosphere during the Last Glacial Maximum, *Nature Geoscience*, *5*(1), 74-79.

Curry, W. B., and D. W. Oppo (2005), Glacial water mass geometry and the distribution of δ13C of ΣCO2 in the western Atlantic Ocean, *Paleoceanography*, *20*(1).

Cutler, K., R. Edwards, F. Taylor, H. Cheng, J. Adkins, C. Gallup, P. Cutler, G. Burr, and A. Bloom (2003), Rapid sea-level fall and deep-ocean temperature change since the last interglacial period, *Earth and Planetary Science Letters*, *206*(3), 253-271.

Duplessy, J., N. Shackleton, R. Fairbanks, L. Labeyrie, D. Oppo, and N. Kallel (1988), Deepwater source variations during the last climatic cycle and their impact on the global deepwater circulation, *Paleoceanography*, *3*(3), 343-360.

Eggleston, S., J. Schmitt, B. Bereiter, R. Schneider, and H. Fischer (2016), Evolution of the stable carbon isotope composition of atmospheric CO2 over the last glacial cycle, *Paleoceanography*, *31*(3), 434-452.

Elderfield, H., M. Greaves, S. Barker, I. R. Hall, A. Tripati, P. Ferretti, S. Crowhurst, L. Booth, and C. Daunt (2010), A record of bottom water temperature and seawater δ 18 O for the Southern Ocean over the past 440kyr based on Mg/Ca of benthic foraminiferal Uvigerina spp, *Quaternary Science Reviews*, *29*(1), 160-169.

Elsig, J., J. Schmitt, D. Leuenberger, R. Schneider, M. Eyer, M. Leuenberger, F. Joos, H. Fischer, and T. F. Stocker (2009), Stable isotope constraints on Holocene carbon cycle changes from an Antarctic ice core, *Nature*, *461*(7263), 507-510.

Ferrari, R., M. F. Jansen, J. F. Adkins, A. Burke, A. L. Stewart, and A. F. Thompson (2014), Antarctic sea ice control on ocean circulation in present and glacial climates, *Proceedings of the National Academy of Sciences*, *111*(24), 8753-8758.

Headley, M. A. (2008), Krypton and xenon in air trapped in polar ice cores: Paleo-atmospheric measurements for estimating past mean ocean temperature and summer snowmelt frequency, Ph.D thesis.

Herguera, J., E. Jansen, and W. Berger (1992), Evidence for a bathyal front at 2000‐M depth in the glacial Pacific, based on a depth transect on Ontong Java Plateau, *Paleoceanography*, *7*(3), 273-288.

Hodell, D. A., K. A. Venz, C. D. Charles, and U. S. Ninnemann (2003), Pleistocene vertical carbon isotope and carbonate gradients in the South Atlantic sector of the Southern Ocean, *Geochemistry, Geophysics, Geosystems*, *4*(1), 1-19.

Huybers, P., and C. Langmuir (2009), Feedback between deglaciation, volcanism, and atmospheric CO 2, *Earth and Planetary Science Letters*, *286*(3), 479-491.

Jaccard, S. L., E. D. Galbraith, D. M. Sigman, G. H. Haug, R. Francois, T. F. Pedersen, P. Dulski, and H. R. Thierstein (2009), Subarctic Pacific evidence for a glacial deepening of the oceanic respired carbon pool, *Earth and Planetary Science Letters*, *277*(1), 156-165.

Kallel, N., L. D. Labeyrie, A. Juillet-Leclerc, and J.-C. Duplessy (1988), A deep hydrological front between intermediate and deep-wafpr, masses in the glacial Indian Ocean, *Nature*, *333*(6174), 651-655.

Keigwin, L. D. (1998), Glacial‐age hydrography of the far northwest Pacific Ocean, *Paleoceanography*, *13*(4), 323-339.

Köhler, P., H. Fischer, and J. Schmitt (2010), Atmospheric δ13CO2 and its relation to pCO2 and deep ocean δ13C during the late Pleistocene, *Paleoceanography*, *25*(1).

Labeyrie, L. D., and J. C. Duplessy (1985), Changes in the oceanic 13C12C ratio during the last 140 000 years: High-latitude surface water records, *Palaeogeography, Palaeoclimatology, Palaeoecology*, *50*(2-3), 217-240.

Lund, D., J. Adkins, and R. Ferrari (2011), Abyssal Atlantic circulation during the Last Glacial Maximum: Constraining the ratio between transport and vertical mixing, *Paleoceanography*, *26*(1).

Lüthi, D., M. Le Floch, B. Bereiter, T. Blunier, J.-M. Barnola, U. Siegenthaler, D. Raynaud, J. Jouzel, H. Fischer, and K. Kawamura (2008), High-resolution carbon

dioxide concentration record 650,000–800,000 years before present, *Nature*, *453*(7193), 379-382.

Mackensen, A., M. Rudolph, and G. Kuhn (2001), Late Pleistocene deep-water circulation in the subantarctic eastern Atlantic, *Global and Planetary Change*, *30*(3), 197-229.

Mackensen, A., H. W. Hubberten, T. Bickert, G. Fischer, and D. Fütterer (1993), The δ 13C in benthic foraminiferal tests of Fontbotia wuellerstorfi (Schwager) relative to the δ 13C of dissolved inorganic carbon in southern ocean deep water: implications for glacial ocean circulation models, *Paleoceanography*, *8*(5), 587-610.

Marchitto, T. M., and W. S. Broecker (2006), Deep water mass geometry in the glacial Atlantic Ocean: A review of constraints from the paleonutrient proxy Cd/Ca, *Geochemistry, Geophysics, Geosystems*, *7*(12).

Martin, J. H. (1990), Glacial‐interglacial CO2 change: The iron hypothesis, *Paleoceanography*, *5*(1), 1-13.

Martínez-Garcia, A., A. Rosell-Melé, S. L. Jaccard, W. Geibert, D. M. Sigman, and G. H. Haug (2011), Southern Ocean dust-climate coupling over the past four million years, *Nature*, *476*(7360), 312.

McManus, J., W. M. Berelson, G. P. Klinkhammer, D. E. Hammond, and C. Holm (2005), Authigenic uranium: relationship to oxygen penetration depth and organic carbon rain, *Geochimica et Cosmochimica Acta*, *69*(1), 95-108.

Menviel, L., A. Mouchet, K. Meissner, F. Joos, and M. England (2015), Impact of oceanic circulation changes on atmospheric δ 13CO2, *Global Biogeochemical Cycles*, *29*(11), 1944-1961.

Ninnemann, U. S., and C. D. Charles (2002), Changes in the mode of Southern Ocean circulation over the last glacial cycle revealed by foraminiferal stable isotopic variability, *Earth and Planetary Science Letters*, *201*(2), 383-396.

Peterson, C. D., L. E. Lisiecki, and J. V. Stern (2014), Deglacial whole‐ocean δ13C change estimated from 480 benthic foraminiferal records, *Paleoceanography*, *29*(6), 549-563.

Schlitzer, R. (2000), Electronic atlas of WOCE hydrographic and tracer data now available, *Eos, Transactions American Geophysical Union*, *81*(5), 45-45.

Schmitt, J., R. Schneider, J. Elsig, D. Leuenberger, A. Lourantou, J. Chappellaz, P. Köhler, F. Joos, T. F. Stocker, and M. Leuenberger (2012), Carbon isotope constraints on the deglacial CO2 rise from ice cores, *Science*, *336*(6082), 711-714.

Schneider, R., J. Schmitt, P. Köhler, F. Joos, and H. Fischer (2013), A reconstruction of atmospheric carbon dioxide and its stable carbon isotopic composition from the penultimate glacial maximum to the last glacial inception, *Climate of the Past*, *9*(6), 2507-2523.

Sigman, D. M., and E. A. Boyle (2000), Glacial/interglacial variations in atmospheric carbon dioxide, *Nature*, *407*(6806), 859-869.

Skinner, L., S. Fallon, C. Waelbroeck, E. Michel, and S. Barker (2010), Ventilation of the deep Southern Ocean and deglacial CO2 rise, *Science*, *328*(5982), 1147-1151.

Stephens, B. B., and R. F. Keeling (2000), The influence of Antarctic sea ice on glacial–interglacial CO 2 variations, *Nature*, *404*(6774), 171-174.

Stuiver, M., and H. A. Polach (1977), Discussion reporting of 14 C data, *Radiocarbon*, *19*(3), 355-363.

Talley, L. D. (2011), *Descriptive physical oceanography: an introduction*, Academic press.

Tschumi, T., F. Joos, M. Gehlen, and C. Heinze (2010), Deep ocean ventilation, carbon isotopes, marine sedimentation and the deglacial CO2 rise, *Climate of the Past*, *6*(5), 1895-1958.

Ziegler, M., P. Diz, I. R. Hall, and R. Zahn (2013), Millennial-scale changes in atmospheric CO2 levels linked to the Southern Ocean carbon isotope gradient and dust flux, *Nature Geoscience*, *6*(6), 457-461.